



1993

Voltage Clamp Analysis of Latent Pacemaker Cells Isolated from Cat Right Atrium

Zhengfeng Zhou
Loyola University Chicago

Follow this and additional works at: https://ecommons.luc.edu/luc_diss



Part of the [Physiology Commons](#)

Recommended Citation

Zhou, Zhengfeng, "Voltage Clamp Analysis of Latent Pacemaker Cells Isolated from Cat Right Atrium" (1993). *Dissertations*. 3116.

https://ecommons.luc.edu/luc_diss/3116

This Dissertation is brought to you for free and open access by the Theses and Dissertations at Loyola eCommons. It has been accepted for inclusion in Dissertations by an authorized administrator of Loyola eCommons. For more information, please contact ecommons@luc.edu.



This work is licensed under a [Creative Commons Attribution-NonCommercial-No Derivative Works 3.0 License](#).
Copyright © 1993 Zhengfeng Zhou

LIBRARY-LOYOLA UNIVERSITY
MEDICAL CENTER

VOLTAGE CLAMP ANALYSIS OF LATENT PACEMAKER
CELLS ISOLATED FROM CAT RIGHT ATRIUM

By

Zhengfeng Zhou

A Dissertation Submitted to the Faculty of the Graduate School
of Loyola University of Chicago in Partial Fulfillment
of the Requirements for the Degree of
Doctor of philosophy

January

1993

Copyright by Zhengfeng Zhou, 1992

All rights reserved.

ACKNOWLEDGEMENTS

I would like to express sincere thanks to my supervisor and mentor, Dr. Stephen L. Lipsius. His guidance, patience and encouragement were essential to the completion of this dissertation.

I also wish to thank my committee members, Drs. Richard D. Nathan, J. Andrew Wasserstrom, Charles L. Webber and David E. Euler for their critical readings and discussions of this dissertation.

My appreciation is also extended to all members of the Department of Physiology for providing the means to complete this study.

Finally, I wish to acknowledge my parents, my wife and my son, whose sacrifice and understanding were of great help to me.

VITA

The author, Zhengfeng Zhou, son of Qiliang Zhou and Zaijuan Li, was born on December 25, 1957, in Beijing, People's Republic of China (P.R.C.).

He graduated from No. 105 High School in Beijing, P.R.C. in 1977. In March of 1978, he enrolled at Beijing Medical University in Beijing, P.R.C. In December of 1982, he received his Doctor of Medicine degree. In December of 1985, he received his Master of Science degree in Physiology. From December of 1985 to September of 1987, he worked as a research associate in the Department of Physiology at Beijing Medical University. In September of 1987, he enrolled in the Graduate School at Loyola University of Chicago in the Department of Physiology.

The author has worked under the direction of Dr. Stephen L. Lipsius. He was the recipient of Arthur J. Schmitt Dissertation Fellowship in 1991-1992.

TABLE OF CONTENTS

	Page
ACKNOWLEDGEMENTS	iii
VITA	iv
LIST OF TABLES	vii
LIST OF FIGURES	viii
LIST OF PUBLICATIONS	xi
LIST OF ABBREVIATIONS	xii
CHAPTER	
I. INTRODUCTION	1
II. LITERATURE REVIEW	4
A. Primary and Latent Pacemakers	4
B. Morphology of Cardiac Pacemaker Cells	6
C. Electrophysiology of Latent Pacemakers	7
D. Isolation of Single Pacemaker Cells	9
E. Ionic Current Mechanisms of Diastolic Depolarization	11
1. Inward Rectifier K^+ Current, I_{K1}	11
2. Hyperpolarization-activated Current, I_f	13
3. Delayed Rectifier K^+ Current, I_K	17
4. Slow Inward Ca^{2+} Currents	21
5. Fast Na^+ Current	23
6. Na-Ca Exchange Current, I_{NaCa}	24
F. Effect of β -adrenergic Stimulation	28
III. METHODS	30
A. Single Cell Isolation Procedure	30

B. Patch-clamp Recording Techniques	32
C. Measurements and Data Analysis	43
D. Solutions, Drugs and Chemical Reagents	44
IV. RESULTS	47
A. Morphology and Passive Membrane Properties	47
B. Pacemaker Action Potential Characteristics	49
C. Membrane Currents During Voltage Clamp	49
1. Hyperpolarization-activated Current, I_f	52
2. Delayed rectifier, I_K	74
3. Ca^{2+} Currents: T-type and L-type	81
4. Fast Na^+ Current	95
5. Na-Ca Exchange Current	95
V. DISCUSSION	120
A. Isolation of Single Latent Pacemaker Cells	120
B. Input Resistance and I_{K1} Current	121
C. I_f Current	122
D. I_K Current	127
E. Ca^{2+} Currents	131
F. Na-Ca Exchange Current	134
SUMMARY AND CONCLUSIONS	142
BIBLIOGRAPHY	147

LIST OF TABLES

TABLE

1. Cell Isolation Solutions	31
2. Internal Pipette Solutions	35
3. Measurements of Spontaneous Action Potentials in Latent Pacemaker Cells	51

LIST OF ILLUSTRATIONS

FIGURE	Page
1. Two types of whole-cell recording methods	33
2. Voltage clamp recording system	38
3. Discontinuous single electrode voltage clamp circuit	39
4. Settling times of voltage clamp	42
5. Measurement of membrane capacitance	45
6. Morphology of latent pacemaker cells	48
7. Latent pacemaker action potentials	50
8. Action potentials and currents recorded from latent pacemaker cell	53
9. Action potentials and I_f	54
10. Voltage dependence of I_f activation	56
11. Envelope of tails test for I_f	58
12. Reversal potential and fully-activated I-V relationship of I_f	60
13. Effect of Na^+ on I_f I-V relationship	62
14. Effect of K^+ on I_f I-V relationship	63
15. Kinetic analysis of I_f	65
16. Effect of Cs^+ on I_f I-V relationship	67
17. Effect of Cs^+ on pacemaker action potentials and I_f	69
18. Effect of ISO on I_f amplitude	72

FIGURE	Page
19. Effect of ISO on I_f activation curve	73
20. Effect of ISO on pacemaker action potentials and I_f	75
21. Voltage dependence of I_K activation	76
22. Fully-activated I-V relationship of I_K	78
23. Separation of I_K tail current from I_f activation	79
24. Effect of external K^+ on I_K reversal potential	82
25. Effect of elevated K^+ on pacemaker action potentials	83
26. Two types of Ca^{2+} currents: $I_{Ca,T}$ and $I_{Ca,L}$	85
27. Voltage dependence of activation and inactivation of $I_{Ca,T}$ and $I_{Ca,L}$	88
28. Effect of cobalt on $I_{Ca,T}$ and $I_{Ca,L}$	90
29. Effect of nifedipine on $I_{Ca,T}$ and $I_{Ca,L}$	91
30. Effect of nickel on $I_{Ca,T}$ and $I_{Ca,L}$	93
31. Effect of nickel on pacemaker action potentials	94
32. TTX-sensitive Na^+ current	96
33. I_{NaCa} in latent pacemaker cells	97
34. Dependence of I_{NaCa} on intracellular Ca^{2+}	100
35. Dependence of I_{NaCa} on SR Ca^{2+} and external Na^+	102
36. Effect of clamp duration on I_{NaCa}	104
37. Voltage dependence of $I_{Ca,L}$ and I_{NaCa}	106
38. Time course of rested $I_{Ca,L}$ and I_{NaCa} recovery	108
39. Differential effects of cadmium on $I_{Ca,L}$ and I_{NaCa}	109

FIGURE	Page
40. Effect of isoproterenol on $I_{Ca,L}$ and I_{NaCa}	111
41. Time and voltage dependence of I_{NaCa} recovery	114
42. Effect of ryanodine on pacemaker action potentials	116
43. Effect of isoproterenol on pacemaker action potentials	118

LIST OF PUBLICATIONS

Articles:

1. Zhou Z. and Ku Yun-Hui. Effect of electrical stimulation of rostral ventrolateral medulla on unit discharge of sympathetic preganglionic neurons in the rat. *Acta Physiologica Sinica*. **39**:123-131, 1987.
2. Zhou Z. and Lipsius S.L. Properties of the pacemaker current (I_p) in latent pacemaker cells isolated from cat right atrium. *Journal of Physiology (London)* **453**:503-523, 1992.
3. Zhou Z. and Lipsius S.L. Na-Ca exchange current in latent pacemaker cells isolated from cat right atrium. *Journal of Physiology (London)* 1992. (in press).
4. Zhou Z. and Lipsius S.L. Delayed rectifier potassium current (I_K) in latent pacemaker cells isolated from cat right atrium. *Pflügers Archiv* (submitted).
5. Zhou Z. and Lipsius S.L. Effect of Isoprenaline on I_f current recorded with conventional and nystatin whole-cell recording methods. *Pflügers Archiv* (submitted).

Abstracts:

1. Zhou Z. and Lipsius S.L. Ionic current mechanisms of latent atrial pacemakers. *Circulation* **82**:III-526, 1990.
2. Zhou Z. and Lipsius S.L. SR Ca^{2+} -mediated inward sodium current in latent atrial pacemaker cells. *Circulation* **84**:II-167, 1991.
3. Zhou Z. and Lipsius S.L. Pacemaker current, i_f recorded from latent atrial pacemaker cells using two different whole-cell recording methods. *Circulation* **84**:II-178, 1991.
4. Zhou Z. and Lipsius S.L. Delayed outward potassium current, I_K in latent atrial pacemaker cells. *Circulation*, 1992. (in press).

LIST OF ABBREVIATIONS

EGTA	Ethyleneglycol-bis-N,N,N',N'-Tetraacetic Acid
HEPES	N-2-hydroxyethylpiperazine-N'-2-ethane-sulfonic Acid (Calbiochem)
DMSO	Dimethylsulfoxide
ISO	Isoproterenol
TTX	Tetrodotoxin
4-AP	4-aminopyridine
TEA-CL	Tetraethylammonium Chloride (Sigma Chemical Company)
TRIS/HCL	TRIZMA Hydrochloride (Sigma Chemical Company)
SR	Sarcoplasmic reticulum
SA	Sinoatrial
AV	Atrioventricular
I_f	Hyperpolarization-activated current
I_K	Delayed rectifier potassium current
I_{K1} or $I_{K,rec}$	Inward rectifier potassium current
$I_{Ca,T}$	T-type Ca^{2+} current
$I_{Ca,L}$	L-type Ca^{2+} current
I_{NaCa}	Na-Ca exchange current
I_{to}	Transient outward current
\dot{V}_{max}	Maximum upstroke velocity

CHAPTER I

INTRODUCTION

There is extensive evidence that latent (subsidiary) pacemakers are located within specific regions of the mammalian right atrium (23,24,120,121,180,196,197). Both *in vivo* and *in vitro* experiments have shown that following surgical excision (120,121,180), exclusion (196,197) or suppression (27,185,186) of the SA node, the site that assumes pacemaker activity is consistently located in the caudal region of the right atrium. Further *in vitro* experiments have localized this latent pacemaker activity to the Eustachian ridge (185,188,189). The Eustachian ridge is a caudal extension of the crista terminalis that lies within the distribution of the posterior internodal pathway, and runs close to the opening of the inferior vena cava (199). Morphological studies have shown that cells thought to be responsible for SA node pacemaker activity, i.e. P cells (119,206), are found in specific extranodal regions of the right atrium. Thus, Sherf and James (199) report that P cells are found in the Eustachian ridge and Bachmann's bundle of human and canine hearts. In addition, P cells within the Eustachian ridge have been correlated with pacemaker activity, and are ultrastructurally similar to those found in SA node (188). These studies indicate that the Eustachian ridge is a functionally important site of latent pacemaker activity, and that this activity may be generated by pacemaker cells similar to those found in SA node.

In vitro electrophysiological studies of latent pacemaker activity have been performed on multicellular preparations of the Eustachian ridge isolated from dog and cat right atria (185,188,189). These studies revealed that spontaneously active Eustachian ridge tissues generate slow response pacemaker action potentials with characteristics similar to those of SA node (188), but different from those of typical atrial muscle (185). Latent pacemaker action potentials exhibit a prominent diastolic depolarization, significantly lower maximum diastolic potential and slower rate of rise than typical atrial muscle. Although significant insights into atrial latent pacemaker function have been gained from multicellular tissues, these preparations limit our ability to determine the ionic current mechanisms underlying pacemaker automaticity.

With the advent of single cell techniques, it is now possible to study the ionic currents in single cardiac cells isolated from specific regions of the heart. Thus, single pacemaker cells have been isolated from SA node, and patch-clamp techniques (93) have been used to study ionic currents in these single pacemaker cells (48,59,159,160,213). In general, experimental evidence indicates that multiple ionic current are involved in the generation of primary pacemaker activity, although the relative contribution of each current is still controversial (38,83,112,113,164). However, comparable studies have not been performed for atrial latent pacemaker function.

Therefore, the specific aims of the present research are: 1) to isolate viable single latent pacemaker cells from the Eustachian ridge of cat right atrium, 2) to study the morphology and passive membrane properties of these single latent pacemaker cells, and 3) to systematically analyze each of the major ionic currents, i.e. I_f , I_K , and Ca^{2+}

currents, in order to gain insight into the ionic mechanisms underlying latent pacemaker activity. In addition, this study will focus on the role of Na-Ca exchange in latent pacemaker function.

CHAPTER II

LITERATURE REVIEW

A. Primary and Latent Pacemakers.

Pacemakers in the mammalian heart are thought to be organized in a hierarchy consisting of a primary site and a number of latent (subsidiary) sites. The sinoatrial (SA) node serves as the primary pacemaker in the mammalian heart (30,75,136). The primary pacemaker controls the beating rate of the whole heart, because it exhibits the fastest inherent rate and it overdrive suppresses latent pacemakers throughout the heart (216). Latent pacemakers have been found in different regions of the heart including atrioventricular (AV) node (128,154,211), coronary sinus (27,76,224), atrioventricular valves (8,184), atrial muscle (Eustachian ridge) (185,186,188), and Purkinje fibers (65,215). In the classical concept of pacemaker hierarchy, it is generally believed that the AV node is the next most automatic pacemaker in the absence of the SA node (75,154,211,212). This concept has been challenged by the findings that after removal or suppression of the SA node the emerged dominant latent pacemaker site is located within the right atrium (74,116,120,121,179-181,196,197). Thus, Sealy *et al.* (196,197) found that after surgical exclusion of the canine SA node, pacemaker rhythms were generated from low right atrial sites. Using electrophysiological mapping techniques,

Jones *et al.* (120,121) showed in the canine that after removal of the SA node along with 3-4 cm of sulcus terminalis, the latent pacemaker site of earliest activation was located at the junction of inferior right atrium with the inferior vena cava. Experiments on the conscious animal showed that these atrial latent pacemakers were capable of assuming pacemaker control of the heart and were regulated by both divisions of the autonomic nervous system (120,121,179,180,187,203). The atrial subsidiary pacemakers differed from both SA node and AV node pacemakers. Their spontaneous rates of discharge were slower than those of the SA node and faster than those of the AV node (121). Further *in vitro* studies localized the latent pacemaker site to the Eustachian ridge, a caudal extension of the crista terminalis that courses close to the opening of the inferior vena cava (185,186,188). Rozanski *et al.* (186) studied latent atrial pacemaker activity in an *in vitro* right atrial preparation isolated from the canine heart. In their experiments, suppression of SA node activity was accomplished by ligating the SA node artery. The appearance of latent pacemaker activity following SA node suppression was facilitated by the presence of β -adrenergic stimulation. The spontaneous rate of latent atrial pacemakers was significantly slower than that of SA node pacemakers. Latent pacemakers were more sensitive to the negative chronotropic effects of ACh than the SA node. In addition, rapid pacing of latent pacemakers resulted in pacemaker suppression with a significantly longer recovery time than those recorded in SA node. These responses are similar to those found in whole animal experiments. These studies indicate that the atrial pacemakers located within the Eustachian ridge are a functionally important component in the hierarchy of cardiac pacemakers.

B. Morphology of Cardiac Pacemaker Cells.

Numerous morphological studies indicate that SA node pacemaker cells have ultrastructural characteristics distinct from typical atrial muscle (117-119,146,147,175). In general, SA node consists of three cell types: 1) "P cell" or leading pacemaker cell, 2) transitional cell or latent pacemaker cell, and 3) working atrial muscle cell (119,147,175). P cells are characterized by a relatively small diameter, sparse myofibrillar content, a relatively large nucleus, ovoid or spindle shaped, with a pale histological appearance (119,147,175). Taylor *et al.* (206) provided direct evidence that P cells are responsible for pacemaking within the SA node. In their experiments, cells exhibiting true pacemaker action potentials were iontophoretically tagged with lanthanum. The lanthanum labeled cells were found to exhibit ultrastructural characteristics typical of P cells.

Morphological studies have found that P cells are not restricted to the SA node (188,199). Thus, Sherf and James (199) reported that P cells are found in the Eustachian ridge and Bachmann bundle of human and canine hearts. Rubenstein *et al.* (188) performed morphological and electrophysiological studies on spontaneously active Eustachian ridge preparations isolated from cat right atrium. In their experiments the site of earliest pacemaker activation was determined by electrophysiological mapping using intracellular recordings. Morphological analysis revealed that P cells were consistently found at the sites which generated atrial latent pacemaker activity (188). Morphometric measurements showed that Eustachian ridge P cells were similar, although not identical, to SA node P cells from the same animals (188). Like in SA node, P cells were typically

clustered in groups of three or more cell profiles, approximately 5 to 7 μM in diameter and irregular in shape. Myofibrillar content was sparse and randomly oriented. However, Eustachian ridge P cells had a unique organization of subsarcolemmal cisternae never seen in SA node P cells. The subsarcolemmal cisternae were prominent and often directly apposed to one another between connected P cells or between a connected P cell and a transitional cell. The possible functional significance of this ultrastructural feature will be discussed below.

C. Electrophysiology of Latent Pacemakers.

In 1951 Draper and Weidmann (65) used intracellular microelectrodes to perform the first transmembrane recordings from mammalian heart muscle. They found that action potentials generated by spontaneously active canine Purkinje fibers exhibited slow diastolic depolarization. In 1955, West (221) was the first to record primary pacemaker action potentials from the rabbit SA node. He showed that pacemaker action potentials of SA node were different from those of non-pacemaker atrial muscle. Pacemaker action potentials exhibited a slow diastolic depolarization, significantly more positive maximum diastolic potential, relatively slow depolarization, slow repolarization, and smaller amplitude (221). Further studies confirmed that a slow depolarization during diastole is a consistent feature of pacemaker activity in the heart (30,44,98,100,221). However, the existence of slow diastolic depolarization does not mean that the cell is functioning as a primary or true pacemaker. True pacemaker cells are those cells which initiate an impulse. Action potentials of true pacemakers are characterized by a prominent diastolic depolarization and a smooth transition from diastolic depolarization into the upstroke of

the action potential. In contrast, latent pacemaker action potentials usually exhibit some degree of diastolic depolarization, along with an abrupt transition into the action potential upstroke (30,141). However, a latent pacemaker cell can be transformed into a true pacemaker when cells with higher automaticity have been suppressed or removed. Lu (143) showed that when separated from the true pacemaker, a latent pacemaker area could generate true pacemaker-type action potentials, although the spontaneous rate was slower than that of the original true pacemaker. This result indicates that some latent pacemaker cells are capable of generating independent pacemaker activity if they have the opportunity to develop their intrinsic rhythmicity.

In addition to SA node primary pacemakers, slow diastolic depolarization has been recorded from different regions of right atrium (46,101,102,132,177). Paes de Carvalho *et al.* (177) studied in detail the sequence of activation of the rabbit atrium. They found that action potentials recorded in the region of the SA ring bundle, a white bundle of tissue paralleling the crista terminalis on the venous border, exhibited slow diastolic depolarization. They speculated that in certain cases the SA ring bundle is able to undertake pacemaker activity. Hogan and Davis (101,102) showed that specialized fibers with action potentials similar to those of ventricular Purkinje fibers were found along the caval border of the crista terminalis of canine right atrium. The action potentials of these so called "plateau fibers" exhibited a long plateau phase and inherent diastolic depolarization. Epinephrine produced an increase in both rate and magnitude of diastolic depolarization. Kreitner (132) also found similar plateau fibers (B cells) in a localized area between the caval border of the crista terminalis and the primary

pacemaker area of rabbit right atrium. The action potential upstroke of these B cells was depressed by TTX and the diastolic depolarization was reduced by about 70% in the presence of 1.5 mM cesium (Cs^+). In contrast, the action potentials of the primary pacemaker cells (A cells) were insensitive to TTX and their diastolic depolarization was not affected by Cs^+ . Action potentials with slow diastolic depolarization have also been recorded from AV node (110,128,195,208), coronary sinus (224), and atrioventricular valves (8,144,183,184).

Transmembrane recordings have been performed in multicellular preparations of the Eustachian ridge isolated from dog and cat right atrium (185,188,189). When isolated *in vitro*, Eustachian ridge tissues beats spontaneously. Electrophysiological recordings revealed that Eustachian ridge tissues generate pacemaker action potentials with characteristics similar to those of SA node, although the spontaneous cycle length of latent pacemakers is more than twice that of SA node (188). Latent pacemaker action potentials exhibited a prominent diastolic depolarization that merged smoothly into the upstroke, characteristic of true pacemaker activity. The diastolic depolarization in latent pacemakers exhibited two distinct slopes: an initial slope that was steep in relation to a secondary, more gradual depolarization. Similar diastolic potentials have been noted in latent pacemaker activities recorded from rabbit atrioventricular valves (183,184).

D. Isolation of Single Pacemaker Cells.

With the development of single cell isolation techniques, single Ca^{2+} tolerant pacemaker cells have been isolated from rabbit (12,48,59,64,159,160,205,213) and guinea pig (2) SA node. Several different morphological types of pacemaker cells have

been used in electrophysiological studies including round or oval (2,159,160,205), elongated or spindle shaped (12,47,48,64,213,230), and spider (48,59). Taniguchi *et al.* (205) found that SA node pacemaker cells appeared rod-like or spindle-shaped in a high-K⁺, low-Cl⁻, Ca²⁺-free "KB" solution (114). However, in normal Tyrode's solution containing 1.8 mM Ca²⁺ the rod cells became round or oblate spheroids. Unlike damaged atrial or ventricular cells, the round SA node pacemaker cells exhibited a relatively smooth and shiny surface (159). Nathan (160) also found that some pacemaker cells were rod shaped on the day of isolation and rounded up after 1 or 2 days in culture. Recently, many investigators have reported isolation of SA node cells which maintain their elongated or spindle shape in normal Tyrode's solution (12,47,48,64, 213, 230). Another cell type, referred to as "spider like" were also isolated from rabbit SA node (48,59). DiFrancesco *et al.* (59) have found that spider cells most frequently exhibited large I_f current. However, Denyer & Brown (48) showed that the spider cells were often groups of two or more cells stuck together. Isolated SA node pacemaker cells are characterized by regular spontaneous activity in normal Tyrode's solution, and spontaneous action potentials similar to those observed in multicellular preparations (59,64,159,160,213). In addition, action potentials recorded from pacemaker cells with different morphologies are very similar (59,64,159,160,213).

Anumonwo *et al.* (1) reported the isolation of latent pacemaker cells from rabbit tricuspid valve. Tricuspid valve cells were rod-like or spindle-shaped in the recovery (KB) solution. Upon exposure to normal Tyrode's solution about 70% of the cells became rounded. Some round cells had smooth surfaces and exhibited rhythmic

contractions. Spontaneous action potentials recorded from these cells showed a mean maximum diastolic potential of -82 mV which was more negative than that of SA node pacemaker cells. In previous work from this laboratory, Wu *et al.* (226) have shown that some cells isolated from cat right atrium exhibited spontaneous pacemaker activity. Based on ionic currents elicited in response to hyperpolarization two types of spontaneously active latent pacemaker cells were found: 1) those exhibiting predominantly I_f , and 2) those lacking I_f and exhibiting only time-independent leak currents. Although both pacemaker cell types were elongated and similar in size, those exhibiting predominantly I_f exhibited a more tortuous appearance with less apparent myofibrillar material. These cells were similar in appearance to pacemaker cells isolated from rabbit SA node (12,48). The exact origin of each pacemaker cell type within the right atrium was not determined.

E. Ionic mechanisms of diastolic depolarization.

Much of our current knowledge of the ionic current mechanisms responsible for pacemaker automaticity has been gained from experiments on the pacemaker cells of SA node. The evidence indicates that multiple current systems are involved in the generation of spontaneous diastolic depolarization, although the relative contribution of each current is still controversial (38,83,112,113,164).

1. Inward Rectifier K^+ current, I_{K1} .

One important finding from studies on SA node cells is that pacemaker cells exhibit little, if any, of the inward rectifying background potassium current termed I_{K1} or $I_{K,rec}$ (83,113,172,213). In working ventricular and atrial muscle cells I_{K1} is the

major background current responsible for the relatively negative resting membrane potential. The lack of I_{K1} in SA node cells is thought to be responsible for the relatively low maximum diastolic potential and high input resistance in these cells (83). This latter property is very important for pacemaker depolarization because it means that a small change in membrane current can cause a relatively large change in membrane potential (38,83). I_{K1} is a K^+ current which activates almost instantaneously upon a change in membrane potential. This current was originally thought to be a time-independent current. However, recent experiments indicate that I_{K1} also exhibits voltage- and time-dependent activation and inactivation (20,133,148,191,226). The I-V relationship of I_{K1} exhibits a strong inward rectification (162,192,226). The conductance of the I_{K1} channel is increased by elevated extracellular K^+ , resulting in a cross-over phenomenon in the I-V relationship (162,192,226). Using a cell-attached patch clamp technique, Noma *et al.* (172) recorded two classes of single K^+ channel currents that differed primarily in their mean open time. The first type was an inward rectifying K^+ channel ($I_{K,rec}$) which was observed most frequently in ventricular cells but rarely seen in SA node pacemaker cells. The second type was an ACh-operated K^+ channel which was observed in SA node pacemaker cells but never seen in ventricular cells. In atrial cells, however, both types of channels were recorded. The open time of the $i_{K,rec}$ channel is much longer (life-time: 50-100 ms) (123,192) than that of the ACh-operated K^+ channel (0.5-1.5 ms) (190,202). The relatively long open time of $i_{K,rec}$ channel results in a relatively high resting membrane conductance in ventricular cells. Although SA node pacemaker cells exhibit a high density of ACh-operated K^+ channels, in the absence of ACh the

spontaneous open time is very short, and therefore this channel contributes little to the resting membrane conductance in pacemaker cells. In the presence of ACh, however, the frequency of channel openings is greatly increased (190,202), resulting in an increase in membrane conductance and hyperpolarization of membrane potential.

The lack of I_{K1} has also been reported in frog sinus venosus pacemaker cells (84) and latent pacemaker cells isolated from rabbit crista terminalis (85) and cat right atrium (226). Wu *et al.* (226) found that in myocytes isolated from the cat right atrium, 93% of the quiescent atrial cells studied exhibited prominent I_{K1} , whereas 94% of atrial cells that exhibited spontaneous pacemaker activity lacked I_{K1} . These data suggest that the lack of background K^+ conductance is essential for atrial pacemaker function.

2. Hyperpolarization-activated current, I_f .

Voltage clamp studies of a variety of cardiac pacemaker tissues have recorded the so-called pacemaker current, I_h (228), I_p (150) or I_f (25,31,32,36,51,52,59,63,71,129, 159,160,213,226). I_f is a time-dependent inward current that is activated by hyperpolarization to voltages more negative than approximately -50 mV and fully activated at -110 mV. I_f is carried by both sodium and potassium ions with a reversal potential of about -20 mV (51,59,89,213). Relatively low concentrations (1-2 mM) of Cs^+ block I_f in a voltage-dependent manner. At potentials more negative than the reversal potential, Cs^+ exerts a strong blocking effect, but at potentials more positive than the reversal potential, Cs^+ has little effect (25,53,59,89).

The pacemaker current was first recorded from cardiac Purkinje fibers as a net inward current that increased with time (214). However, it was interpreted as a decaying

outward K^+ current, I_{K2} (42,62,151,166,178,214). This conclusion was based on the observations that the I_{K2} reversal potential was close to the K^+ equilibrium potential and varied with the extracellular K^+ concentration in a way expected for a K^+ current (42,62,166). In addition, total membrane conductance measured during hyperpolarization decreased with time, supporting I_{K2} as a deactivating outward current (214). However, it was also noted that the I_{K2} reversal potential was always slightly more negative than the expected K^+ equilibrium potential (42,62,166). This was thought to be due to the depletion of K^+ in extracellular clefts caused by background K^+ current, I_{K1} during the hyperpolarization (62). In addition, the current disappeared when external Na^+ was removed (151). Further studies performed by DiFrancesco (51-54) demonstrated that after blocking I_{K1} with barium (Ba^{2+}), I_{K2} behaved as an activating inward current rather than a decaying outward current. Thus, in Ba^{2+} -containing solution the total membrane conductance increased during hyperpolarization (52,54). In addition, in the presence of Ba^{2+} , I_{K2} exhibited a reversal potential of about -30 mV, suggesting that I_{K2} could not be a pure K^+ current (51,53). Therefore, DiFrancesco (52,54) reinterpreted the pacemaker current, I_{K2} , in Purkinje fibers as an inward current, I_f , which is activated by hyperpolarization and carried by both Na^+ and K^+ ions, very much like I_f found in SA node (31,32,63,228). The former interpretation of I_{K2} as a decaying outward K^+ current was explained as a superimposition of two current components: the hyperpolarization-activated inward current, I_f and a current caused by I_{K1} due to K^+ depletion during hyperpolarization imposed by the voltage clamp (52,54,164).

In SA node and Purkinje fiber pacemakers, I_f activation exhibits either a short

delay in onset, yielding a sigmoidal time course or no delay in onset (36,53,59,89,213,228). I_f currents without delay in onset were best fitted by a single exponential function (59,89,228). I_f currents that exhibited a sigmoidal time course have been analyzed differently by different authors. van Ginneken & Giles (213) used a Hodgkin-Huxley model with an activation variable raised to the second power to describe the sigmoidal time course of I_f activation. In contrast, DiFrancesco (55) proposed a rather complex kinetic model with 5 closed states and 3 open states. For reconstruction purposes, DiFrancesco & Noble (60) used a simple first-order Hodgkin-Huxley model to approximate I_f kinetics. Thus, a single exponential function was used to fit the sigmoidal current after ignoring the initial several millisecond of the current (36,53,59). The time course of I_f activation has been reported to be relatively slow in the pacemaker voltage range. At -70 mV, the time constant for I_f activation is about 1 sec in SA node pacemaker cells (89,213) and about 3 sec in Purkinje cells (36). The fully-activated I-V relationship of I_f is linear at voltages more negative than the reversal potential and showed outward rectification at more positive voltages (59,213). The average fully-activated slope conductance is about 12 nS (213). DiFrancesco *et al.* (59) found that lowering extracellular Na^+ concentration shifted the reversal potential to more negative voltages but did not change the slope conductance (51,59). In contrast, changing K^+ concentration not only shifted reversal potential but also increased the slope conductance when extracellular K^+ was elevated (53,59). These results suggest that both Na^+ and K^+ ions are charge carriers for I_f . In addition, extracellular K^+ ions have an activation-like effect on I_f . Recent work suggests that the activation-like effect of K^+ may be due

to an increase in Na^+ conductance through the I_f channel (81).

Although I_f has been extensively studied in SA node pacemaker tissues, its relative contribution to primary pacemaker activity has been debated. It has been proposed that I_f may not contribute to the pacemaker depolarization because of its relatively small amplitude within the pacemaker potential range (-45 to -65 mV) and its slow time course of activation (89,171,228). Noma *et al.* (171) showed that 2 mM Cs^+ significantly suppressed I_f , but the rate of diastolic depolarization was slowed only slightly. However, it has been argued that since SA node pacemaker cells have relatively high input resistances, even a few picoamps of inward current may result in a significant depolarization of the membrane potential (83). DiFrancesco (57) showed that in SA node pacemaker cells the slope of diastolic depolarization was about 100 mV/s which required only 3 pA of inward current in a cell with a capacitance of 30 pF. van Ginneken & Giles (213) recently reported that a small but significant amount (about 5-10 pA) of I_f was activated within the pacemaker potential range in SA node pacemaker cells. In addition, I_f current density has been shown to be linearly related to the slope of diastolic depolarization (173). These findings are consistent with those of Denyer & Brown (49) who found that in single SA node cells 2 mM Cs^+ consistently slowed spontaneous rate by 20-30 %. These results indicate that I_f contributes significantly to primary pacemaker function. However, because Cs^+ induced block of I_f does not stop pacemaker activity, it appears that I_f is not an essential current for primary pacemaker function.

Because I_f amplitude increases at more negative potentials, I_f may contribute more significantly to the diastolic depolarization in more hyperpolarized cells such as Purkinje

cells (165). Consistent with this idea, Anumonwo *et al.* showed that in tricuspid valve pacemaker cells, which exhibited a maximum diastolic potential of -82 mV, 2 mM Cs^+ blocked I_f and markedly increased spontaneous cycle length (1). Because latent atrial pacemakers exhibit a somewhat more negative pacemaker voltage range than SA node cells, I_f may contribute more to latent than primary pacemaker activity. A contribution of I_f to latent atrial pacemaker activity was suggested by experiments in multicellular Eustachian ridge preparations in which $1-2$ mM Cs^+ decreased the slope of diastolic depolarization and significantly increased pacemaker cycle length (189). Single myocytes isolated from cat right atrium that exhibited pacemaker activity also exhibited a Cs^+ -sensitive I_f current (226). However, the origin of these latent pacemakers within the right atrium was not determined. At the present time, little is known about the role of I_f in right atrial latent pacemaker function.

3. Delayed Rectifier K^+ current, I_K .

Another mechanism proposed to contribute to the pacemaker depolarization in SA node is deactivation of the delayed rectifying potassium current, I_K (33,35,83,113,207). I_K is a time-dependent outward current which is activated by depolarization to voltages more positive than -40 mV and fully activated at about $+20$ mV. (61,159,169,200). I_K is mainly carried by potassium ions with a reversal potential of about -80 mV (159,169,200). The fully-activated I-V relationship is linear at voltages more negative than about -20 mV and exhibits inward-going rectification at more positive voltages (159). Normally, this current activates during the depolarization of the action potential, and is thought to be the major outward current responsible for initiating repolarization.

After repolarization, I_K decays during diastole and within the pacemaker potential range (83,113,207). However, in order to elicit depolarization the decay of I_K must be associated with a constant background inward current (38). Possible inward current candidates have been proposed by Hagiwara *et al.* (91) and DiFrancesco (57).

Brown *et al.* (33,35) compared the relative contribution of different time-dependent currents to SA node pacemaker activity. They found that both I_K decay and I_f activation were present in the pacemaker voltage range. However, the relative amounts of activating I_f and decaying I_K varied from preparation to preparation. In general, about 80% of total depolarizing current resulted from I_K decay. The role of I_K decay in the spontaneous activity was tested by switching off the clamp circuit at various phases of the I_K tail current (169). The results supported the idea that the I_K tail current was mainly responsible for generating the diastolic depolarization. In contrast, Yanagihara & Irisawa (229) showed that the change in I_K during diastolic depolarization was very small and spontaneous action potentials could be observed even in the absence of I_K . These results indicated that the decay of I_K can hardly be a major factor determining the pacemaker depolarization. In bull-frog sinus venosus pacemakers the slow deactivation of I_K was reported to be the main pacemaker mechanism (84). The role of I_K in latent atrial pacemaker function is not known.

There is still controversy about the components and kinetics of I_K in SA node pacemaker cells. Experiments on multicellular preparations showed that the time course of I_K decay was a simple exponential and was independent of the magnitude of the preceding depolarization (169). This finding indicated that I_K current in SA node can

be described by a Hodgkin-Huxley model with one conductance mechanism. DiFrancesco *et al.* (61) found that the single exponential decay of I_K was only obtained when the depolarizing clamp duration was relatively short. When the pulse duration was prolonged, however, the outward current tail became a two exponential process because of the presence of a slow component which took more than 5 sec to reach steady-state at the holding potential. Similar two components of delayed outward currents have been reported in other cardiac preparations: i_{x1} and i_{x2} in sheep Purkinje fibers (167,168), I_1 and I_2 frog atrium (174), and I_K and I_x in cat ventricle (152). Based on kinetics of activation and deactivation, reversal potentials, and degree of rectification, it was proposed that two distinct currents were responsible for the time-dependent outward current (152,167,168,174). However, the results obtained from multicellular preparations should be interpreted with caution since the kinetics of K^+ currents may be distorted by accumulation of K^+ ions in the extracellular spaces resulting from prolonged depolarization (9,152,163).

In single cell preparations the accumulation of K^+ has been shown to be minimal. It was found that in single frog atrial and sinus venosus pacemaker cells there was only one type of delayed outward current, I_K (84,107,201). I_K tail currents exhibited a single exponential decay even with long (10 sec) depolarizing clamp pulses. The activation of I_K during depolarization exhibited a sigmoidal time course in onset. The kinetics of I_K could be described using a single Hodgkin-Huxley model with an activation variable n raised to the second power (84,107,201).

The kinetic properties of I_K in single mammalian cardiac cells, however, seem

to be more complicated than those in frog cells. In SA node pacemaker cells, both activation and decay of I_K were best fitted by two exponential functions (2,159). Similar two-exponential time courses of I_K activation and deactivation have been observed in other single mammalian cardiac cells (6,86,193,194,220). These results suggested that the two-exponential kinetics are not an artifact of ion accumulation. In Purkinje cells, although two exponential functions were required for fitting both activation and deactivation of I_K , an envelope test indicated that neither the fast nor the slow component fulfilled a Hodgkin-Huxley model (86). It was proposed that there was only one type of I_K channel with two different closed states and one open state (86). Matsuura *et al.* (149) showed that I_K decay was mono-exponential at voltages more negative than -50 mV but was bi-exponential at more positive voltages. The time course of activation was sigmoidal and could be best fitted by an exponential with an activation variable n raised to the second power. According to the Hodgkin-Huxley model, with n raised to the second power, a bi-exponential decay of tail current would be expected at voltages where the steady-state activation variable (n_∞) is not zero. At voltages where $n_\infty = 0$, the time course of tail current decay would become mono-exponential (149,201). Therefore, the results were consistent with a Hodgkin-Huxley model with n raised to the second power. In contrast, Balser *et al.* (6) found that the sigmoid time course of I_K activation could not be described by higher-order Hodgkin-Huxley models with an activation variable raised to the second or fourth power. Instead, they found that the sigmoid time course was best described by a four-state Markovian chain model (three closed states and one open state). Recently, Sanguinetti & Jurkiewicz (193,194) showed that I_K in guinea

pig atrial and ventricular cells resulted from the activation of two distinct K^+ currents, $I_{K,r}$ and $I_{K,s}$. $I_{K,r}$ was specifically blocked by a benzenesulfonamide antiarrhythmic agent, E-4031, and activated very rapidly relative to the slower activating $I_{K,s}$. In guinea pig SA node pacemaker cells, however, an E-4031-sensitive current, $I_{K,r}$ was not present (2). In summary, the kinetics of I_K in mammalian cardiac cells are not fully understood. Whether the two-exponential activation and deactivation behavior represents complex kinetic behavior of a single I_K channel type or is the result of two distinct K^+ currents is still an open question.

Another potassium current, transient outward current (I_{to}) has been found in a few SA node pacemaker cells (48) and in pacemaker cells isolated from rabbit crista terminalis (85). This current may contribute to the repolarization of the action potential. However, its role in pacemaker activity is not clear.

4. Slow Inward Ca^{2+} Currents.

Two types of slow inward Ca^{2+} currents, T-type and L-type, have been identified in a variety of cardiac cells (10,26,99,124,225) including SA node pacemaker cells (79,90). Both Ca^{2+} currents are time-dependent inward currents activated by depolarization of the membrane potential. The long lasting (L-type, $I_{Ca,L}$) Ca^{2+} current is the classical slow inward Ca^{2+} current which is activated at voltages more positive than -40 mV with a peak at about 0 mV (79,90). The low threshold, transient type (T-type, $I_{Ca,T}$) Ca^{2+} current has an activation threshold between -50 to -60 mV (79,90). The amplitudes of both Ca^{2+} currents are significantly increased with increasing extracellular Ca^{2+} concentration. However, $I_{Ca,T}$ exhibits a lower K_m for Ca^{2+} ions

than $I_{Ca,L}$, indicating that $I_{Ca,T}$ had a higher channel affinity for Ca^{2+} ions (90).

$I_{Ca,T}$ and $I_{Ca,L}$ have different sensitivities to inorganic blockers. Low concentrations of nickel (Ni^{2+}) have been reported to selectively block $I_{Ca,T}$ (26,90,124,225). In SA node pacemaker cells, Hagiwara *et al.* (90) showed that $40 \mu M$ Ni^{2+} abolished $I_{Ca,T}$ but had no effect on $I_{Ca,L}$. Others have reported that the blocking effect Ni^{2+} is less selective (99,156,210). Fermini & Nathan (79) found that $40 \mu M$ Ni^{2+} did not block $I_{Ca,T}$ in cultured SA node pacemaker cells, and higher concentrations reduced both $I_{Ca,T}$ and $I_{Ca,L}$. Most studies have reported that low concentrations of cadmium (Cd^{2+}) selectively block $I_{Ca,L}$ (26,156,161,225). In rabbit SA node pacemaker cells, however, $20 \mu M$ Cd^{2+} significantly blocked both $I_{Ca,T}$ and $I_{Ca,L}$ (90). In addition, both Ca^{2+} currents were abolished in SA node cells (90) or reduced in canine atrial cells by $2 mM$ cobalt (Co^{2+}) (10).

It has been reported that $I_{Ca,T}$ current density is ten times larger in SA node pacemaker cells than in atrial cells (90). However, this comparison was made between data obtained under different experimental conditions. Although the authors corrected for the influence of different Ca^{2+} concentrations, they did not account for the differences in temperature ($37^{\circ}C$ versus $22^{\circ}C$) and species (rabbit versus dog) (10,90). Tseng and Boyden (210) compared $I_{Ca,T}$ current density of Purkinje cells with that of ventricular cells under the same experimental conditions. They found that $I_{Ca,T}$ current density in Purkinje cells was twice as much as that in ventricular cells. In addition, $I_{Ca,T}$ current density of Purkinje cells was comparable to that of SA node pacemaker cells (90,210). Whether atrial subsidiary pacemaker cells have a higher density of $I_{Ca,T}$

compared with typical atrial muscle cells has yet to be determined.

Ca^{2+} currents are thought to play a major role in primary pacemaker activity by contributing to the late phase of the diastolic depolarization (35,164). The role of $I_{\text{Ca,L}}$ has been debated because its activation threshold is more positive than the pacemaker potential range (90). However, recent studies using an action potential clamp technique and a $I_{\text{Ca,L}}$ channel blocker demonstrated that $I_{\text{Ca,L}}$ played a significant role in the pacemaker depolarization (64). In addition, SA node pacemaker cells exhibited a large nifedipine-sensitive $I_{\text{Ca,L}}$ "window" current. The voltage range of the $I_{\text{Ca,L}}$ "window" current was similar to that of the pacemaker potential and thereby may contribute to the diastolic depolarization (50). However, neither of these experiments distinguish whether $I_{\text{Ca,L}}$ plays a direct or indirect role in pacemaker function. The contribution of $I_{\text{Ca,T}}$ to pacemaker potential is supported by the finding that in SA node pacemaker cells $40 \mu\text{M}$ Ni^{2+} , which specifically blocked $I_{\text{Ca,T}}$, inhibited the late diastolic depolarization and increased spontaneous cycle length (64,90). In addition, Fermini and Nathan (79) found a significant overlap of $I_{\text{Ca,T}}$ activation and inactivation curves in the pacemaker voltage range, suggesting that $I_{\text{Ca,T}}$ "window" current may contribute to SA pacemaker activity. In tricuspid valve pacemaker cells $40 \mu\text{M}$ Ni^{2+} also prolonged spontaneous cycle length, but $I_{\text{Ca,T}}$ was not studied in these cells (1).

5. Fast Na^+ current.

In multicellular preparations, pacemaker action potentials recorded from the central region of SA node are resistant to TTX (131,142,227), suggesting that the fast Na^+ current is either not present or inactivated in the primary pacemaker cells. On the

other hand, TTX-sensitive Na^+ current has been recorded in some single pacemaker cells isolated from SA node (48,160). Nathan (160) found that there are two types of cultured SA node pacemaker cells; type I cells were TTX resistant and type II cells exhibited TTX-sensitive Na^+ current. Presumably, the type I cells were dominant and type II were subsidiary SA node pacemaker cells. However, a recent study showed that TTX-sensitive Na^+ current was also present in type II cells isolated from the central region, i.e. the site of earliest excitation (14). Thus, it is unclear whether type II cells are dominant or subsidiary pacemaker cells. Voltage clamp analysis of Na^+ current cultured in SA node pacemaker cells indicated that the activation and inactivation curves overlapped between -60 and -50 mV, generating a "window" current (157,158). The presence of a TTX-sensitive Na^+ "window" current in the pacemaker potential range suggests that the Na^+ current may contribute to the pacemaker potential. However, action potential recordings showed that TTX reduced only maximum upstroke velocity (\dot{V}_{max}) and the overshoot but had no effect on spontaneous beating rate (158). These results indicate that fast Na^+ current may be present in SA node pacemaker cells but only contributes to the action potential upstroke.

6. Na-Ca Exchange Current.

It is now well recognized that in a variety of tissues, Na-Ca exchange is electrogenic and thereby can substantially influence membrane voltage (21). Voltage clamp studies on single cardiac myocytes have identified a Na-Ca exchange current under a variety of experimental conditions (106,108,109,126,127,137,138,153). Kimura *et al.* (126) found that after blocking Ca^{2+} and K^+ channels as well as the Na-K pump, a Na-

Ca exchange current (I_{NaCa}) was recorded in ventricular cells. The magnitude and reversal potential of I_{NaCa} were dependent on external and internal Na^+ and Ca^{2+} concentrations. Under conditions of 140 mM external Na^+ , 10 mM internal Na^+ , 127 nM internal Ca^{2+} and 2 mM external Ca^{2+} , the I_{NaCa} reversal potential was about -24 mV. This value was close to the thermodynamically expected value for 3 Na^+ :1 Ca^{2+} stoichiometry.

A slow inward tail current that is attributable to activation of Na-Ca exchange has been recorded in single atrial and ventricular cells (66,69,72,78,82,155). Fedida *et al.* (78) recorded an inward current in guinea pig ventricular cells that was closely correlated with the contraction of the cell but not with $I_{Ca,L}$. This inward current appeared as a slow inward tail current after a brief depolarizing pulse. It has been shown that this slow inward tail current was abolished by loading the cell with EGTA (69,78,155), suggesting that the current is mediated by intracellular Ca^{2+} . In support of this idea, the inward tail current has been shown to exhibit a linear relationship to intracellular Ca^{2+} concentration measured with fura-2 or indo-1 in ventricular cells (7,66). In rat ventricular (155) and rabbit atrial (69) cells the inward tail current was abolished by 1-3 μ M ryanodine, an agent that eliminates SR Ca^{2+} release (182) and abolishes intracellular Ca^{2+} transients (5,145,222). In guinea pig ventricular cells, however, 1 μ M ryanodine had no effect on the inward tail current (78). The same dose of ryanodine also had no effect on the contraction of guinea pig ventricular cells. Egan *et al.* (72) showed that at higher doses (8-10 μ M) ryanodine abolished at least 80% of the inward tail current in guinea pig ventricular cells. These results suggest that the slow inward tail current is

activated by an intracellular Ca^{2+} transient which is mediated via SR Ca^{2+} release. The inward tail current has been shown to depend on extracellular Na^+ (69,78,155). Two possible mechanisms may be responsible for intracellular Ca^{2+} -activated Na^+ influx; the Na-Ca exchange mechanism (126,127) or a non-specific cation channel (43,73). Lithium (Li^+) can pass through Ca^{2+} -activated non-specific cation channels (73), but is unavailable to the Na-Ca exchange mechanism (126). Replacing extracellular Na^+ with Li^+ significantly inhibited the inward tail current (69,78,155). These results provide further support for the idea that the inward tail current is due to activation of Na-Ca exchange current rather than a Ca^{2+} -activated non-specific cation channel.

It has been shown in guinea pig ventricular (78) and rabbit atrial cells (82) that the duration of the depolarizing clamp has little effect on the time course of I_{NaCa} decay. In rabbit ventricular cells, however, I_{NaCa} decay following long depolarizations was significantly faster than that after relatively short depolarizations (82). It was proposed that this difference in kinetics is due to the difference in the amount of SR in rabbit ventricular and atrial cells. The atrial myocytes have more SR and the SR which is present appears to exhibit more prominent Ca-induced release of Ca^{2+} than ventricular myocytes (82). The findings that EGTA and ryanodine abolished I_{NaCa} indicate that SR Ca^{2+} release is the major source of Ca^{2+} to activate I_{NaCa} (69,78,155). The influx of Ca^{2+} through Ca^{2+} channels may not be sufficient to activate I_{NaCa} . In fact, in the presence of EGTA and ryanodine the Ca^{2+} entry is increased rather than decreased due to the slow-down of $I_{\text{Ca,L}}$ inactivation. The dependence of I_{NaCa} on SR Ca^{2+} release is also supported by the findings that I_{NaCa} amplitude is not related to $I_{\text{Ca,L}}$ on a beat to

beat basis (69,72). In atrial cells, the voltage dependence of I_{NaCa} and $I_{Ca,L}$ differ from each other. The I-V relationship of $I_{Ca,L}$ was bell-shaped with a peak at about +10 mV, whereas I_{NaCa} increased between -40 and -20 mV and was relatively constant between -10 and +40 mV (69). In addition, brief application of Cd^{2+} significantly inhibited $I_{Ca,L}$ without affecting I_{NaCa} amplitude (72). Similar results have been reported using other Ca^{+} channel blockers; nifedipine (155) and diltiazem (69). These results indicate that I_{NaCa} is relatively insensitive to changes in $I_{Ca,L}$ and that only a fraction of $I_{Ca,L}$ is sufficient to trigger maximal I_{NaCa} .

The Na-Ca exchange current has been proposed as a component contributing to the action potential duration and plateau (66,69,72,155). In addition, Na-Ca exchange plays a significant role in the decline of intracellular Ca^{2+} during contractile relaxation (16) and in the loss of intracellular Ca^{2+} that underlies the diastolic decay of contraction with time, i.e. rest decay (105). However, the contribution of Na-Ca exchange to cardiac pacemaker function is less well understood. Experiments on multicellular SA node preparations by Brown *et al.* (33,34) reported two components of slow inward current; a fast inward component due to a channel gated current fraction, and a second slower component due to Na-Ca exchange and mediated by SR Ca^{2+} release. They proposed that both fast and slower components of slow inward current may contribute to the last third of the pacemaker depolarization and into the upstroke. However, Noble (164) has indicated that it is unlikely that the Na-Ca exchange component contributes to the primary pacemaker potential. Hagiwara & Irisawa (88) reported a Na-Ca exchange current in single pacemaker cells isolated from SA node. At this time, it appears that

the role of Na-Ca exchange in primary pacemaker activity is not settled.

Previous studies from this laboratory in cat multicellular Eustachian ridge tissue indicated that a major component of latent pacemaker activity was mediated by SR Ca^{2+} release (189). Thus, ryanodine, an agent that interferes with SR Ca^{2+} release (182), specifically inhibited the late phase of diastolic depolarization, resulting in a significant increase in pacemaker cycle length. Moreover, in the absence of a functionally intact SR latent atrial pacemakers generated dysrhythmic electrical activities (140,189). Several studies have shown a clear relationship between intracellular Ca^{2+} released from the SR and sarcolemmal Na-Ca exchange currents (66,69,155). These findings are consistent with the hypothesis that a component of latent pacemaker activity is mediated by SR Ca^{2+} release via Na-Ca exchange. However, direct study of Na-Ca exchange current in latent atrial pacemaker cells has not been performed.

F. Effect of β -adrenergic Stimulation.

Experiments in whole animal (180) and multicellular preparations (185,189) have shown that atrial latent pacemaker activities are modulated by β -adrenergic stimulation. In SA node pacemaker cells, β -adrenergic stimulation accelerated spontaneous pacemaker rate by increasing the slope of diastolic depolarization (32). The mechanisms responsible for the effect β -adrenergic stimulation potentially involve several ionic current systems. It has been shown that β -adrenergic agonists, isoproterenol (ISO) and adrenaline, increased the I_f amplitude and shifted the steady-state activation curve to more positive voltages in Purkinje and SA node pacemaker cells (32,36,59,89). In addition, the time course of I_f activation became faster in the presence of ISO (89). The effect of

isoproterenol on I_f was mediated by activation of adenylate cyclase and increased levels of cyclic AMP, because superfusion of forskolin and intracellular application of cyclic AMP produced similar enhancement of I_f (89). β -adrenergic agonist also increased slow inward Ca^{2+} current (32,90) in SA node pacemaker cells. Recent single channel recordings of Ca^{2+} currents in SA node pacemaker cells demonstrated that ISO significantly increased the open probability of $I_{Ca,L}$ channels, but had no effect on $I_{Ca,T}$ channels (90). In addition, in guinea-pig ventricular cells, ISO induced a Na^+ -dependent Cl^- current (4,95,96). This current is inward at diastolic voltages. Thus, if the ISO-induced Cl^- current is present in pacemaker cells, it could contribute to the positive chronotropic effect of ISO. However, a recent study reported that the ISO-induced Cl^- current was not present in SA node pacemaker cells (204). An increase of I_K by β -adrenergic agonists has also been reported (13,31,68,97). An increased I_K should not contribute to the positive chronotropic effect of β -agonist, since the increase in outward current would by itself tend to slow the pacemaker depolarization. Therefore, an increased I_f and $I_{Ca,L}$ in the pacemaker voltage range may contribute to the positive chronotropic effect of β -agonists in SA node pacemakers. (32,59,89,90).

CHAPTER III

METHODS

A. Single Cell Isolation Procedure.

Adult cats of either sex, weighing 1.5-3.5 kg, were anesthetized with pentobarbital sodium (30-50 mg/kg, i.p.) and injected with heparin (500 units/kg, i.p.). The enzyme dispersion procedure used to isolate single latent atrial pacemaker cells was modified from a method previously described to isolate single atrial myocytes (225). After a mid-sternal thoracotomy the heart was quickly removed and transferred to a beaker containing prewarmed (36°C) Tyrode's solution (Table 1; solution 1), and then mounted on a Langendorff perfusion apparatus. The heart was perfused with normal Tyrode's solution (Table 1; solution 1) for 5-6 min at 37°C until blood was washed out completely. This was followed by a 5 min perfusion with a Ca^{2+} -free Tyrode's solution (Table 1; solution 2), and a final perfusion for 30-40 min with an enzyme solution (Table 1; solution 3) containing 36 μM Ca^{2+} and 0.1% albumin. The enzyme solution was recirculated with a pump. During the enzyme perfusion phase, 50 μl of Ca^{2+} stock solution (54 mM) was added to the perfusate every 8 min to yield a final Ca^{2+} concentration of about 150 μM . Following this perfusion procedure the atria were removed from the heart and the right atrium was opened to expose the endocardium.

Table 1. Cell Isolation Solutions

	1	2	3	4	5
	Normal Tyrode	Ca-free Tyrode	Perfusion Enzyme	Incubation Enzyme	HEPES Tyrode
NaCl (mM)	137	137	137	137	137
KCl (mM)	5.4	5.4	5.4	5.4	5.4
CaCl ₂ (mM)	1.8	--	0.036	0.036	1.8
MgCl ₂ (mM)	1.0	1.0	1.0	1.0	1.0
NaHCO ₃ (mM)	12	12	12	12	--
NaH ₂ PO ₄ (mM)	0.6	0.6	0.6	0.6	--
Glucose (mM)	11	11	11	11	11
Albumin (%)	--	--	0.1	0.1	--
Collagenase(%)	--	--	0.07	0.1	--
Protease (%)	--	--	--	0.01	--
Elastase (%)	--	--	--	0.1	--
HEPES (mM)	--	--	--	--	5
pH	7.4 *	7.4 *	7.4 *	7.4 *	7.4 **
Osmolarity (mOsm/L)	296 ***	294 ***	--	--	293 ***

* Bicarbonate-buffered Tyrode's solutions were bubbled with 95% O₂-5% CO₂ to yield pH 7.4.

** HEPES-buffered Tyrode's solution was titrated with NaOH to pH 7.4.

*** Measured by Advanced Micro-osmometer, Model 3MO

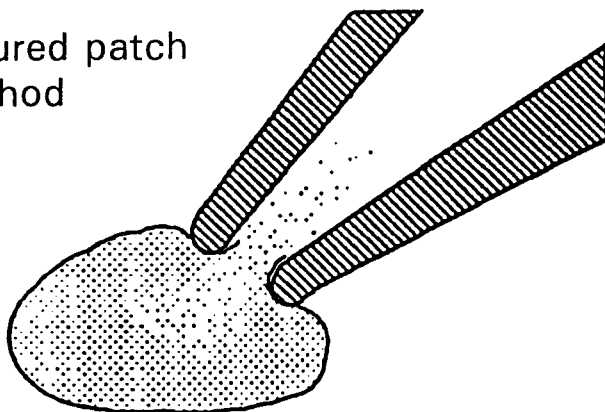
Latent pacemaker cells were isolated from the Eustachian ridge of the right atrium. The Eustachian ridge is a caudal extension of the crista terminalis that courses close to the opening of the inferior vena cava (188). Previous work has identified the Eustachian ridge as a functionally important site of latent pacemaker activity (185,188,189). The Eustachian ridge region ($\approx 6 \times 3$ mm) was excised and incubated in an enzyme solution (Table 1; solution 4) for 30-40 min at 36°C while being agitated in a shaking water bath. The tissue suspension was filtered through a nylon mesh ($210 \mu\text{m}$) using Tyrode's solution containing $200 \mu\text{M Ca}^{2+}$ and 0.05% albumin. After the cells settled for about 30 min the solution was suctioned off and gradually replaced with HEPES-buffered solution (Table 1; solution 5). Cells were stored in this solution at room temperature until use. A similar procedure was used to isolate regular atrial myocytes from right atrial appendage.

B. Patch-Clamp Recording Techniques.

Cells used for study were transferred to a small tissue bath (0.5 ml) mounted on the stage of an inverted microscope (Nikon Diaphot). After cells settled for about 10 min, they were superfused with prewarmed HEPES-buffered Tyrode's solution containing (in mM): NaCl 137, KCl 5.4, MgCl_2 1.0, CaCl_2 1.8, HEPES 5, glucose 11, and titrated with NaOH to pH 7.4, at a rate of 1-3 ml/min. All experiments were performed at a temperature of $34\text{-}36^\circ\text{C}$.

Ruptured patch recording method. Action potentials and ionic currents were recorded in the whole-cell configuration using suction pipettes, as described by Hamill *et al.* (93) (Figure 1A). Pipettes were pulled from borosilicate glass (Sutter Instrument

A. Ruptured patch method



B. Nystatin-perforated patch method

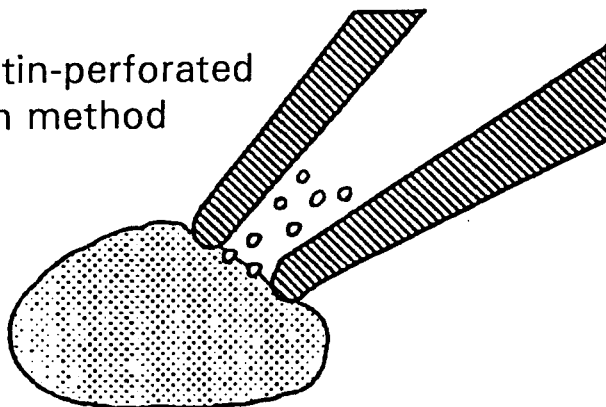


Figure 1. A: Standard ruptured patch recording method. B: Nystatin-perforated patch recording method. (modified from Horn & Marty, 1988)

Co.) in a six step process using a horizontal programmable puller (Flaming Brown, model PC 80, Sutter instrument Co.). Pipette tips were fire polished by passing current through a platinum wire in close proximity to the pipette tip. The pipettes had inner diameters of 1-1.5 μm and when filled with standard internal pipette solution (see Table 2) had resistances of 3-6 $\text{M}\Omega$. With the standard pipette solution filling the pipette, there was a liquid junction potential of about -10 mV between internal pipette and bath solutions. All recordings were corrected for this junction potential. In studies of T- and L- type Ca^{2+} currents, pipettes were filled with a CsCl pipette solution (see Table 2). Under these conditions, the liquid junction potential was only -3-5 mV which was not corrected in the recordings. Pipettes were connected to an amplifier headstage via a Ag-AgCl wire. A Ag-AgCl reference electrode was used to connect the bath solution and the ground input of the headstage. The headstage was mounted on a hydraulic micromanipulator (Narashige). The following procedures were routinely performed to improve gigaseal formation: 1) the pipette solution was filtered through a 0.2 μM syringe filter (Nalgene, Nalge Co.). 2) a slight positive pressure was applied to the pipette as it was moved through the air-water interface. 3) a fresh pipette was used for each cell. After the pipette tip was positioned near the cell, the positive pressure was relieved. Upon touching the cell membrane gentle suction was applied to form a gigaseal. Additional suction was applied to rupture the membrane patch.

Nystatin-perforated patch recording method. With the nystatin-perforated patch method, action potential and ionic current signals were recorded in the whole cell configuration, and nystatin was added to the internal pipette solution to permeabilize

Table 2. Internal Pipette Solutions

	Standard	Nystatin	Ca ²⁺ currents
K-glutamate	120	100	--
KCl	20	40	--
MgCl ₂	1.0	1.0	1.0
EGTA	1.0	0.5	10
Na ₂ -ATP	4.0	4.0	--
HEPES	5.0	5.0	5.0
CsCl	--	--	120
K ₂ -ATP	--	--	5.0
pH	7.2 *	7.2 *	7.2 **

* titrated with KOH to pH 7.2.

** titrated with CsOH to pH 7.2.

rather than rupture the membrane patch, as described by Horn and Marty (104) (Figure 1B). Nystatin is a polyene antibiotic that forms voltage-insensitive ion pores in the membrane patch under the recording pipette. These pores are somewhat selective for cations over anions (40,130), but are impermeant to Ca^{2+} , other multivalent ions and molecules > 0.8 nm in diameter (103,130). Suction pipettes were filled with the nystatin internal pipette solution (see Table 2) as follows: first, nystatin was dissolved in DMSO at a concentration of 50 mg/ml and then added to internal pipette solution to yield a final concentration of 150 ug/ml. Nystatin stock solution was added to the pipette solution while the pipette solution was being ultrasonicated. After 5 min of ultrasonication the nystatin-containing pipette solution appeared slightly yellow without any precipitate. Pipettes were filled by putting the pipette tip directly in nystatin-containing pipette solution for about 2 min and then backfilling the pipettes with the same solution. It has been reported that filling the pipette tip with the nystatin-containing solution may interfere with gigaseal formation (104,130). In our experiments, nystatin did not appear to reduce the success rate for gigaseal formation. The advantage of filling the pipette tip with the nystatin-containing solution is that the time needed to achieve a low access resistance was significantly shortened. In our experiments, the access resistance began to drop almost immediately after gigaseal formation and decreased to as low as 20 M Ω after about 5 min. After about 1-2 hours, it was usual for nystatin precipitate to appear at the bottom of the plastic beaker, requiring re-sonication of the solution. Usually the nystatin-containing pipette solution could be used for about 4-5 hours at which time fresh nystatin pipette solution was made.

Electronic equipment: Figure 2 shows a schematic diagram of the experimental recording setup. An Axoclamp-2A amplifier (Axon Instruments, Inc.) was used to record action potentials in bridge mode and ionic currents in discontinuous single electrode voltage clamp mode (dSEVC). In the voltage clamp mode the amplifier cycling (sampling) rate was 8-12 kHz. A Compaq 286 computer was used to generate voltage clamp protocols as well as acquire and analyze voltage and current signals using a Pclamp program (version 5.0, Axon Instruments, Inc.). The membrane potential and current traces were monitored on a dual beam storage oscilloscope (Tektronix 5113). A second oscilloscope (Tektronix 2213A) was used to monitor the decay of the pipette voltage. The membrane potential and current signals were sampled by a 12-bit resolution A/D converter (Tecmar Labmaster) and stored on the computer hard disk. In addition, the voltage and current signals were recorded digitally on video tape using a 2 or 4 channel PCM A/D VCR adaptor (PCM-2 or PCM-4, Medical Systems Corp.).

In the dSEVC mode a single electrode switches between passing current and recording voltage. This method eliminates possible errors arising from electrode series resistance. The principle of the dSEVC method was first introduced by Brennecke & Lindemann (28,29) and implemented experimentally by Wilson and Goldner (223). Figure 3 shows the schematic diagram of the dSEVC circuit. A1 is a high input-impedance amplifier which measures the total voltage composed of both membrane potential (V_m) and voltage drop (V_e) across the resistance of the electrode resulted from current (I_0) injection through the electrode. In order to eliminate V_e the switch S1 is operated in current passing and voltage recording positions alternately. During the

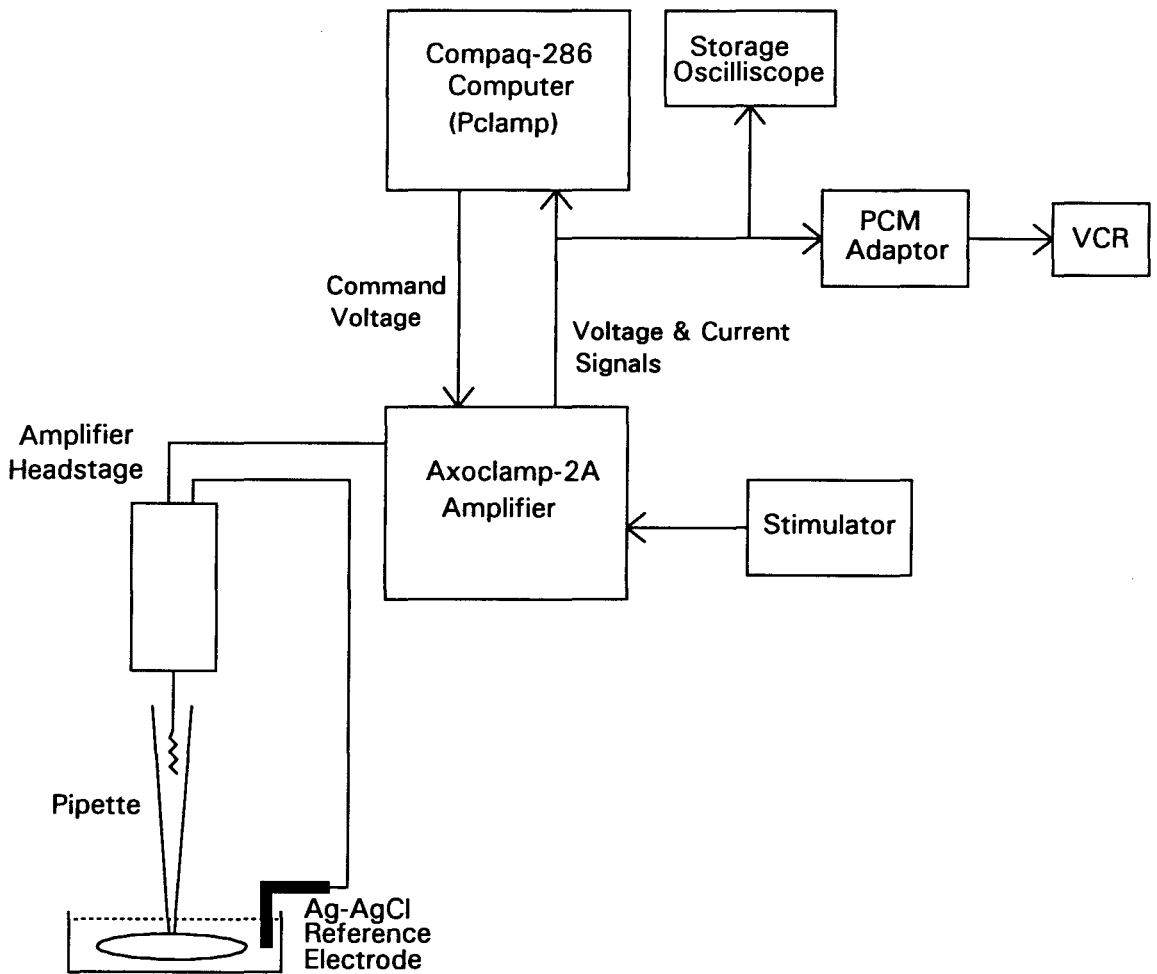


Figure 2. Schematic diagram of voltage clamp recording system.

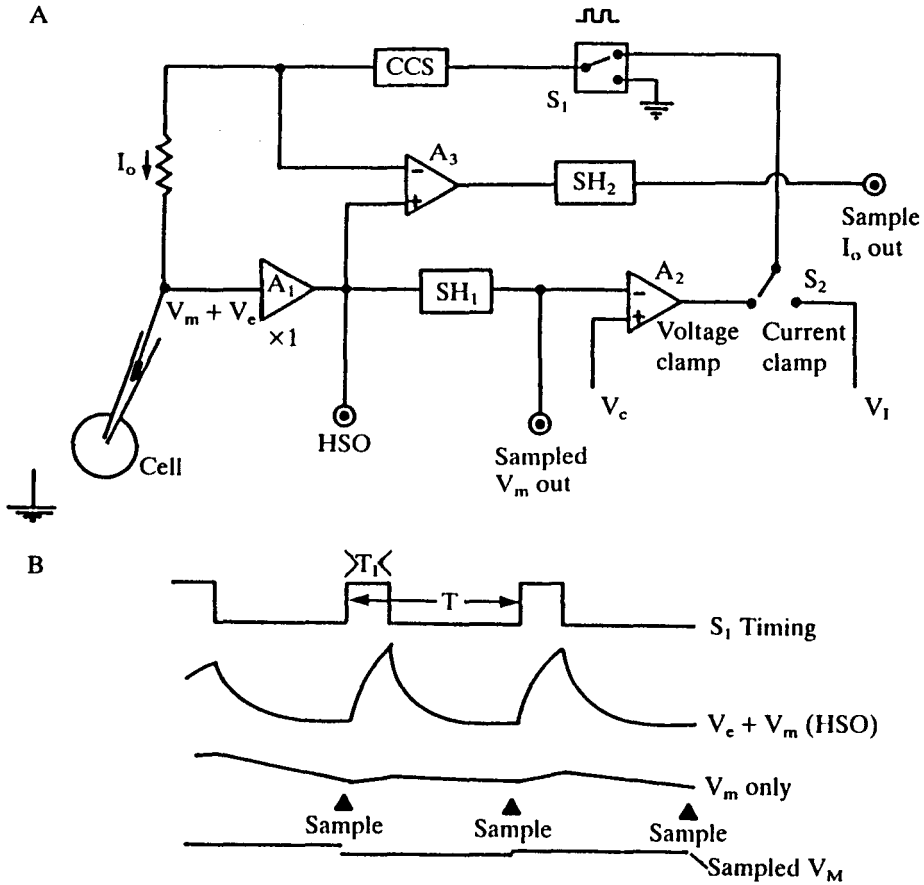


Figure 3. A: schematic diagram of dSEVC circuit. B: diagram showing the timing of the states of switch S_1 and the corresponding signals recorded at HSO and Sampled V_m out. A_1 : high input-impedance amplifier, SH_1 : voltage sample and hold device, A_2 : voltage clamp feedback amplifier, S_2 : voltage clamp and current clamp switch, S_1 : electronic switch for current passing and voltage recording, CCS : controlled current source, V_c : command voltage, V_i : current injection command, V_e : electrode voltage, V_m : membrane potential, A_3 : current measurement amplifier, SH_2 : current sample and hold device, T : cycling time, T_1 : the time for which current is passed. See text for further detail. (reproduced from Halliwell *et al*, 1987).

voltage recording phase no current is passing through the electrode and V_e decays to zero with the time constant of $R_e \times C_s$, where R_e is the electrode resistance and C_s is the stray capacitance. The output of A1 is fed to a sample and hold device (SH1), which takes samples when the decay of V_e is completed and holds the voltage until the next sample. Under this condition the output of SH1 reflects the true membrane potential. This voltage is sent to a clamp feedback amplifier (A2) where the voltage is compared with the clamp command voltage (V_c). The output of A2 is connected to S1 and in turn to a controlled current source (CCS). When S1 is in current passing position, the CCS injects current into the cell through the electrode which is directly proportional to the input voltage of the CCS. The duty cycle is designed to allow current passing for 30% of each cycle and voltage recording for 70% of each cycle (80). The sample point of SH1 is set at the end of the voltage recording phase (or just before the next current injection) to allow maximum decay of V_e . The cycling rate of S1 is usually between 3-20 kHz (92). In theory, the cycling rate should be at least ten cycles per membrane time constant in order that the pulses of current are smoothed. In addition, the cycling rate is at least twice the frequency component of the fastest current that is to be resolved. In the present experiments, the cycling rate was 8-12 kHz. Since latent pacemaker cells exhibit relatively high input resistances, the membrane time constants were about 20-50 ms. Therefore, the cycling rate used is fast enough to smooth the membrane potential response during current pulse injections. In addition, the fastest current analyzed in the present experiments had a time to peak of about 2-4 ms (e.g. T- or L- type Ca^{2+} currents). Therefore, the cycling rate (sample rate) used in the present experiments was

sufficient to reliably measure these currents. However, the cycling rate was not high enough to accurately measure fast Na^+ current, which had a time to peak of less than 1 ms. The maximum cycling frequency is limited by the time constant of the electrode. During a voltage recording period sufficient time must be allowed for V_e to decay completely. As discussed above, the decay rate of V_e is determined by the electrode time constant. If the electrode time constant is too long, the decay of V_e may not be complete within the voltage recording period at a given cycling rate. In this case, the electrode transient contributes a significant component of the sample voltage causing error in V_m measurement. Therefore, during an experiment it is important to observe the decay of V_e at the input of SH1 (at point of HSO) and to ensure that the decay is complete.

In order to evaluate the performance of the dSEVC, the settling times for both ruptured patch and nystatin perforated patch methods were determined. Figure 4 shows the current and membrane voltage responses to a 10 mV depolarizing voltage clamp step from a holding potential of -60 mV. With the ruptured patch method, the membrane potential increased to the new level exponentially with a time constant of 111 μs ($126 \pm 9 \mu\text{s}$, $n=6$) which was similar to the time constant of the decay of the capacitive current transient of 114 μs ($132 \pm 14 \mu\text{s}$, $n=6$). The V_m settling time, which was measured as the time in which V_m achieved 95% of the command step (115), was 333 μs ($380 \pm 27 \mu\text{s}$, $n=6$). With nystatin-perforated patch method, the time constants of the membrane potential and the decay of capacitive transient were 342 μs ($352 \pm 12 \mu\text{s}$, $n=5$) and 360 μs ($370 \pm 19 \mu\text{s}$, $n=5$), respectively, and the settling time was 1020

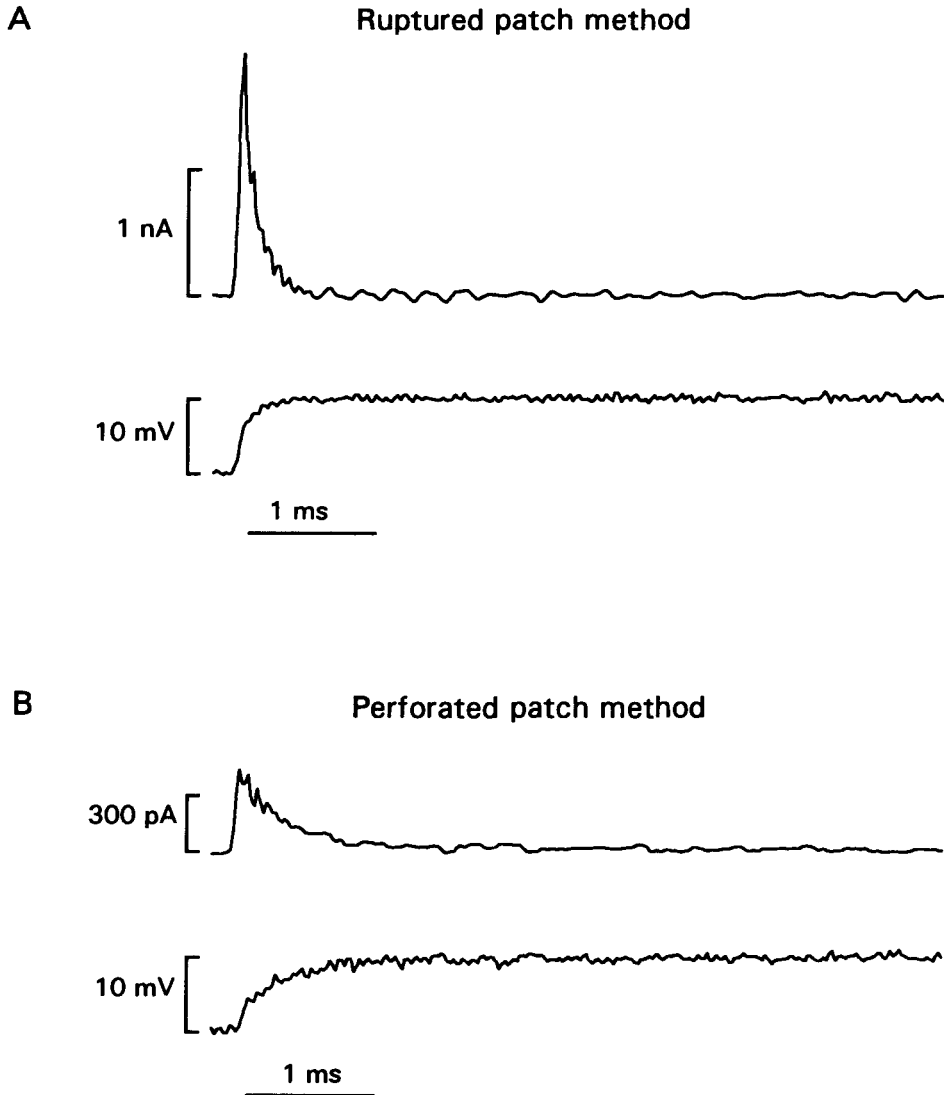


Figure 4. Settling times of voltage clamp. The current and membrane voltage responses to a 10 mV depolarizing voltage clamp step with ruptured patch recording method (A), and nystatin-perforated patch recording method (B).

μs ($1057 \pm 36 \mu\text{s}$ $n=5$). Since the time to peak Ca^{2+} currents was longer than 2 ms, the settling times of both ruptured patch and nystatin methods allowed accurate measurement of these currents.

In some experiments, action potentials were clamped during the later phase of the diastolic depolarization. This was accomplished by using a window discriminator (Frederick Haer & Co.) to trigger the voltage clamp amplifier from current clamp mode to voltage clamp mode. In current clamp mode, spontaneous action potentials were recorded and fed into the window discriminator. The threshold of the window discriminator was set at the same level as the clamp command voltage. When the unclamped action potentials went above the threshold, the window discriminator sent out a TTL pulse to switch the amplifier to voltage clamp mode and the cell was clamped at the same level.

In some experiments, pacemaker cycle length was measured without using a patch electrode. This was accomplished by monitoring contractile events, which were associated with pacemaker activity, with a video-based edge detector (Crescent Electronics). Cycle length was determined by averaging ten consecutive cycles in cells exhibiting regular pacemaker activity.

C. Measurements and Data Analysis.

The input resistance (R_{in}) was determined from the voltage response to a constant hyperpolarizing current pulse of 10 pA delivered during the diastolic interval. R_{in} was calculated by dividing the resulting change in membrane potential by the current amplitude. The membrane capacitance (C_m) was measured by delivering a ramp voltage

clamp pulse ($dV/dt=5V/s$) and dividing the half-amplitude of the current jump at the turning point of the ramp pulse by the ramp slope (Figure 5) (126). When appropriate, currents were normalized in reference to C_m of each cell to yield current density (pA/pF). Data are presented as means \pm standard error of the mean (SE). Student's t -test was used for statistical analysis and differences with p values <0.05 were considered statistically significant.

D. Solutions, Drugs and Chemical Reagents.

All solutions were made on the same day of each experiment from fresh double-deionized water which had a resistance of over $18 M\Omega$ (Aqua-Summa, Culligan Co.) The solutions used for cell isolation are listed in Table 1. The internal pipette solutions used for standard ruptured patch, nystatin-perforated patch and measurement of Ca^{2+} currents are listed in Table 2.

When the hyperpolarizing-activated inward current (I_f) was analyzed, the following compounds were used to block other currents that might interfere with the analysis of I_f : 3 mM Ni^{2+} to block slow inward Ca^{2+} currents and Na-Ca exchange current (126), 3 mM Ba^{2+} to block K^+ currents (87,176), and 2 mM 4-aminopyridine (4-AP) to block transient outward current (125). In some experiments, 20 μM TTX was used to block fast Na^+ current. When extracellular Na^+ concentration was reduced, NaCl was replaced with equimolar quantities of TRIS/HCl. Extracellular K^+ concentrations were changed without compensation for total osmolarity.

In studies of T- and L- type Ca^{2+} currents, external solution was a Na-free solution containing (in mM): TEA-Cl 137, KCl 5.4, $MgCl_2$ 1.0, $CaCl_2$ 2.7, HEPES 5,

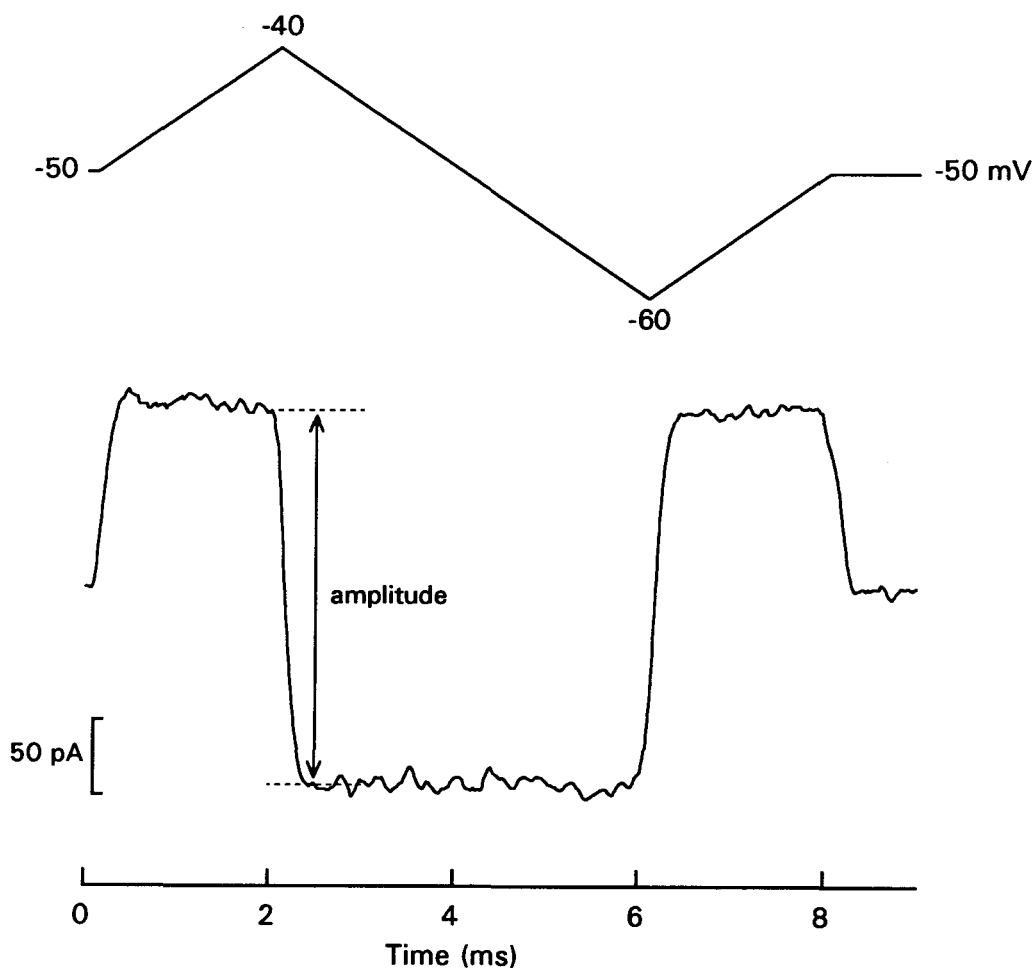


Figure 5. Measurement of membrane capacitance. The cell was held at -50 mV, and a ramp clamp to -40 mV and -60 mV was applied. The slope of the ramp (dV/dt) was 5 V/sec. The cell capacitance was calculated by dividing the half-amplitude of current jump at the turning point of the ramp pulse by the ramp slope. The current was the average of 5 clamps.

glucose 11, TTX 30 μM , 4-AP 1.0 and titrated with TEA-OH to pH 7.4. In addition, internal K^+ was replaced by Cs^+ (see Table 2). In studies of I_{K} current, the extracellular K^+ concentrations were changed by replacement of NaCl with equimolar quantities of KCl. In studies of Na-Ca exchange current, when extracellular Na^+ concentration was reduced, NaCl was replaced with equimolar quantities of LiCl.

List of drugs and chemical reagents:

Collagenase (type II, 171 units/mg, Worthington,)

Protease (type XIV, 5.4 units/mg, Sigma Chemical Company)

Elastase (type III, 80 units/mg, Sigma Chemical Company)

Albumin (Sigma Chemical Company)

Na_2 -ATP (grade I, Sigma Chemical Company)

K_2 -ATP (from Equine Muscle, Sigma Chemical Company)

Ethyleneglycol-bis-N,N,N',N'-Tetraacetic Acid (Sigma Chemical Company)

N-2-hydroxyethylpiperazine-N'-2-ethane-sulfonic Acid (Calbiochem)

Nystatin (Sigma Chemical Company)

Dimethyl Sulfoxide (Sigma Chemical Company)

Tetrodotoxin (Calbiochem)

4-aminopyridine (Sigma Chemical Company)

Tetraethylammonium Chloride (Sigma Chemical Company)

TRIZMA Hydrochloride (Sigma Chemical Company)

Nifedipine (Sigma Chemical Company)

Ryanodine (Penick, Lyndhurst, New Jersey)

CHAPTER IV

RESULTS

A. Morphology and Passive Membrane Properties.

Figure 6 shows two typical latent atrial pacemaker cells isolated from the Eustachian ridge of cat right atrium. Both cells were beating spontaneously in normal Tyrode's solution containing 1.8 mM Ca^{2+} . Pacemaker activity was associated with spontaneous contractions, characterized by distinct twitches that were synchronous throughout the cell. In general, approximately 5 to 20% of the cells isolated in an individual experiment exhibited spontaneous, rhythmic pacemaker activity. The mean spontaneous beating rate of pacemaker cells (monitored by video-based edge detection) was 69 ± 4 beats/min ($n=15$). Pacemaker cells were elongated with tapered ends, and appeared somewhat bent or crinkled, without obvious striations. Pacemaker cells exhibited a mean diameter and length of $7.4 \pm 0.5 \mu\text{m}$ and $93.1 \pm 5.9 \mu\text{m}$, respectively ($n=15$). The mean total membrane capacitance and input resistance were 27.8 ± 3.1 pF ($n=19$) and 2.2 ± 0.2 G Ω ($n=21$), respectively. These morphological and passive membrane properties are similar to those found in rabbit SA node pacemaker cells (11,12,47,48) and pacemaker cells from cat right atrium (226).

B. Pacemaker Action Potential Characteristics.

Figure 7 shows typical pacemaker action potentials recorded from a latent atrial



Figure 6. Typical latent pacemaker cells isolated from the Eustachian ridge of cat right atrium. Both cells exhibited rhythmic spontaneous activity. Cell at lower left was photographed during contractile event. Calibration bar = 40 μm .

(see Figures 17,20,25,31). Action potentials recorded from single latent pacemaker cells were comparable to those obtained from latent pacemakers in multicellular Eustachian ridge preparations (188,189).

C. Membrane Currents During Voltage Clamp.

Figure 8 shows typical pacemaker action potentials and membrane currents

B. Pacemaker Action Potential Characteristics.

Figure 7 shows typical pacemaker action potentials recorded from a latent atrial pacemaker cell using a ruptured-patch whole-cell recording configuration. These action potentials exhibited a relatively slow rate of rise (< 10 V/s) and a pacemaker voltage range between -71 to -54 mV. In some cells the diastolic slope exhibited two phases; an initial steeper slope followed by a more gradual slope. Table 3 summarizes the action potential variables obtained from single latent pacemaker cells ($n=15$). As expected for latent pacemakers, the slope of diastolic depolarization was small (35 mV/s) and the spontaneous cycle length was long (901 ± 67 ms) compared with those reported in SA node ($57,159,213$). The maximum diastolic potential was about -68 mV. Although spontaneous action potentials could be recorded for as long as 20 minutes in some cells, usually spontaneous activity gradually slowed and finally stopped within 5 minutes of rupturing the membrane patch. Similar results have been reported in rabbit SA node ($59,159$) and frog sinus venosus pacemaker cells (25). Action potentials were, therefore, recorded immediately after breaking the membrane. In later experiments we used a nystatin-perforated patch method to record pacemaker action potentials for at least 30 minutes without significant change in action potential configuration and spontaneous rate (see Figures 17,20,25,31). Action potentials recorded from single latent pacemaker cells were comparable to those obtained from latent pacemakers in multicellular Eustachian ridge preparations ($188,189$).

C. Membrane Currents During Voltage Clamp.

Figure 8 shows typical pacemaker action potentials and membrane currents

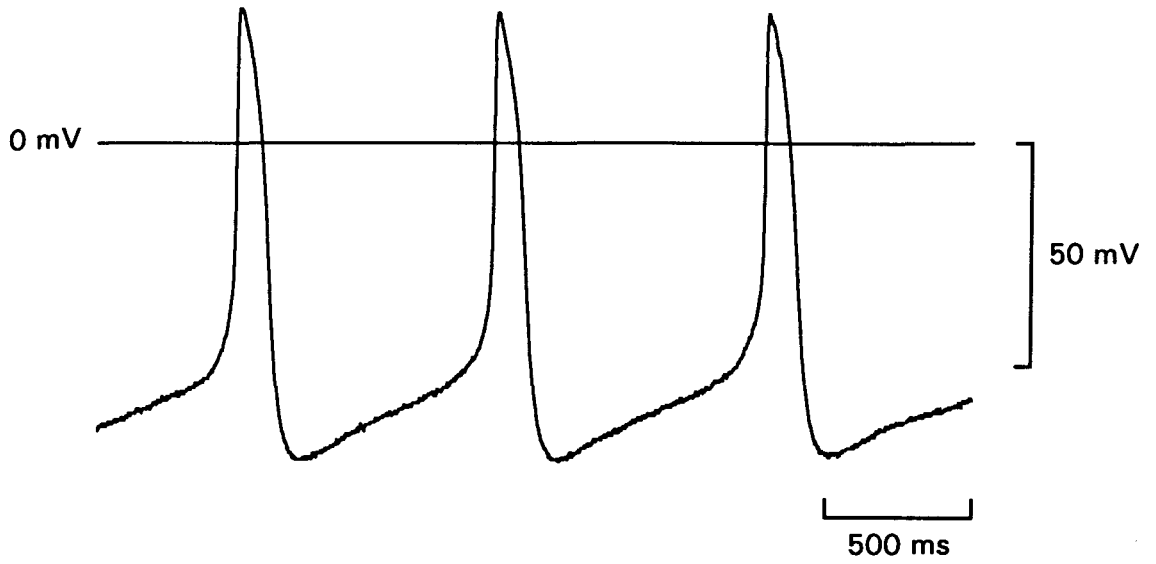


Figure 7. Pacemaker action potentials recorded from a single spontaneously active cell isolated from Eustachian ridge of cat right atrium.

Table 3. Measurements of Spontaneous Action Potentials in Latent Pacemaker Cells

Parameter	Mean	\pm SE	n
Maximum Diastolic Potential (mV)	-68.2	1.2	15
Overshoot (mV)	27.5	1.5	15
Amplitude (mV)	95.7	1.8	15
Take-off Potential (mV)	-54.4	1.5	15
Duration (60%) (ms)	141.1	11.2	15
Upstroke Velocity (V/s)	6.5	1.6	15
Slope of Diastolic Depolarization (mV/s)	35.4	3.4	15
Spontaneous Cycle Length (ms)	900.7	66.8	15

recorded from a single latent atrial pacemaker cell. Panel A shows spontaneous action potentials that exhibited a maximum diastolic potential of -70 mV, an overshoot potential of $+35$ mV, and cycle length of 896 ms (rate= 67 /min). Following the action potential recordings the cell was held at -40 mV and clamped for 1 sec to more negative (panel B) and more positive (panel C) voltages ranging between -120 and $+30$ mV. As shown in Panel B, hyperpolarizing clamp pulses elicited an increasing inward current that was larger at more negative voltages. In addition, hyperpolarization elicited little instantaneous inward current. This time- and voltage-dependent inward current corresponds to the hyperpolarization-activated current, I_f similar to that reported in SA node pacemaker cells (59,160,213). In panel C, depolarizing clamps elicited an initial inward current followed by an increasing outward current. Repolarization to the holding potential elicited decaying outward tail currents. The initial inward current can be attributed to activation of L-type Ca^{2+} current (90,159) and the increasing outward current corresponds to delayed rectifier, I_K (159,200). In the following experiments each of these currents as well as T-type Ca^{2+} current and Na-Ca exchange current will be analyzed in detail.

1. Hyperpolarization-activated Current, I_f .

Figure 9 shows an experiment where both action potentials and I_f currents were recorded from a single latent atrial pacemaker cell. Action potentials exhibited a pacemaker potential with a voltage range between -69 and -45 mV. Following these voltage recordings, the cell was clamped at a holding potential of -40 mV and hyperpolarized to voltages between -50 and -100 mV in 10 mV increments.

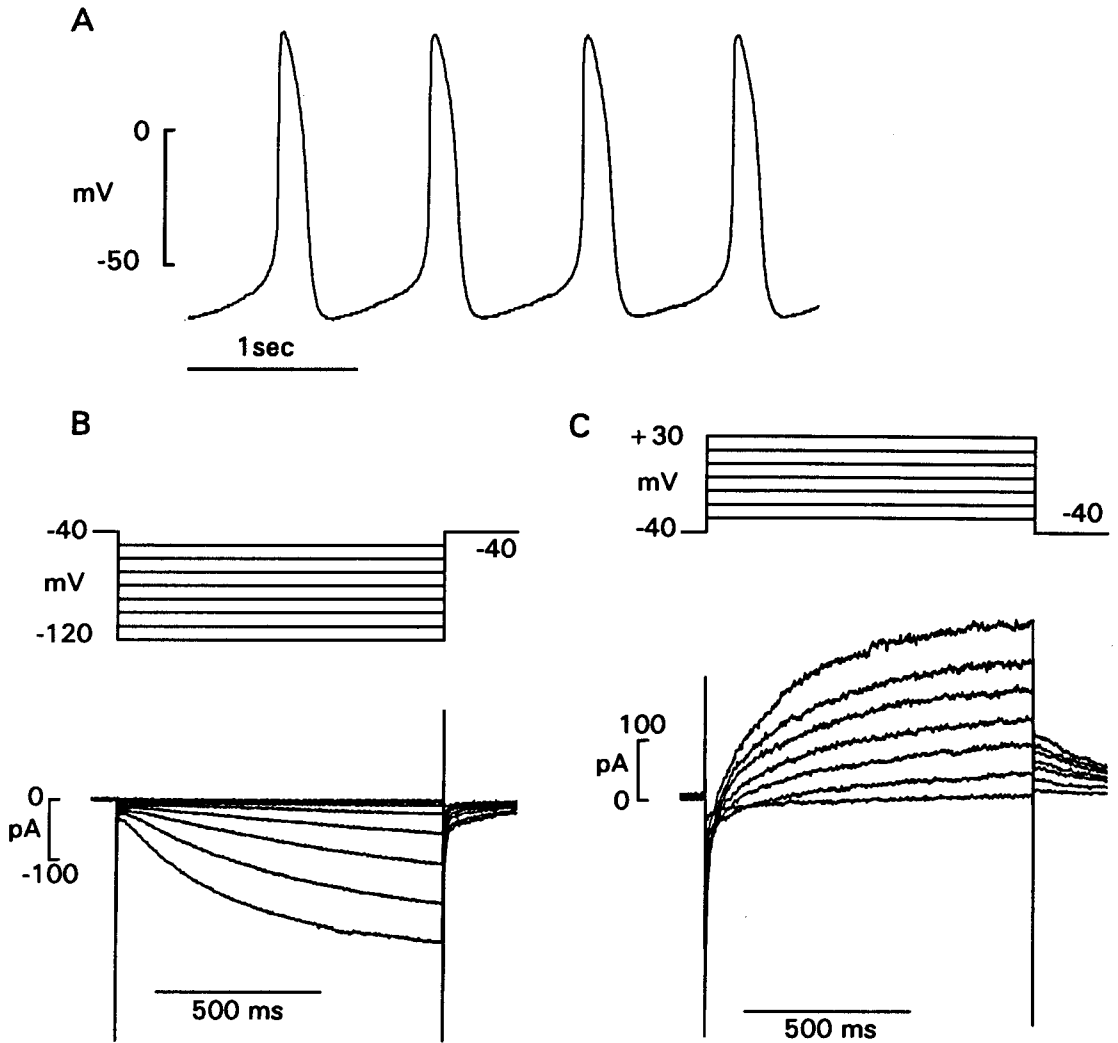


Figure 8. Recordings of pacemaker action potentials (A) and membrane currents (B & C) from a single pacemaker cell. Voltage clamp protocols and membrane currents in response to hyperpolarization (B) and depolarization (C) from a holding potential (V_h) of -40 mV. Hyperpolarizing clamp pulses were delivered in 10 mV increments between -50 and -120 mV for 1 sec. Depolarizing clamp pulses were delivered in 10 mV increments between -30 and $+30$ mV for 1 sec.

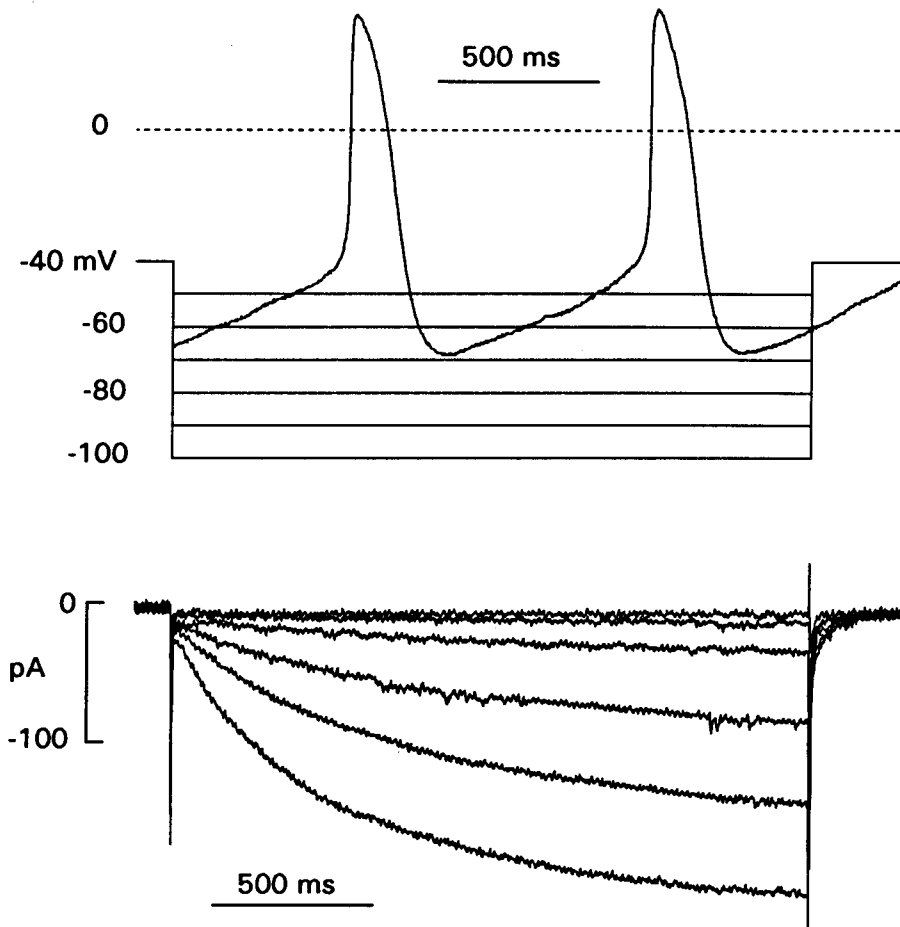


Figure 9. Action potentials (top) and I_f currents (bottom) recorded from a single latent pacemaker cell. Top: voltage clamp protocols superimposed on spontaneous action potentials to illustrate voltage range of the pacemaker potential. Bottom: I_f currents recorded from the same cell. Membrane currents were elicited by hyperpolarizing clamp pulses between -50 and -100 mV from V_h of -40 mV.

Hyperpolarization elicited a relatively small initial inward current jump, indicating that the inward rectifying current, I_{K1} was very small or absent in these cells (226). This was later confirmed by the fact that barium had no significant effect on this initial inward current (Figure 10). In addition, hyperpolarization elicited an inward current that increased with time and at more negative voltages. This time- and voltage-dependent inward current corresponds to the hyperpolarization-activated current, I_f found in SA node (48,59,159,160,213), Purkinje (36,51,52) and other cardiac pacemaker cells (1,25,226). Of the 213 cells selected for study, 201 cells (94%) exhibited I_f in response to hyperpolarization. This experiment shows that the threshold for I_f activation was between -50 and -60 mV, well within the pacemaker voltage range. It should also be noted that I_f amplitude varied among different pacemaker cells. Typically, maximum I_f amplitude elicited at -120 mV ranged from 100 to 300 pA and was no greater than 400 pA. These values are considerably smaller than those reported in SA node pacemaker cells (59,213), where I_f amplitudes of more than 1000 pA are not uncommon. I_f also exhibited various degrees of run-down following rupture of the membrane patch. Similar findings have been reported in SA node pacemaker cells (59). In 5 experiments, I_f decreased to $77 \pm 4\%$ of control at 10 minutes after breaking the membrane. To minimize run-down, most experiments were performed within 5 to 10 min of breaking the membrane.

Voltage dependence of I_f activation. In Figure 10, the voltage dependence of I_f activation was determined by using an experimental protocol similar to that described by DiFrancesco *et al.* (59). From a holding potential of -40 mV the cell was

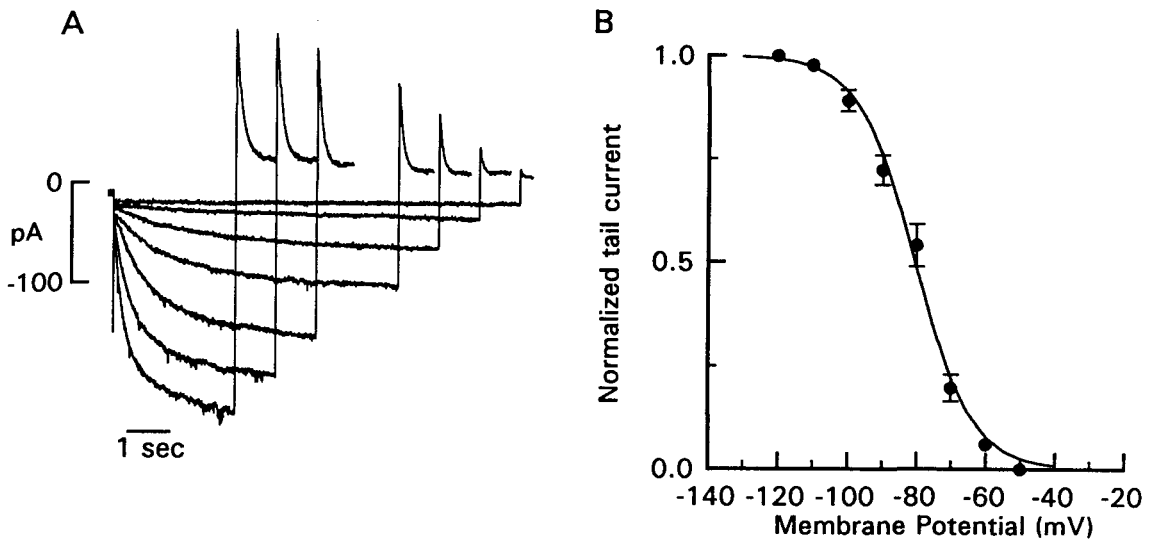


Figure 10. Activation curve of I_f . A: selected membrane currents used to determine the voltage dependence of I_f activation curve. The cell was held at -40 mV and hyperpolarized between -60 and -120 mV for 3 to 10 sec and then clamped to $+10$ mV for 1 sec. B: tail current amplitudes are normalized with respect to maximal tail current amplitude and plotted against the voltage imposed during hyperpolarization. Data points (●) are means \pm SE obtained from 4 cells. The solid curve was obtained by fitting the data with a Boltzmann equation. External solution contained 3 mM Ni^{2+} , 3 mM Ba^{2+} and 2 mM 4-AP.

hyperpolarized to various test voltages between -60 and -120 mV to activate I_f , and then clamped to a fixed positive voltage to elicit deactivating outward tail currents (Figure 10A). Longer hyperpolarizing clamp pulses were used at less negative voltages where the time course of I_f activation was slower. As shown in Figure 10B, the activation curve (smooth curve) was obtained by fitting the data with a Boltzmann equation: $q_\infty = \{1 + \exp[(V_t - V_{0.5})/k]\}^{-1}$, where q_∞ = steady-state activation variable, determined as the ratio of the tail current amplitude to maximal tail current amplitude, V_t = hyperpolarizing test voltage, $V_{0.5}$ is voltage at which activation is half-maximal and k is the slope factor. The activation curve is S-shaped and shows that I_f was activated at voltages more negative than -50 mV and fully-activated at about -120 mV. The half-maximal activation voltage and slope factor were -80.5 ± 1.6 and 8.1 ± 0.4 mV, respectively. The half maximal activation voltage in latent pacemaker cells is more negative than that reported in rabbit SA node cells (89,213).

To ensure correct interpretation of the I_f activation curve it is important to demonstrate that I_f tail currents accurately reflect I_f activation. In other words, if channel conductance does not change instantaneously, then the initial amplitude of the tail currents should reflect I_f activated during hyperpolarization as a function of time. A common way of demonstrating this is to perform an "envelope of tails" test (59,84,213). This was accomplished by activating I_f at a single voltage for different periods of time and then returning the membrane to a more positive fixed voltage. As shown in Figure 11A, the time course of the envelope curve (dashed line) describing the peak tail currents was similar to I_f activation. In panel B, the I_f current shown in panel

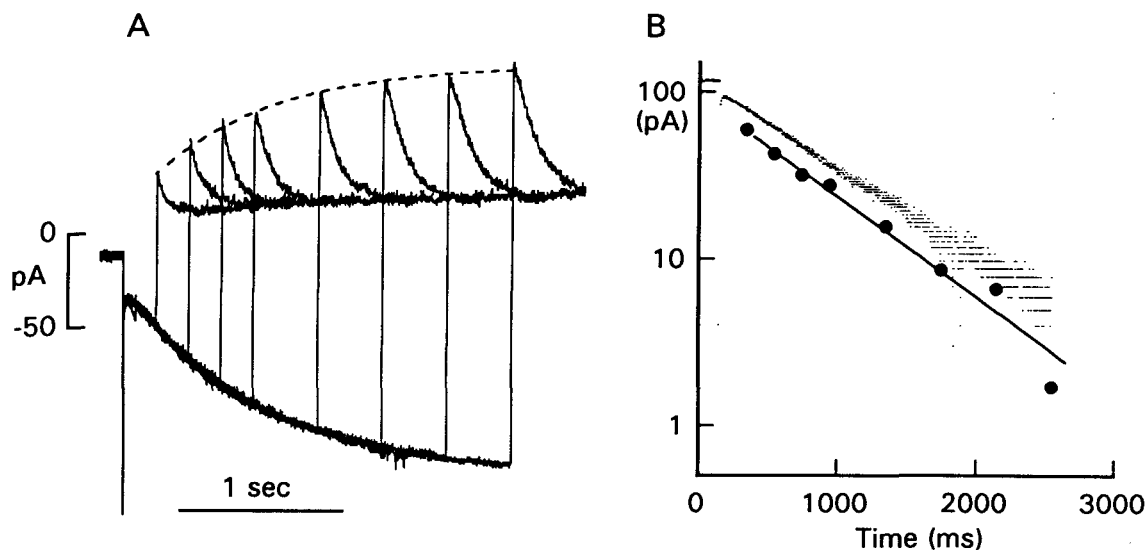


Fig. 11. Envelope of tails test for I_f . A: I_f tail currents were recorded at +10 mV following hyperpolarizing clamp steps to -100 mV ranging from 200 to 2400 ms in duration. Holding potential was -40 mV. Eight traces of I_f activation are superimposed. B: I_f elicited at -100 mV is plotted on a semilogarithmic scale against time, and peak I_f tail current amplitudes (●) are plotted on the same scale against the duration of the preceding clamp step. The straight line was determined by least squares analysis of the tail current amplitudes. External solution contained 3 mM Ni^{2+} , 3 mM Ba^{2+} and 2 mM 4-AP.

A, and the peak tail current amplitudes are plotted on a semilogarithmic scale as a function of time. It is apparent that the time course of both I_f activation and the envelope of tails are similar, with time constants of 808 and 737 ms, respectively. These results indicate that the peak tail currents are a reliable measure of the amount of I_f activation.

Ionic selectivity of I_f . The reversal potential of I_f was determined by hyperpolarizing the cell to -120 mV for 1.5 sec to activate I_f and then returning to more positive voltages in 10 mV increments. The records in Figure 12A show a typical experiment where I_f tail currents reversed direction at about -25 mV, suggesting that I_f is carried by more than one ion species. Similar results were found in a total of ten experiments. The properties of the I_f channel were further analyzed by determining the fully-activated current-voltage (I-V) relationship, according to the method of DiFrancesco (51). From a holding potential of -40 mV the cell was clamped to voltages at which I_f current was either fully activated (-120 mV) or fully deactivated (-20 mV). From each of these voltages the membrane was clamped to identical voltages ranging from -105 to -30 mV. The fully-activated I-V relationship was determined by measuring the difference in peak tail current amplitudes (arrows). In panel C, the difference current was plotted against the imposed voltages. The fully-activated I-V relationship is approximately linear between -120 and -30 mV, and shows outward rectification at more positive voltages. The I-V relationship also shows that the current changed direction at -25.6 ± 0.7 mV ($n=21$), which is similar to the reversal potential determined in Figure 12A. Similar values have been reported for I_f in SA node pacemaker cells (59,213). Measured over the linear portion of the I-V relationship (-30 to -120 mV) the fully-

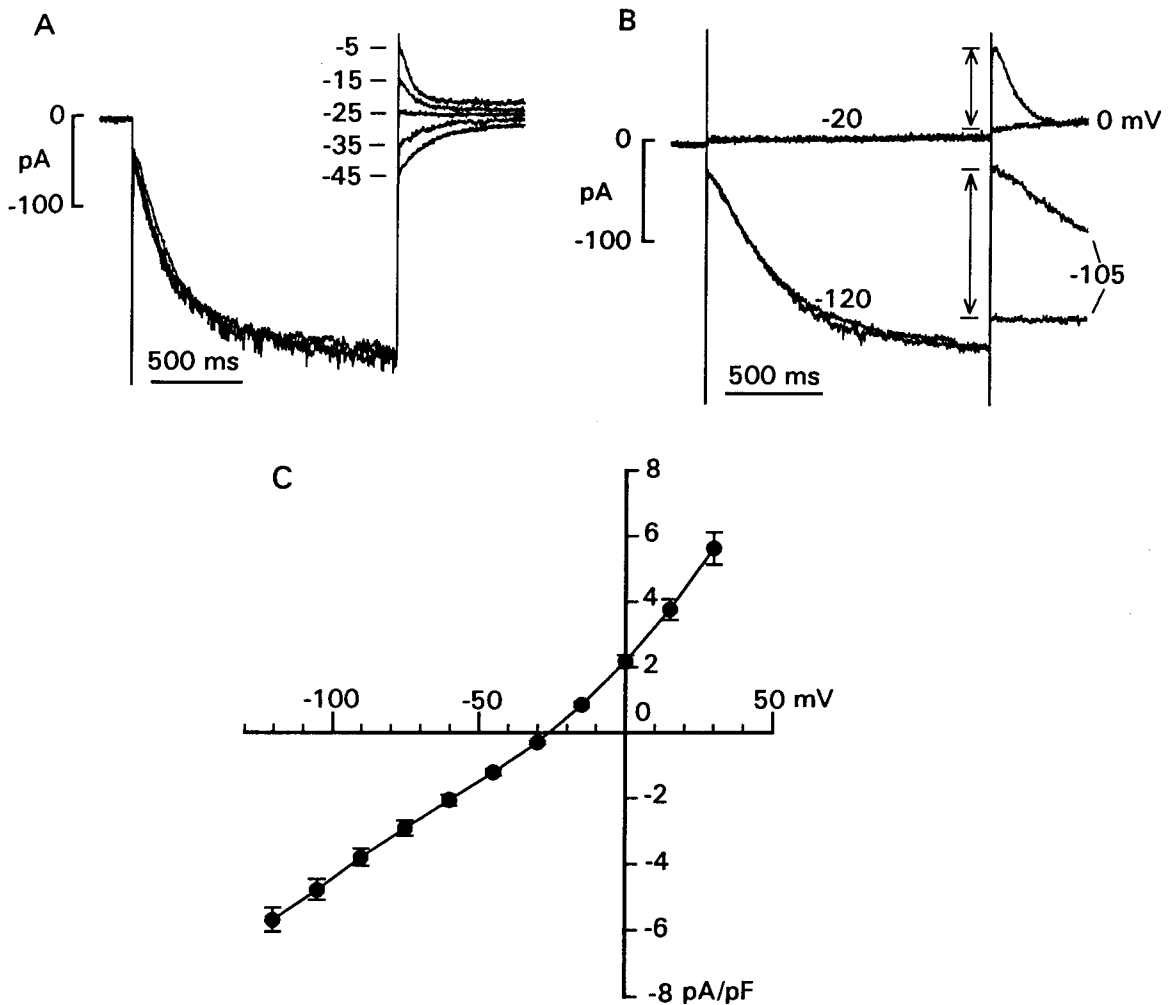


Figure 12. A: Determination of I_f reversal potential. From V_h of -40 mV, the cell was hyperpolarized to -120 for 1.5 sec and then clamped between -45 and -5 mV as indicated. Five traces of I_f are superimposed. External solution contained $20 \mu\text{M}$ TTX, 3 mM Ni^{2+} , 3 mM Ba^{2+} and 2 mM 4-AP. B: selected currents used to determine the fully-activated I-V relationship. The cell was held at -40 mV and clamped to -120 mV or -20 mV for 1.5 sec followed by clamp steps to identical voltages ranging from -105 to $+30$ mV. Differences between the initial tail current amplitudes (arrows) were plotted (panel C) against the voltages at which the tail currents were elicited. External solutions contained 3 mM Ni^{2+} , 3 mM Ba^{2+} and 2 mM 4-AP. C: fully-activated I-V relationship for I_f determined from 21 cells. Currents are expressed as current density (pA/pF).

activated conductance was 1.75 ± 0.14 nS ($n=21$). This value is significantly smaller than the fully-activated conductance of I_f reported in SA node (59,213).

The reversal potential measurements suggest that I_f may be carried by both Na^+ and K^+ ions, as shown in other cardiac pacemaker cells (25,36,51,53,59,63). This was tested by changing extracellular Na^+ or K^+ concentrations and determining the effects on the fully-activated I-V relationship. In Figure 13A, when the extracellular Na^+ was reduced from 137 mM to 30 mM I_f amplitude was decreased. Panel B shows that reducing the external Na^+ shifted the fully-activated I-V relationship more outward and changed the reversal potential from -26.6 ± 0.6 to -41.5 ± 1.6 mV ($n=4$). Reducing the external Na^+ also decreased the slope of the I-V relationship, indicating a decrease in conductance. The change in slope is more evident at more negative voltages. At voltages more negative than about -50 mV, where the I-V curve is approximately linear, the reduction in external Na^+ decreased the slope by about 25%. Others have shown that lowering external Na^+ shifts the fully-activated I-V relationship to more negative voltages in Purkinje fibers (51) and single SA node pacemaker cells (59). However, in contrast to the present results, those studies reported no change in the slope of the fully-activated I-V relationship with a reduction in external Na^+ . These results indicate that Na^+ is a charge carrier of I_f .

Figure 14 shows the effects of lower (panels A & B) and higher (panels C & D) extracellular K^+ concentrations on I_f . In panel A, reducing the external K^+ from 5.4 to 2 mM decreased I_f amplitude. In panel B, the reversal potential of the fully-activated I-V relationship was shifted from -24.1 ± 3.6 to -31.2 ± 3.8 mV ($n=4$) and the slope

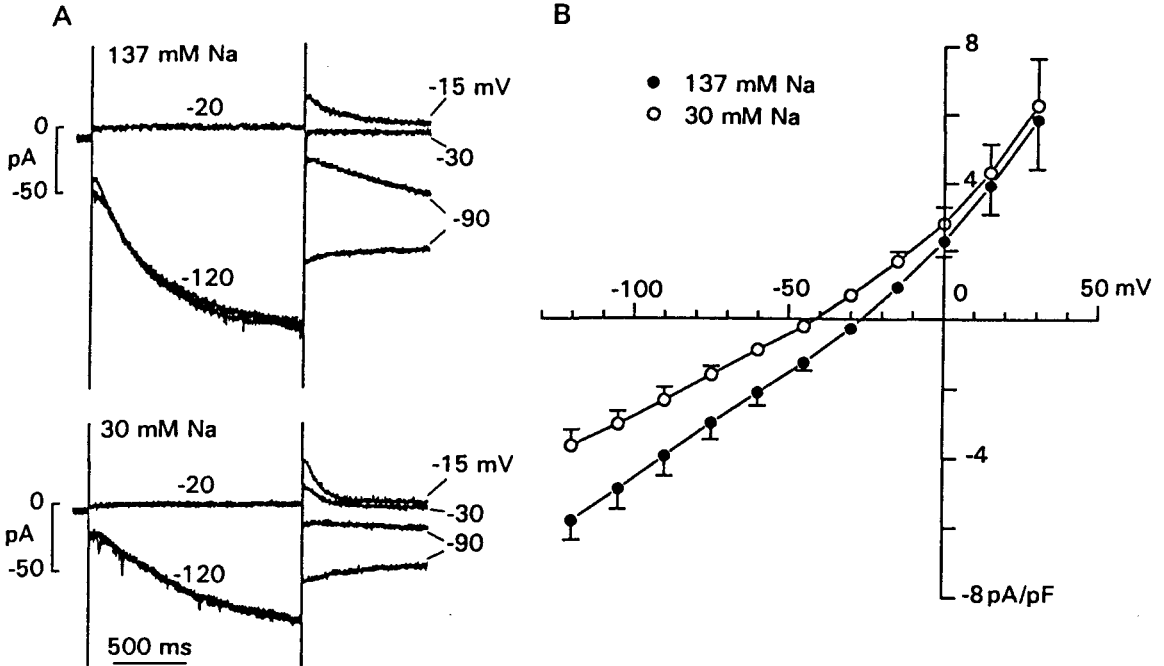


Figure 13. Effects of low extracellular Na⁺ on I_f. A: selected currents recorded in 137 mM (top) and 30 mM (bottom) external Na⁺ solutions. Tail currents shown are those elicited from -120 to -90, -30, -15 mV and from -20 to -90 mV. B: fully-activated I-V relationship in 137 mM (●) and 30 mM (○) Na⁺ determined in 4 cells. External solutions contained 3 mM Ni²⁺, 3 mM Ba²⁺ and 2 mM 4-AP.

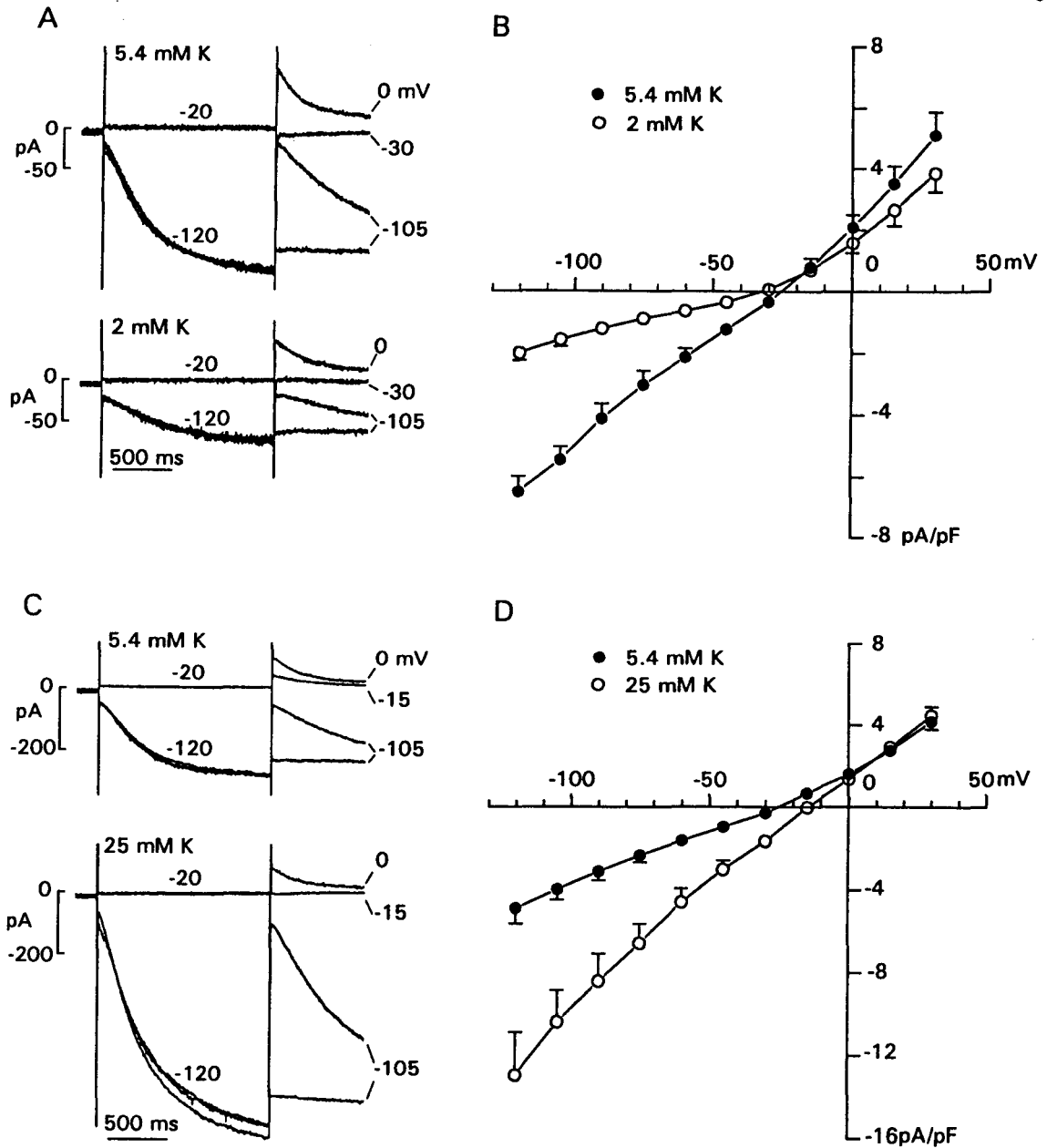


Figure 14. Effects of different extracellular K concentrations on I_f . A: selected currents recorded in 5.4 mM (top) and 2 mM (bottom) external K^+ solutions. B: fully-activated I-V relationship in 5.4 mM (●) and 2 mM (○) K^+ determined in 4 cells. C: selected currents recorded in 5.4 mM (top) and 25 mM (bottom) external K^+ solutions. D: fully-activated I-V relationship in 5.4 mM (●) and 25 mM (○) K^+ determined in 5 cells.

of the I-V relationship was decreased. The two I-V curves crossover one another at about -18 mV. As shown in panels C & D, when external K^+ was increased from 5.4 to 25 mM I_f amplitude increased, the reversal potential shifted from -25.4 ± 0.6 to -14.7 ± 0.7 mV ($n=5$), and the slope of the I-V relationship increased. These results indicate that K^+ is a charge carrier of I_f , similar to that reported in SA node (59,63) and Purkinje fibers (51,53). In addition, it has been reported that the increase in slope of the fully-activated I-V relationship induced by elevated K^+ indicates that K^+ exerts an activation-like affect on I_f (53,59). The present findings indicate that I_f in latent atrial pacemaker cells is carried by both Na^+ and K^+ ions, as reported in Purkinje tissues (36,51,53) and SA node pacemaker cells (59,63).

Kinetics of I_f . Figure 15A shows I_f currents recorded from two different latent pacemaker cells in which activation of I_f exhibited either a short delay in onset, yielding a sigmoidal time course or little, if any, delay in onset. Similar features have been described for I_f in SA node (59,213) and Purkinje cells (36). Of the 7 cells studied, 4 cells exhibited I_f activation without delay, and 3 cells exhibited a sigmoidal time course. I_f currents that exhibited a sigmoidal time course could not be fit adequately with either a single exponential function or an exponential raised to the power of 2 (213). There is considerable evidence that sigmoidal I_f currents do not exhibit kinetic properties consistent with a Hodgkin-Huxley model (55,56,58,94). We therefore have restricted the present kinetic analysis of I_f to those currents that exhibited no delay in onset of activation and hence, were best fit by a single exponential function. This is illustrated in Figure 15B which shows a semilogarithmic plot of I_f activation. The inset in panel

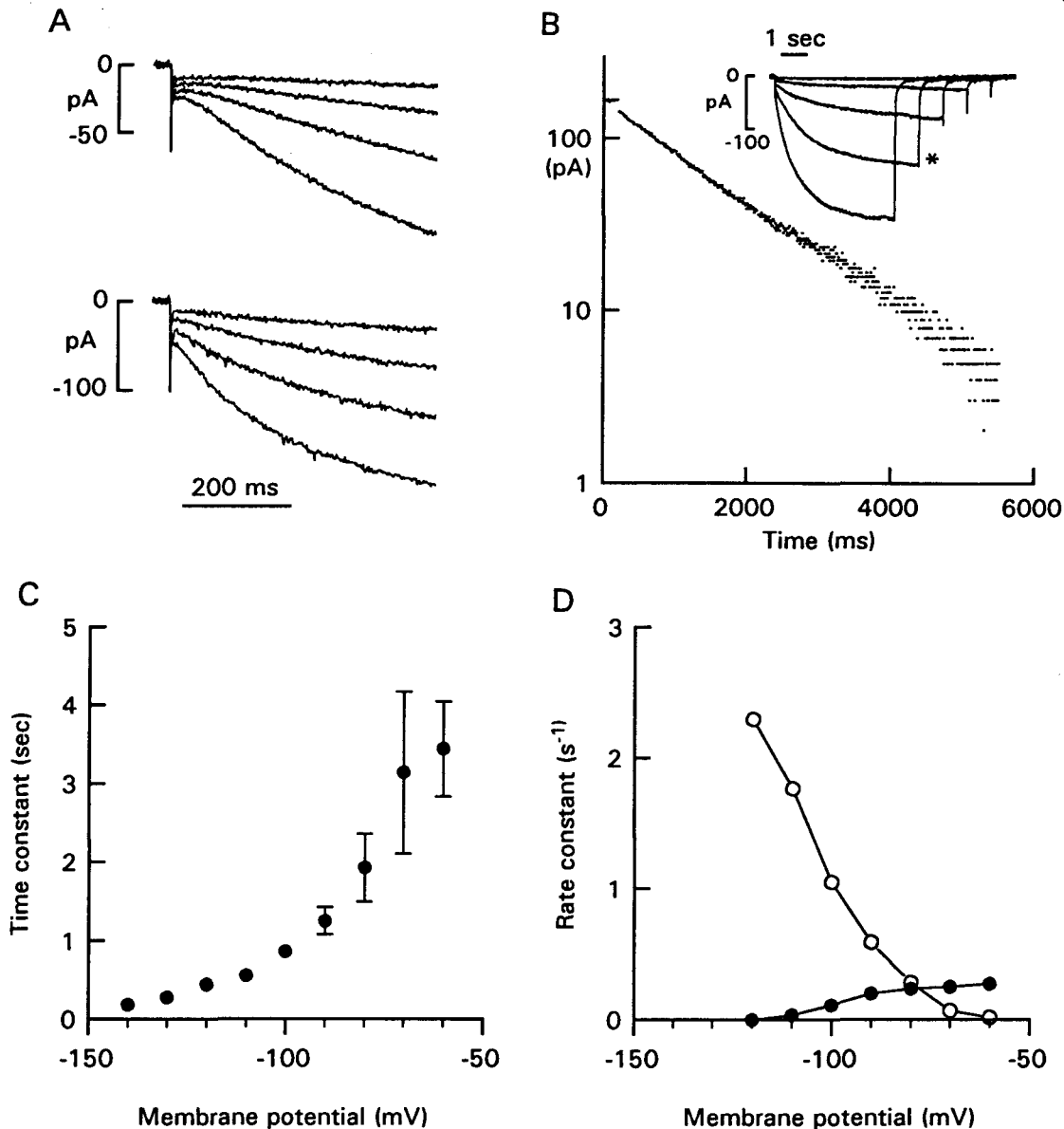


Figure 15. Kinetic analysis of I_f . A: I_f from two different latent pacemaker cells showing sigmoidal time course of activation (top) and no delay in activation (bottom). I_f currents were elicited by clamps between -80 and -110 mV from V_h of -40 mV. B: (inset) I_f currents exhibiting no delay in onset in a cell held at -40 mV and clamped between -60 and -100 mV for 5 to 9 sec. The current trace at -90 mV (*) was plotted on a semilogarithmic scale against time. C: activation time constants of I_f . Data points (\bullet) are means \pm SE obtained from 4 cells. D: rate constants α (\circ) and β (\bullet) of I_f activation. Lines are drawn through data points.

B shows I_f currents elicited by hyperpolarizing clamps to different voltages. Longer hyperpolarizing clamp durations were delivered at less negative voltages. Figure 15C shows the time constants of I_f activation at different voltages for the 4 cells that exhibited single exponential kinetics. Mean time constants were 3.20 ± 1.03 sec at -70 mV and 0.44 ± 0.03 sec at -120 mV. As shown in Figure 15D, the forward (open circles) and backward (closed circles) rate constants for the four cells were determined by the following equations:

$$\alpha = q_{\infty} / \tau, \quad (1)$$

$$\beta = (1 - q_{\infty}) / \tau \quad (2)$$

where α is forward rate constant, β is backward rate constant, τ is the activation time constant and q_{∞} is the activation variable as determined by a Boltzmann function (see Figure 10).

Effects of cesium. Relatively low concentrations of cesium (Cs^+) are known to block I_f in cardiac pacemakers (36,53,59,89). Figure 16A shows selected current recordings used to determine the fully-activated I-V relationship as described above (see Figure 12). Cs^+ blocked I_f elicited by hyperpolarizing clamp steps but exerted only a small effect on I_f tail currents elicited by clamps more positive than about -25 mV. Cs^+ also decreased the initial background inward current elicited by hyperpolarization. The fully-activated I-V relationship in panel B shows that 2 mM Cs^+ decreased I_f to less than 10% of control at voltages more negative than the reversal potential, and had little effect on current at more positive voltages. Similar voltage-dependent block of I_f by Cs^+ has been reported in SA node (59,89), frog sinus venosus (25) and Purkinje tissues (36,53).

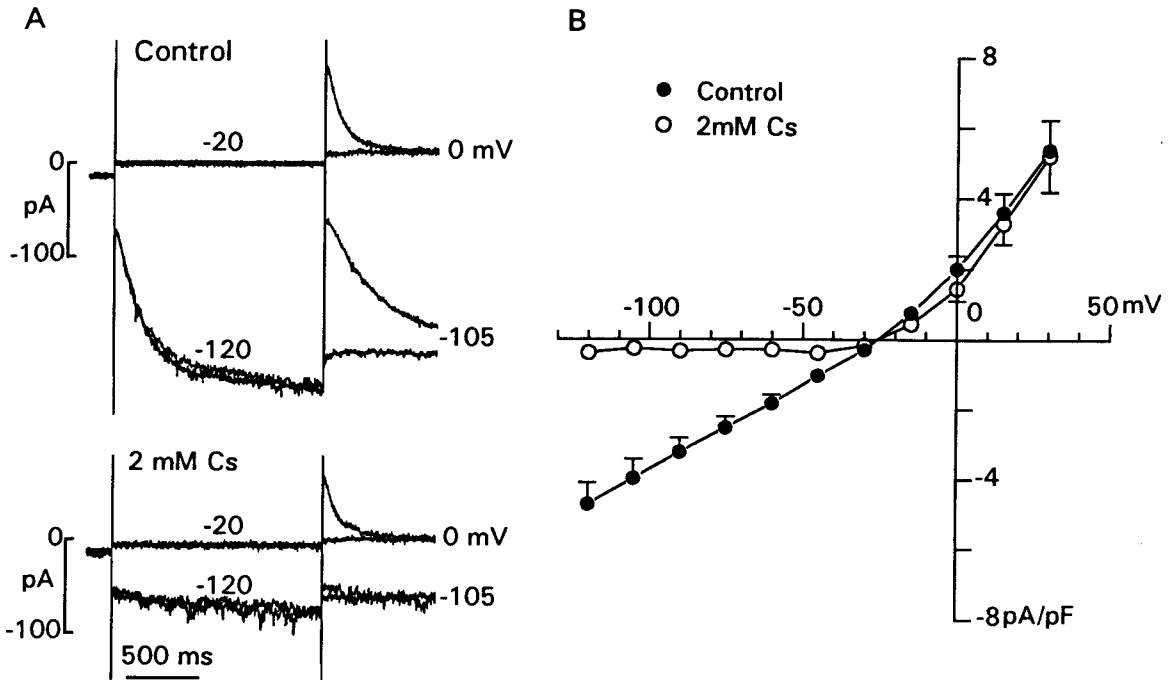


Figure 16. Effect of Cs⁺ on fully-activated I-V relationship of I_f. A: selected current recordings in control (top) and in 2 mM Cs⁺ (bottom) solutions used to determine fully-activated I-V relationship (see Figure 12). Tail currents at -105 and 0 mV were elicited from clamps to -120 and -20 mV. B: fully-activated I-V relationships in control (●) and 2 mM Cs⁺ (○) determined in 4 cells. External solutions contained 3 mM Ni²⁺, 3 mM Ba²⁺ and 2 mM 4-AP.

To determine the contribution of I_f to latent atrial pacemaker activity, Cs^+ was tested on spontaneous action potentials and I_f recorded from a single pacemaker cell. This was accomplished by using a nystatin-perforated patch recording method (104,130). With this method we could record normal spontaneous, pacemaker action potentials and I_f for at least 30 minutes without discernable change in either signal. Apparently, the perforated patch method avoids the run-down of pacemaker activity and I_f that may result from diffusional changes in internal constituents due to rupture of the membrane patch. As shown in Figure 17A hyperpolarization elicited I_f that was activated at voltages more negative than -50 mV, which is within the pacemaker potential range (-68 to -55 mV) of this cell. Moreover, these findings are similar to those obtained with the ruptured patch whole-cell recording method used in the experiments described above (see Figure 7). Panel B shows that 2 mM Cs^+ decreased the slope of diastolic depolarization and significantly increased pacemaker cycle length, although spontaneous activity did not cease. Note that the diastolic slope was depressed starting from its early development. These findings are consistent with the effects of Cs^+ on multicellular pacemaker preparations (189) and indicate that the contribution of I_f is already evident during the initial phase of the pacemaker potential. Cs^+ had no significant effect on other action potential parameters, although this cell exhibited a small hyperpolarization of the maximum diastolic potential. Cs^+ also significantly inhibited I_f ($< 10\%$ of control at -70 mV) activated during hyperpolarization and decreased the initial background inward current. Panel C shows that on washout of Cs^+ both pacemaker action potentials and I_f recovered. In 8 cells tested, 2 mM Cs^+ increased mean cycle length from 884 ± 28

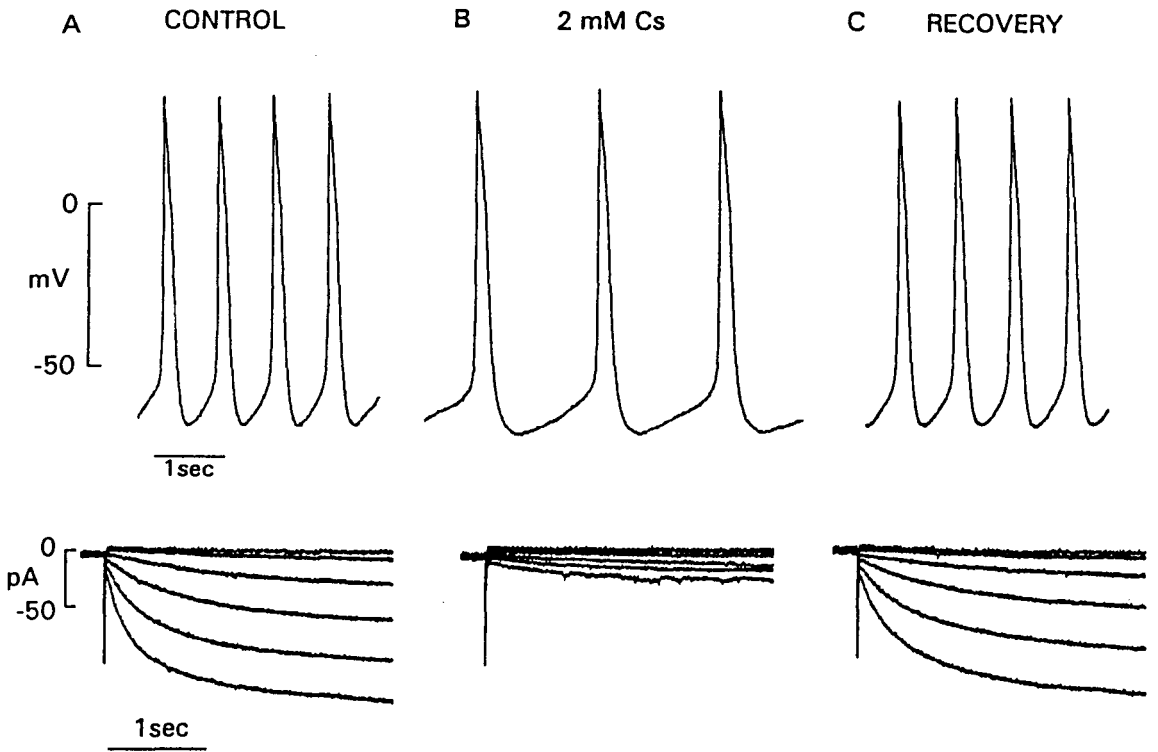


Figure 17. Effects of Cs^+ on pacemaker action potentials and I_f recorded from a single latent pacemaker cell. A: control pacemaker action potentials (top) and I_f (bottom) in normal Tyrode's solution. Currents were elicited by hyperpolarizing clamps between -50 and -100 mV from V_h of -40 mV. B: effect of 2 mM Cs^+ . C: recovery following washout of Cs^+ .

ms to 1782 ± 146 ms, which represents a $48 \pm 5\%$ decrease in spontaneous rate ($P < 0.01$). Following washout of Cs^+ , cycle length returned to 935 ± 40 ms. Cs^+ -induced hyperpolarization of the maximum diastolic potential was variable and not statistically significant.

To determine whether the results obtained in these experiments were influenced by the recording method (49), we studied the effect of Cs^+ on the spontaneous beating rate of latent atrial pacemaker cells without applying a patch electrode to the cell. Instead, pacemaker cycle length was determined by measuring contractile events with a video-based edge detector. In 15 cells tested, cycle length was 913 ± 48 ms in the absence and 1918 ± 142 ms in the presence of 2 mM Cs^+ , which corresponds to a $50 \pm 3\%$ decrease in spontaneous rate ($p < 0.01$). Washout of Cs^+ returned cycle length to 961 ± 48 ms. These values are not statistically different from those obtained using the nystatin-perforated patch recording method. Whether measured with or without patch electrodes, Cs^+ significantly slowed beating rate in all cells tested but did not stop spontaneous activity. These results indicate that a Cs^+ -sensitive I_f current contributes significantly to latent pacemaker activity. In addition, the run-down in pacemaker activity seen with the ruptured-patch recording method cannot solely be due to run-down of I_f activation because Cs^+ block of I_f failed to stop pacemaker activity.

Effect of isoproterenol. It has been reported that the response of I_f to β -adrenergic stimulation are variable among different pacemaker cells isolated from SA node (59, however see 89). We therefore tested whether the response of latent pacemaker cells to isoproterenol is influenced by the recording method used. As shown

in Figure 18 A, when the ruptured patch method was used to record I_f , ISO ($1\mu\text{M}$) elicited variable changes in I_f amplitude among different cells. In panel A (top), ISO increased I_f , while in another cell (bottom), ISO decreased I_f . As a result, ISO elicited no net change in mean I_f amplitude ($n=6$) (panel C). The variability in the response to ISO may be due to loss of some intracellular substances that are essential for mediating the effect of ISO on I_f . It is well known that the effects of ISO are mediated in many cell systems through cytosolic second messenger systems (89,122). In addition, the ruptured patch recording method allows diffusion of internal constituents between the cell interior and the internal pipette solution (93). It is important to use a method which avoids intracellular dialysis. We therefore used a nystatin-perforated patch recording method to avoid loss of intracellular constituents (104,130) and to study the effect of ISO on I_f . Panel B shows a typical response to ISO when I_f was recorded with the nystatin method. ISO elicited a significant increase in I_f , and this response was consistent in all cells tested ($n=8$). Panel C shows that using nystatin method ISO induced a $90 \pm 22\%$ ($P < 0.001$, $n=8$) increase in I_f at -80 mV.

Figure 19 shows the effect of ISO on the I_f activation curve with ruptured patch and nystatin recording methods. Panel A shows that with the ruptured patch method there was no significant change in the I_f activation curves between control (\bullet) and $1\mu\text{M}$ ISO (\circ) ($n=4$). Half-maximal activation voltages in control and ISO were -75.3 ± 2.2 mV and -73.9 ± 4.5 mV, respectively. Panel B shows the I_f activation curves in control (\bullet) and $1\mu\text{M}$ ISO (\circ) with nystatin perforated patch method ($n=3$). ISO elicited a significant shift in the half-maximal activation voltage from -78.7 ± 2.5 mV to -67.6

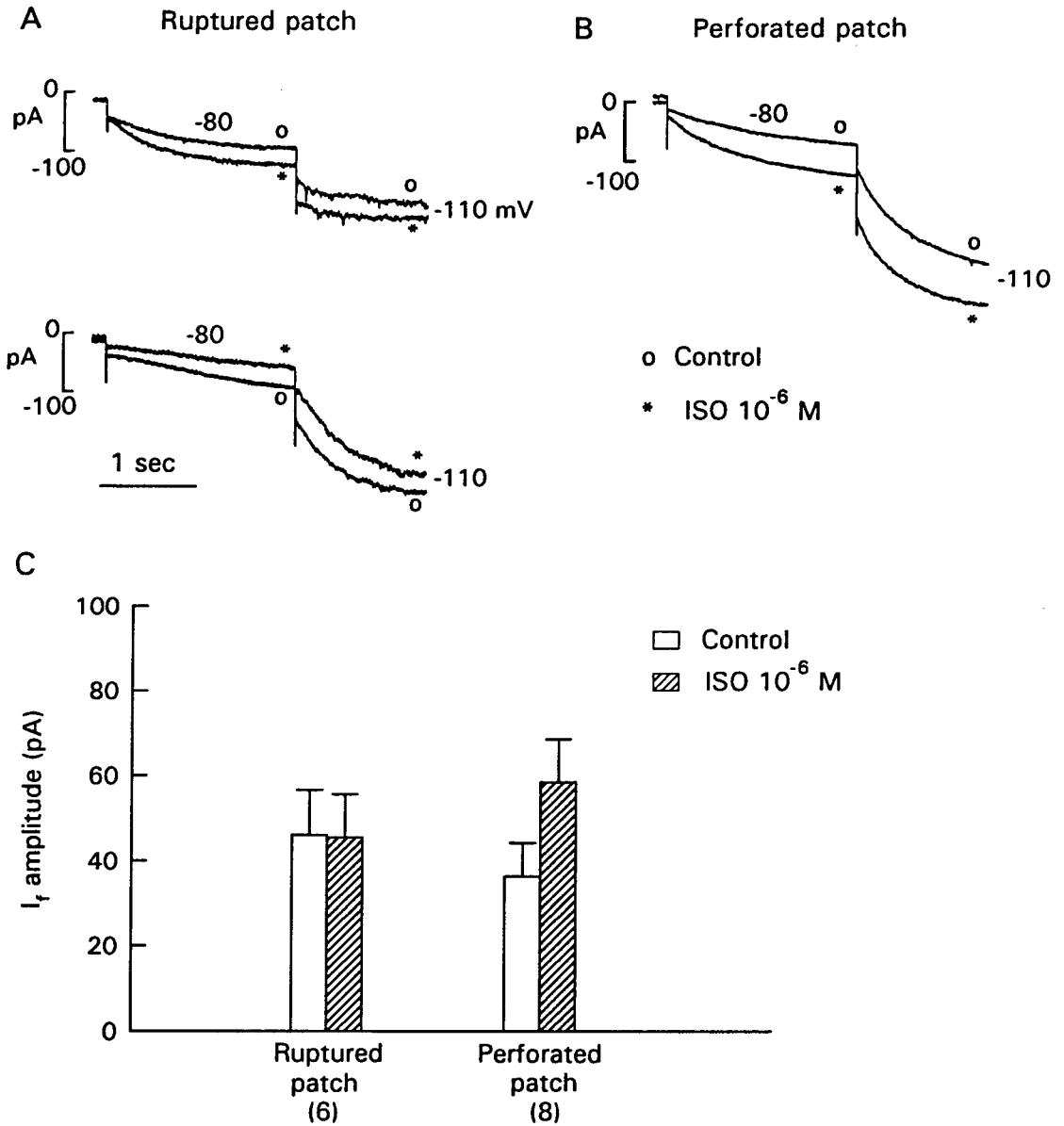


Figure 18. Effects of isoproterenol (ISO) on I_f . A: responses of I_f to ISO with ruptured patch recording method. ISO elicited variable changes in I_f among different cells ($n=6$); increased (top) or decreased (bottom). B: response of I_f to ISO with nystatin-perforated patch method. With nystatin perforated patch method ISO increased I_f in all cells ($n=8$). I_f currents were elicited by two step hyperpolarization clamps to -80 and -110 mV from V_h of -40 mV. C: effects of ISO on I_f elicited by hyperpolarizing clamps to -80 mV from a V_h of -40 mV.

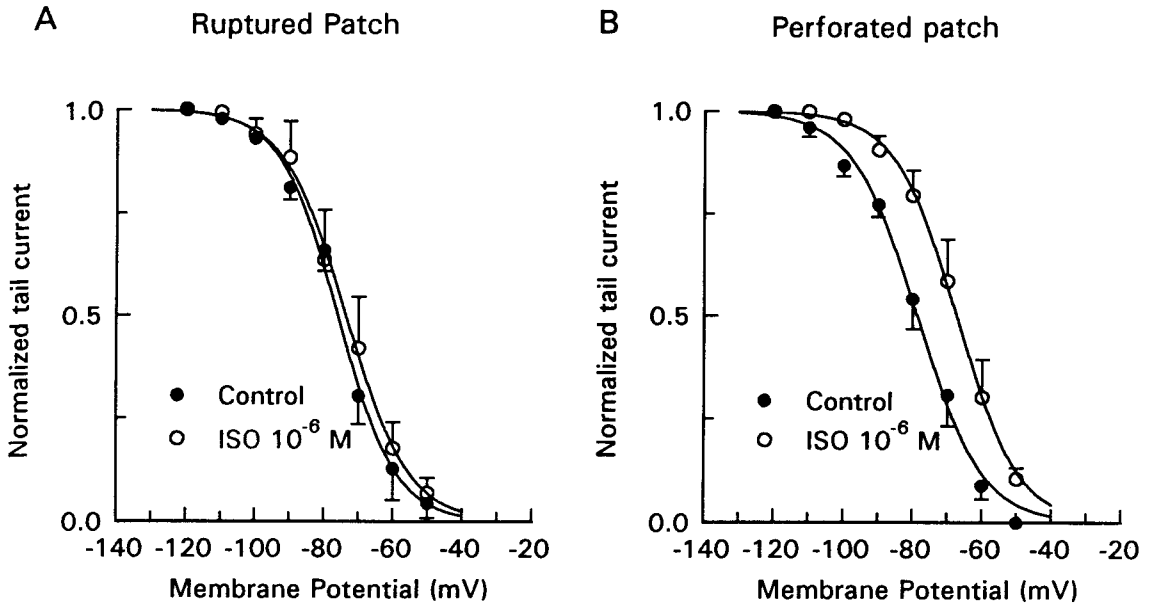


Figure 19. Effect of ISO on I_f activation curve with ruptured patch and nystatin-perforated patch recording methods. A: I_f activation curves in control (●) and $1 \mu\text{M}$ ISO (○) with ruptured patch method ($n=4$). B: I_f activation curves in control (●) and $1 \mu\text{M}$ ISO (○) with nystatin-perforated patch recording method ($n=3$). External solution contained 3 mM Ni^{2+} , 3 mM Ba^{2+} and 2 mM 4-AP .

± 3.3 mV ($p < 0.05$).

In Figure 20, the nystatin recording method was used to study the effects of ISO on pacemaker action potentials and I_f currents recorded from a single latent pacemaker cell. Panel A shows the control spontaneous action potentials and I_f . In panel B, $1 \mu\text{M}$ ISO significantly increased the slope of diastolic depolarization, decreased pacemaker cycle length, and increased I_f elicited by hyperpolarization. In 5 cells tested, ISO decreased mean pacemaker cycle length from 862 ± 84 to 542 ± 31 ms ($P < 0.01$) and increased I_f amplitude in all cells.

2. Delayed Rectifier I_K :

Voltage dependence of I_K activation. Figure 21 shows the determination of the voltage dependence of I_K activation. In panel A, a pacemaker cell was depolarized from a holding potential of -50 mV and then repolarized back to the holding potential following each clamp step. I_K was elicited during each depolarization and I_K tail currents were elicited upon repolarization. As shown in panel B, peak I_K tail current amplitudes were normalized with respect to maximal tail current amplitude and plotted against the voltage imposed during depolarization. The activation curve (smooth curve) was obtained by fitting the data with a Boltzmann equation: $q_\infty = 1 - \{1 + \exp[(V_t - V_{0.5})/k]\}^{-1}$. The activation curve is sigmoidal and shows that I_K is activated at voltages more positive than -40 mV and fully activated at about $+30$ mV. The half-maximal activation voltage and slope factor were -8.6 ± 1.6 and 12.6 ± 0.7 mV, respectively.

Fully-activated I-V relationship. The fully-activated I-V relationship for I_K was determined according to a method described by Nakayama *et al.* (159). As shown in

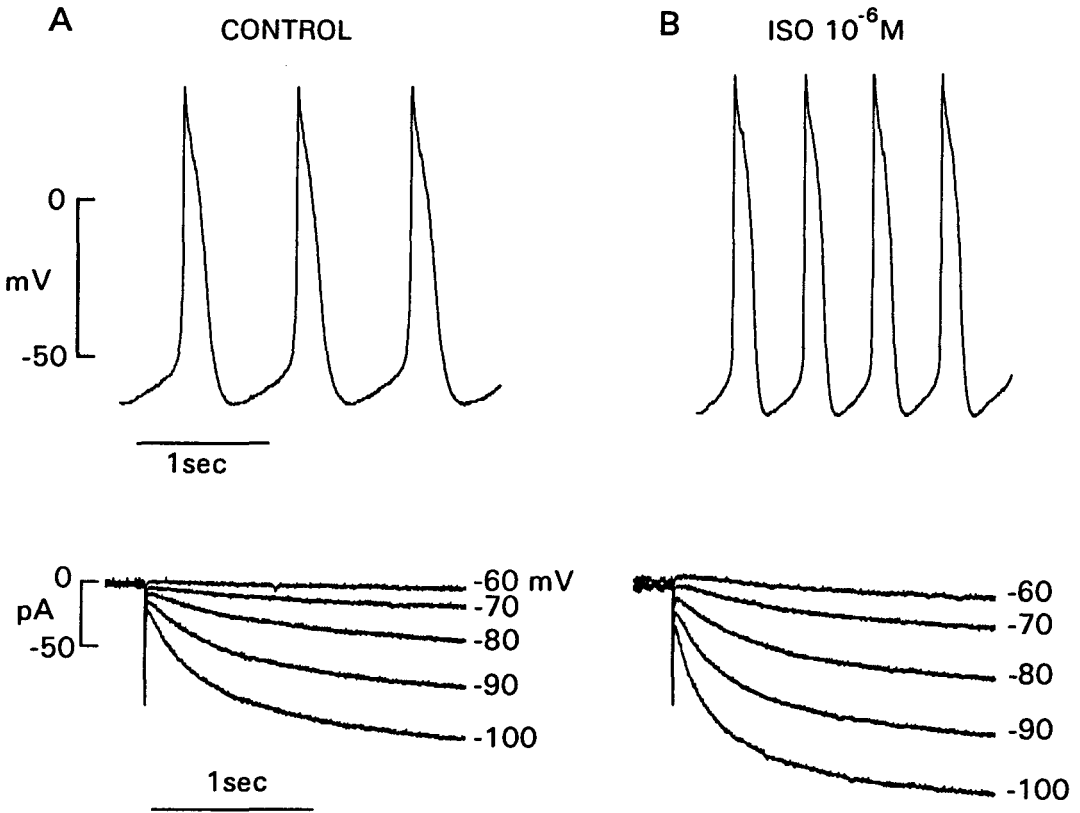


Figure 20. Effect of ISO on pacemaker action potentials and I_f recorded from a single latent pacemaker cell using nystatin-perforated patch recording method. A: control pacemaker action potentials (top) and I_f (bottom) in normal Tyrode's solution. Currents were elicited by hyperpolarizing clamps between -60 and -110 mV from V_h of -40 mV. B: effect of $1 \mu\text{M}$ ISO.

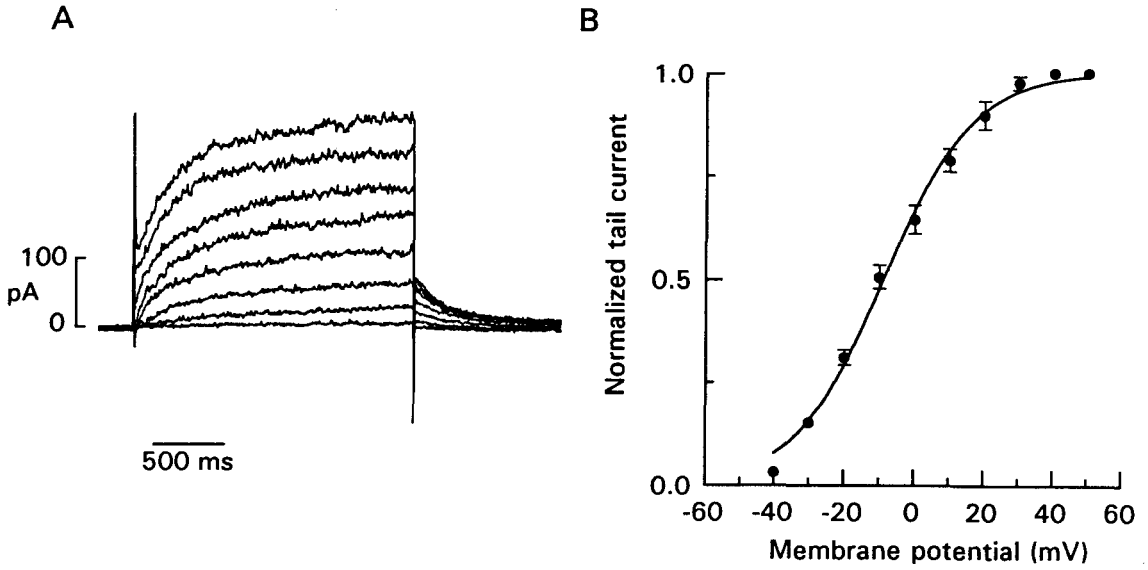


Figure 21. Activation curve of I_K . A: Membrane currents used to determine the activation curve for I_K . The cell was held at -50 mV and depolarized between -40 and $+30$ mV for 2 sec, and then clamped back to -50 mV. B: normalized tail currents are plotted against the voltage imposed during depolarization. The data are means \pm SE obtained from 6 cells. The solid curve is a best fit to the data by a Boltzmann equation.

Figure 22, a pacemaker cell was held at -50 mV and clamped to $+30$ mV, a voltage at which I_K is fully activated. This was followed by test clamp pulses to voltages between -100 and $+20$ mV. Then the same test clamp pulses were applied from -50 mV, a voltage where I_K is not activated. The fully-activated I-V relationship of I_K was determined by measuring the difference in the initial current amplitudes at the same test voltages (as indicated by arrows). In panel B, the difference currents were plotted against the imposed test voltages. The fully-activated I-V relationship was linear between -100 and about -30 mV and inwardly rectified at more positive voltages. In addition, I_K current reversed direction at about -80 mV ($n=4$).

Separation of I_K tail current from I_f activation. To determine the reversal potential of I_K , tail currents elicited upon repolarization were examined in the voltage range between -60 and -100 mV. However, latent pacemaker cells also exhibit I_f activation in the same voltage range. Because I_f activation will influence the measurements of I_K reversal potential we employed the following voltage clamp protocol to separate I_K tail currents from I_f activation. As shown in Figure 23A, pacemaker cells were held at -45 mV and then clamped to more negative voltages with and without a preceding depolarizing clamp. The depolarizing pulse to $+20$ mV for 2 sec activated I_K during depolarization. Therefore, hyperpolarization that followed a depolarizing clamp elicited tail currents that consisted of both I_K deactivation and I_f activation, whereas hyperpolarization from -45 mV to the same voltages without a preceding depolarization elicited I_f alone. Typical current recordings elicited by this protocol are shown in panel A. Without a preceding depolarization, hyperpolarization between -60

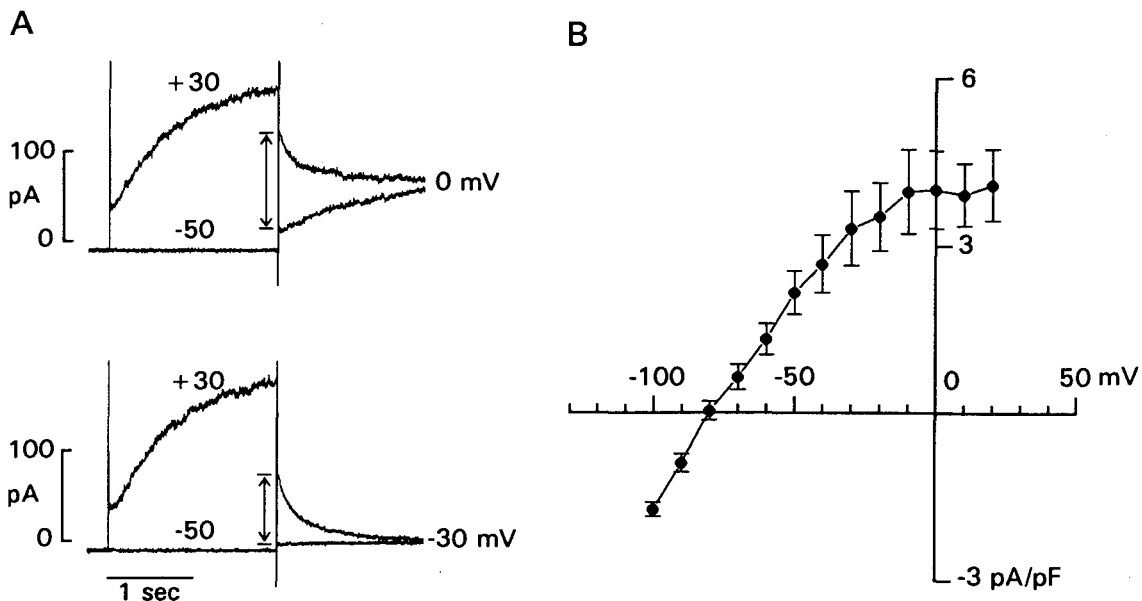


Figure 22. Fully-activated I-V relationship for I_K . A: selected currents used to determine the fully-activated I-V relationship. From V_h of -50 mV, two test clamp pulses were applied to voltages between -100 and $+20$ mV with or without a preceding depolarizing clamp to $+30$ for 2 sec. The difference between the initial tail current amplitude (arrows) was plotted against the test voltage at which the current was elicited. B: fully-activated I-V relationship for I_K from 4 cells. Currents were normalized against total cell capacitance and expressed as current density (pA/pF).

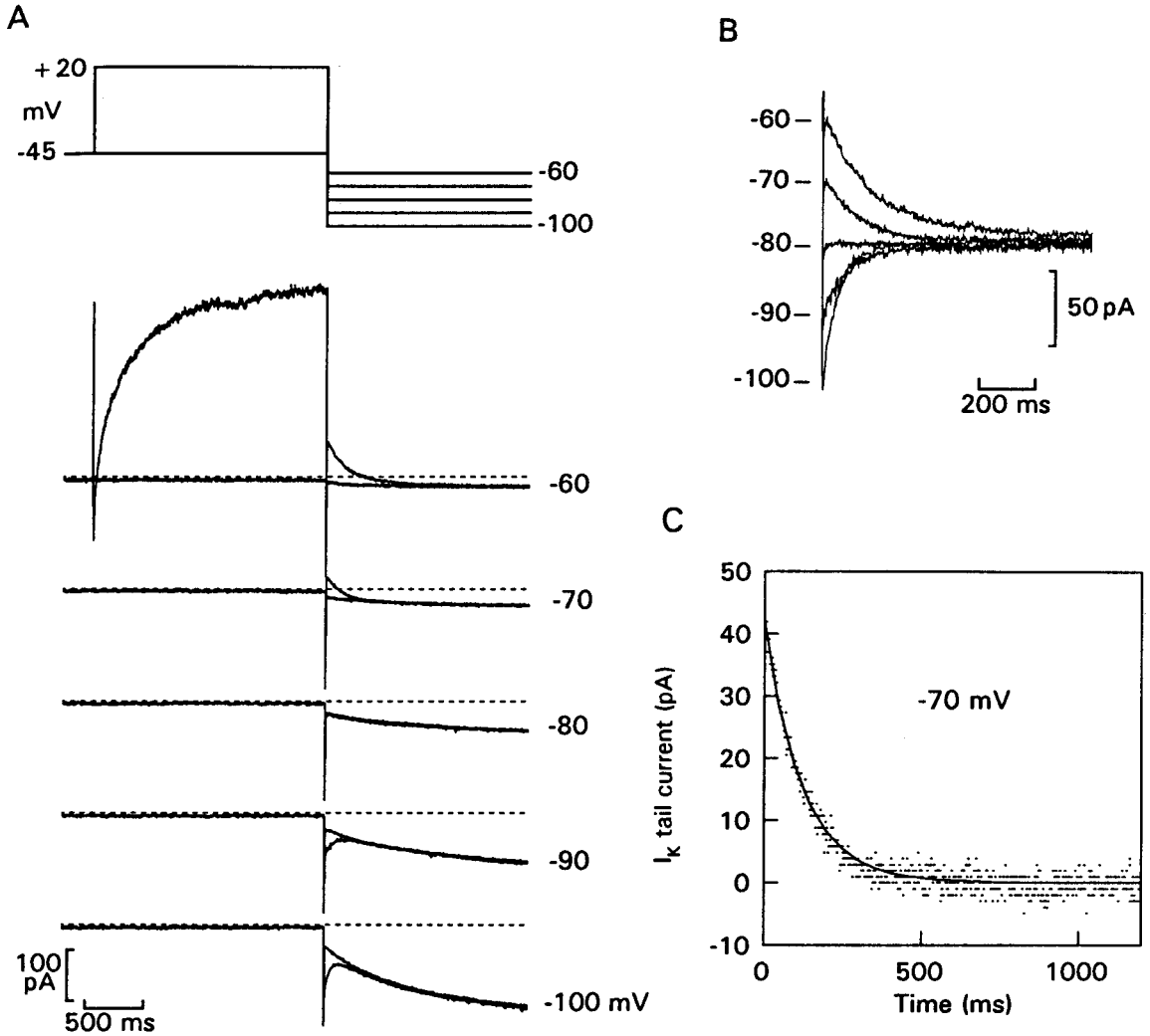


Figure 23. Separation of I_K tail currents from I_f activation. A: the voltage clamp protocols (top). From a V_h of -45 mV a cell was clamped between -60 and -100 mV with or without 2 sec conditional pulses to $+20$ mV to activate I_K . Currents recorded with each protocols are shown superimposed (bottom). The interrupted lines indicate the zero current level. B: I_K tail currents obtained by subtraction of I_f from total current tails. The tail current reversed at about -80 mV. C: the decay of I_K was best fit by a single exponential function.

and -100 mV elicited only I_f , which showed typical characteristics, i.e. increased with time and was larger at more negative voltage. When I_K was activated by depolarizing clamps to $+20$ mV, currents elicited by hyperpolarizing clamps to the same voltages exhibited additional outward tail currents that were larger at -60 than at -70 mV and inward in direction at -90 and -100 mV. At -80 mV, currents elicited by the two different protocols were superimposed, indicating the tail current reversal potential. Clearly, tail current amplitude was larger at voltages that were further from the tail current reversal potential. I_K currents were separated from I_f by subtracting currents elicited by hyperpolarization without a pre-conditioning pulse from those elicited following a depolarizing pulse. Panel B shows the subtracted I_K tail currents. Indeed, I_K tail currents exhibited a reversal potential of about -80 mV. In 6 cells, I_K reversal potential was -78.2 ± 0.3 mV, which is close to the calculated K^+ equilibrium potential (-86 mV). These results support the idea that I_K is selectively carried by K^+ ions. Panel C shows that I_K tail currents (separated from I_f), elicited at -70 mV exhibited a single exponential decay, with a time constant of 159 ± 16 ms ($n=6$). Because latent pacemaker action potentials exhibit a maximum diastolic potential of about -70 mV, and a cycle length of about 900 ms, these results suggest that deactivation of I_K may contribute to the kinetics of the initial portion of the diastolic depolarization in latent atrial pacemakers.

Effect of extracellular K^+ on I_K reversal potential. The ionic selectivity of I_K was further studied by measuring the reversal potential of I_K in different extracellular K^+ concentrations ($[K^+]_o$). I_K tail currents were obtained as described above and used to

examine the I_K reversal potential in $[K^+]_o$ of 2.5, 5.4, 10.8 and 25 mM. Figure 24A shows subtracted I_K tail currents recorded in different $[K^+]_o$, as indicated in each panel. As expected the reversal potential shifted to more positive voltages as the $[K^+]_o$ was increased from 2.5 to 25 mM. In panel B, the reversal potentials measured in each $[K^+]_o$ were plotted against $[K^+]_o$ on a semilogarithmic scale. The linear regression line showed a slope of 51.5 mV per tenfold change in $[K^+]_o$. These results confirm that I_K is, in fact, carried primarily by K^+ ions.

Effect of elevated K^+ on action potentials. Latent atrial pacemakers recorded from multicellular Eustachian ridge preparations are relatively insensitive to elevated concentrations of extracellular K^+ (139). We therefore used the nystatin recording method to determine the effect of elevated K^+ on pacemaker action potentials recorded from single latent pacemaker cells. Figure 25A shows spontaneous pacemaker action potentials in normal Tyrode's solution. As shown in panel B, raising the extracellular K^+ from 5.4 to 10.8 mM shifted the maximum diastolic potential more positive and shortened pacemaker cycle length. As shown in panel C, returning to normal K^+ (5.4 mM) restored action potential configuration. In 5 cells tested, 10.8 mM K^+ shifted the maximum diastolic potential from -69.4 ± 0.9 mV to -58.0 ± 0.5 mV ($p < 0.001$) and shortened pacemaker cycle length from 850 ± 24 ms to 682 ± 46 ms which represents a $26.5 \pm 7.3\%$ increase in spontaneous rate ($p < 0.05$).

3. Ca^{2+} Currents: T-type and L-type.

Ca^{2+} currents were isolated for study by altering the ionic composition of both the internal (see Table 2) and external solutions (see methods) and by using appropriate

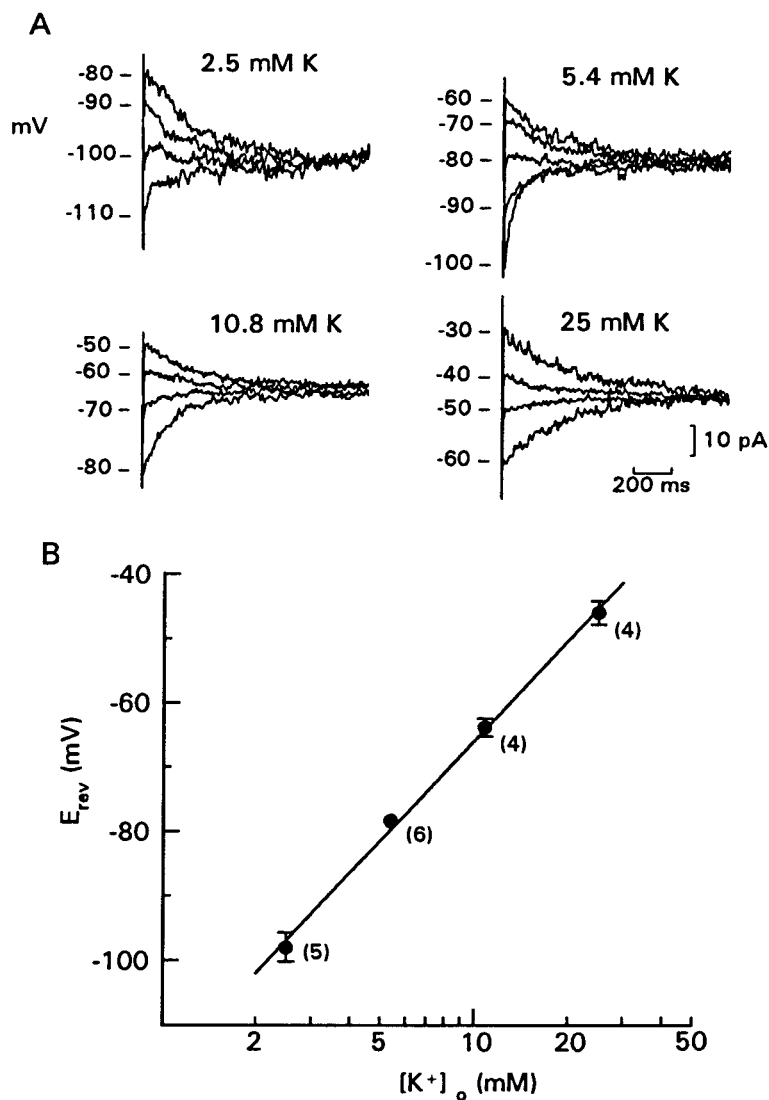


Figure 24. Effect of extracellular K^+ concentration on the reversal potential of I_K . The reversal potentials of I_K were measured in different extracellular K^+ concentrations using the voltage clamp protocol shown in Figure 23. A: subtracted I_K tail currents in $[K^+]_o$ of 2.5, 5.4, 10.8, and 25 mM as indicated. B: reversal potentials were plotted against $[K^+]_o$ on a semilogarithmic scale. Data are means \pm SE and the number of cells tested in each K^+ concentration are shown in parentheses. The straight line is the least-squares fit of the data.

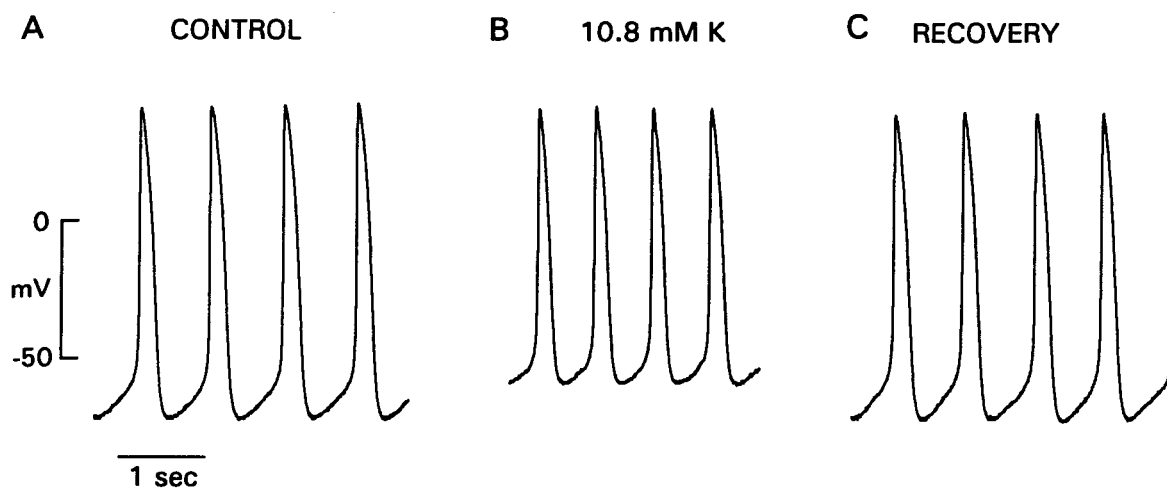


Figure 25. Effect of elevated K^+ concentration on pacemaker action potentials. A: control pacemaker action potentials in normal ($5.4 \text{ mM } K^+$) Tyrode's solution. B: effect of 10.8 mM extracellular K^+ . C: recovery after returning to normal Tyrode's solution.

channel blocking agents. I_K current was inhibited by 120 mM Cs^+ in the pipette solution and 140 mM TEA in the bath solution, and the fast Na^+ current was blocked by 30 μM TTX in Na-free external solution. $I_{Ca,T}$ and $I_{Ca,L}$ were separated based on their voltage dependence of activation and inactivation, using the following voltage clamp protocols. From a holding potential of -80 mV depolarizing clamp pulses between -70 and $+50$ mV were used to elicit both $I_{Ca,T}$ and $I_{Ca,L}$. To elicit $I_{Ca,L}$ alone the cell was held at -80 mV, and a conditioning pulse to -40 mV for 1 sec was imposed to inactivate $I_{Ca,T}$. Then the cell was clamped to voltages between -30 and $+50$ mV to elicit $I_{Ca,L}$. This protocol was used to minimize run-down of L-type current (17). $I_{Ca,T}$ was obtained by subtracting those currents elicited from -40 mV from those currents elicited from a holding potential of -80 mV. As shown in Figure 26 A-a, from a holding potential of -80 mV depolarizing test pulses to voltages more positive than -50 elicited a rapidly decaying transient inward current. At -50 and -40 mV the currents are attributable to activation of $I_{Ca,T}$. At more positive voltages the currents are due to activation of both $I_{Ca,T}$ and $I_{Ca,L}$ (total Ca^{2+} currents). Figure 26 A-b shows the currents elicited by depolarizing clamp pulses that were preceded by a 1 sec conditioning pulse to -40 mV. At -30 mV only a small inward current was elicited. At test pulses of -10 and $+20$ mV, the currents were smaller than those elicited by the same test pulses without a conditioning step. At $+40$ mV, however, the two currents were similar. The currents elicited from -40 mV are attributed to activation of $I_{Ca,L}$. Figure 26 A-c shows the difference currents obtained by the subtraction procedure and attributed to activation of $I_{Ca,T}$. Figure 26B shows the I-V relationships of $I_{Ca,T}$ (\blacksquare), $I_{Ca,L}$ (\circ) and total Ca^{2+}

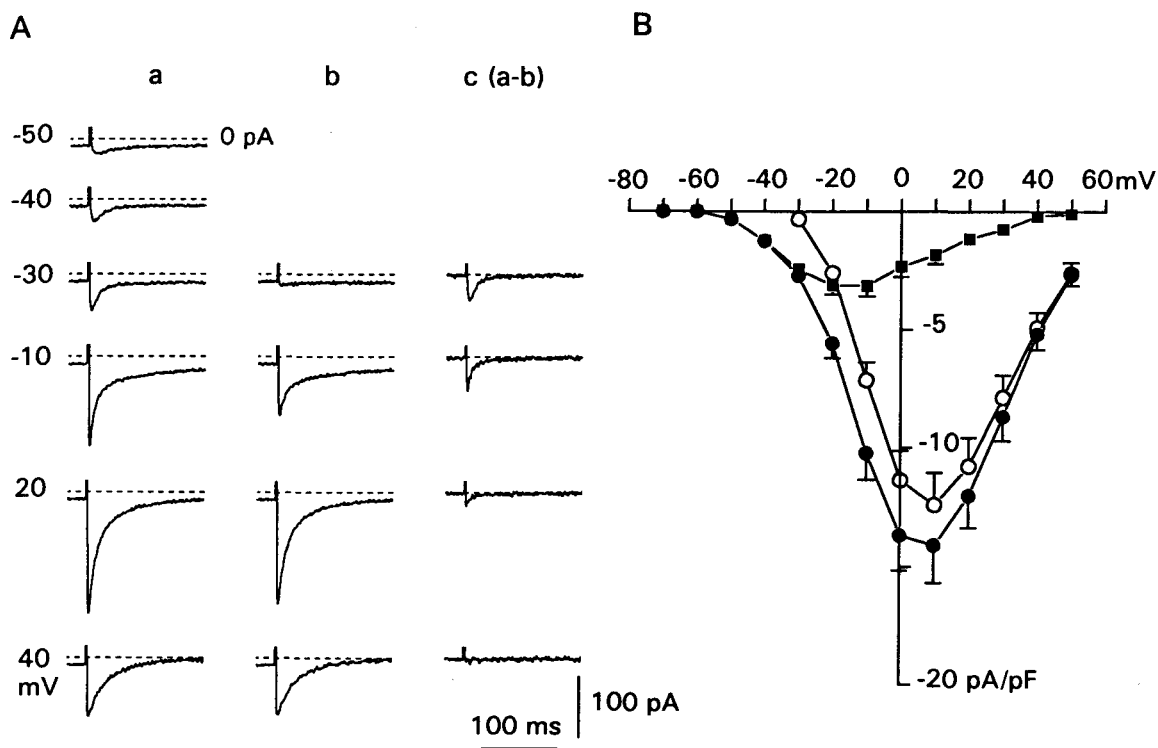


Figure 26. Two types of Ca^{2+} currents in a latent pacemaker cell. A: selected membrane currents elicited by depolarizing clamps to various voltages from V_h of -80 mV without (a) or with a 1-sec conditioning pulse to -40 mV (b), and the difference current (c). B: peak I-V relationships of current elicited by clamps without conditioning pulse as shown in A-a (●), with conditioning pulse as shown in A-b (○), and the difference current as shown in A-c (■).

currents (●) obtained from 15 cells. The data are normalized with respect to membrane capacitance and expressed as current density (pA/pF). The I-V relationship of $I_{Ca,T}$ exhibited a threshold at -50 mV and a peak at -10 mV. The I-V relationship of $I_{Ca,L}$ showed a threshold at -30 mV and a peak at +10 mV. Maximal $I_{Ca,T}$ and $I_{Ca,L}$ were 3.3 ± 0.4 pA/pF and 12.5 ± 1.3 pA/pF, respectively. Peak $I_{Ca,T}$ to $I_{Ca,L}$ ratio was 0.29 ± 0.04 .

It has been reported that in SA node pacemaker (90) and Purkinje cells $I_{Ca,T}$ (210) current density is higher than in atrial and ventricular cells. Previous work from this laboratory showed that $I_{Ca,T}$ current density in cat atrial cells was 1.01 pA/pF, which is significant smaller than that of latent pacemaker cells (225). However, these experiments were performed in 5.4 mM Ca^{2+} and room temperature. In order to eliminate the influence of different experimental conditions, Ca^{2+} currents were recorded from working right atrial cells under the same conditions as those for latent pacemaker cells. It was found that under conditions of 2.7 mM Ca^{2+} and 35°C, maximal $I_{Ca,T}$ amplitude in working atrial cells was 0.68 ± 0.21 pA/pF. These experiments demonstrate that under the same experimental conditions $I_{Ca,T}$ current density of latent pacemaker cells is significantly higher than that of normal working atrial muscle cells ($P < 0.001$).

Voltage dependence of activation and inactivation. The voltage dependence of steady-state inactivation for Ca^{2+} currents was determined by using a double pulse protocol. A 1-sec conditioning pulse to various voltages was followed by a fixed test pulse for 300 ms to elicit $I_{Ca,T}$ or $I_{Ca,L}$. For $I_{Ca,T}$ the test pulse was to -30 mV and the conditioning pulses varied from -90 to -40 mV. For $I_{Ca,L}$ the test pulse was to +20 and

the conditioning pulses varied from -40 to $+10$ mV. The inactivation parameter f was determined by dividing peak current by maximum peak current. The voltage dependence of activation for Ca^{2+} currents was determined according to a method described by Fermini and Nathan (79). The activation parameter d was estimated from the peak conductance: $d = I_{\text{Ca}}/[g_{\text{Ca,max}}(Vm - E_{\text{rev}})]$; where I_{Ca} is the peak current at membrane potential (Vm), $g_{\text{Ca,max}}$ is the maximal Ca^{2+} conductance, and E_{rev} is the apparent reversal potential, which was obtained by fitting the linear portion of the I-V relationships through zero current (115). In Figure 27, the calculated activation and inactivation parameters for $I_{\text{Ca,T}}$ and $I_{\text{Ca,L}}$ were plotted against the imposed voltages. The activation and inactivation curves (smooth curve) were obtained by fitting the data with Boltzmann equations: $d = 1 - \{1 + \exp[(V_t - V_{0.5})/k]\}^{-1}$ and $f = \{1 + \exp[(V_t - V_{0.5})/k]\}^{-1}$, respectively, where V_t is either the depolarizing pulse voltage for activation or the conditioning pulse voltage for inactivation. The results show that $I_{\text{Ca,T}}$ was activated at voltages more positive than -60 mV and fully activated at about -10 mV, whereas $I_{\text{Ca,L}}$ was activated at voltages more positive than -30 mV and fully activated at about $+20$ mV. The half-maximal activation voltage and slope factor for $I_{\text{Ca,T}}$ were -31.4 ± 0.2 and 7.3 ± 0.5 mV, respectively, and for $I_{\text{Ca,L}}$ were -6.2 ± 2.0 and 6.7 ± 0.5 ($n=5$), respectively. The half-maximal inactivation voltage and slope factor for $I_{\text{Ca,T}}$ were -57.2 ± 1.8 and 5.1 ± 0.5 mV, respectively, and for $I_{\text{Ca,L}}$ were -27.6 ± 1.0 and 4.1 ± 0.4 mV, respectively. Overlap of the activation and inactivation curves indicates that a region of steady-state "window" currents exists for both $I_{\text{Ca,T}}$ and $I_{\text{Ca,L}}$. For $I_{\text{Ca,T}}$ this region was between -60 and -30 mV and for $I_{\text{Ca,L}}$ between -40 and 0 mV. The voltage

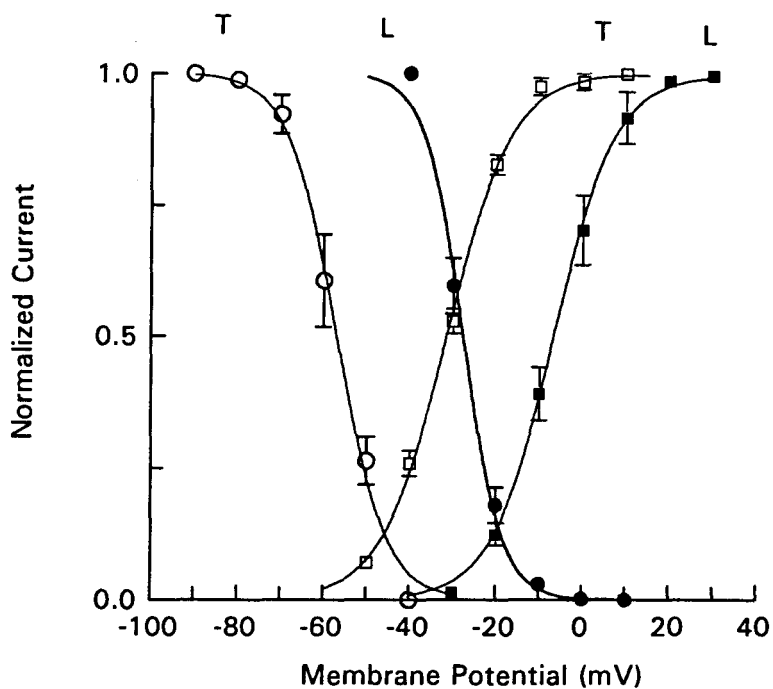


Figure 27. Voltage-dependence of activation and inactivation for $I_{Ca,T}$ and $I_{Ca,L}$. Open symbols show the steady-state activation (\square) and inactivation (\circ) curves for $I_{Ca,T}$. Closed symbols show the steady-state activation (\blacksquare) and inactivation (\bullet) curves for $I_{Ca,L}$. Continuous curves were obtained by fitting data with Boltzmann equations.

range of $I_{Ca,T}$ "window" current is consistent with the late pacemaker potential, and therefore suggests that $I_{Ca,T}$ may contribute to pacemaker activity in latent pacemaker cells.

Effect of cobalt. Cobalt (Co^{2+}) has been reported to block both types of Ca^{2+} currents in SA node pacemaker (90) and atrial cells (10). Figure 28A shows that in latent pacemaker cells, 2 mM Co^{2+} abolished currents elicited by depolarizing clamps to -40 mV (top traces) and $+10$ mV (bottom traces) from a holding potential of -80 mV. In panel B the I-V relationships of total peak current indicate that both $I_{Ca,T}$ and $I_{Ca,L}$ were blocked by 2 mM Co^{2+} ($n=4$). In addition, these results confirmed that fast Na^+ current (see Figure 32) was effectively eliminated under our experimental conditions.

Effect of nifedipine. It has been reported that nifedipine selectively inhibits $I_{Ca,L}$ without affecting $I_{Ca,T}$ (90,99). In addition, the blocking effect of nifedipine on $I_{Ca,L}$ has been reported to be voltage-dependent (99). Figure 29A shows the effect of 1 μ M nifedipine on $I_{Ca,T}$ and $I_{Ca,L}$ in a latent pacemaker cell. The top traces show that nifedipine had no effect on $I_{Ca,T}$ elicited by a depolarizing clamp from -80 to -40 mV. In contrast, the bottom traces show that when $I_{Ca,L}$ was elicited by a depolarizing pulse from -40 to $+10$ mV, nifedipine abolished all inward current. However, when Ca^{2+} currents were elicited from a more negative potential of -80 mV by a depolarizing clamp to $+10$ mV (without a conditioning pulse to -40 mV), nifedipine only inhibited about 25% of total inward current (middle traces). The results suggest that the effect of nifedipine on $I_{Ca,L}$ is voltage-dependent, similar to its effect reported in Purkinje cells (99). Fig 29B shows the I-V relationships from a holding potential of -80 mV without

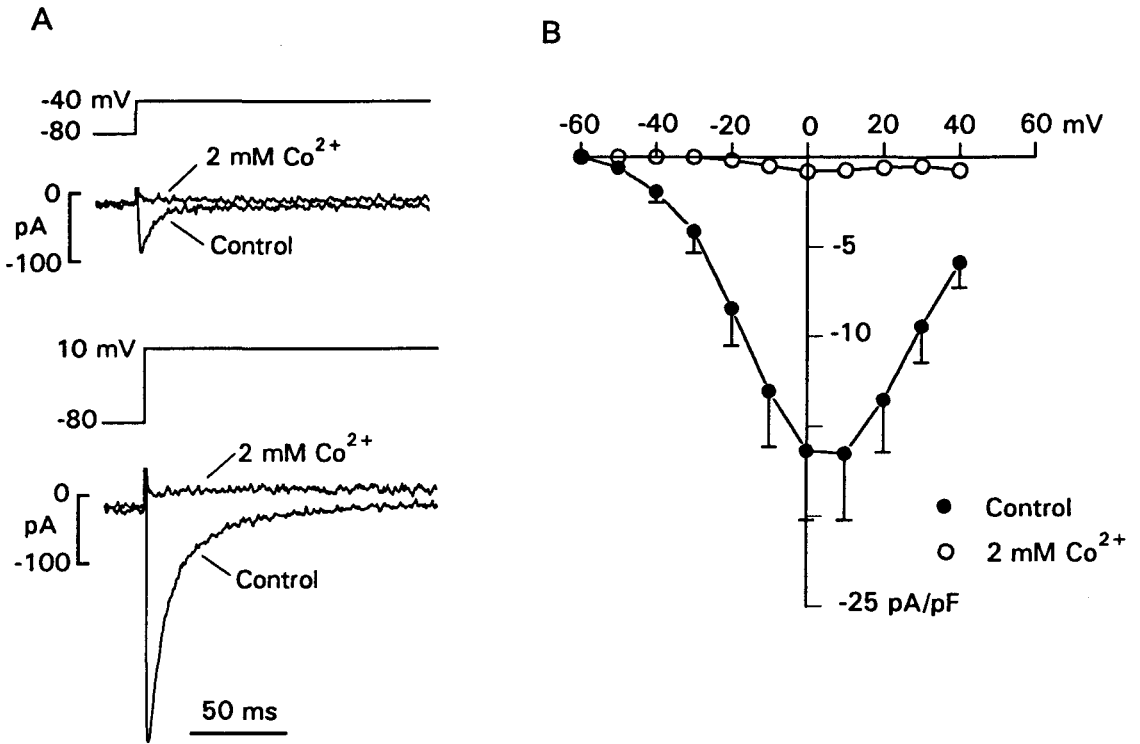


Figure 28. Effects of cobalt (Co^{2+}) on $I_{Ca,T}$ and $I_{Ca,L}$. A: $I_{Ca,T}$ and $I_{Ca,L}$ currents were elicited from V_h of -80 by depolarizing clamps to -40 (top) and +10 mV (bottom), respectively. In the presence of 2 mM Co^{2+} both currents were abolished. B: peak current I-V relationships in control (●) and in the presence of 2 mM Co^{2+} (○).

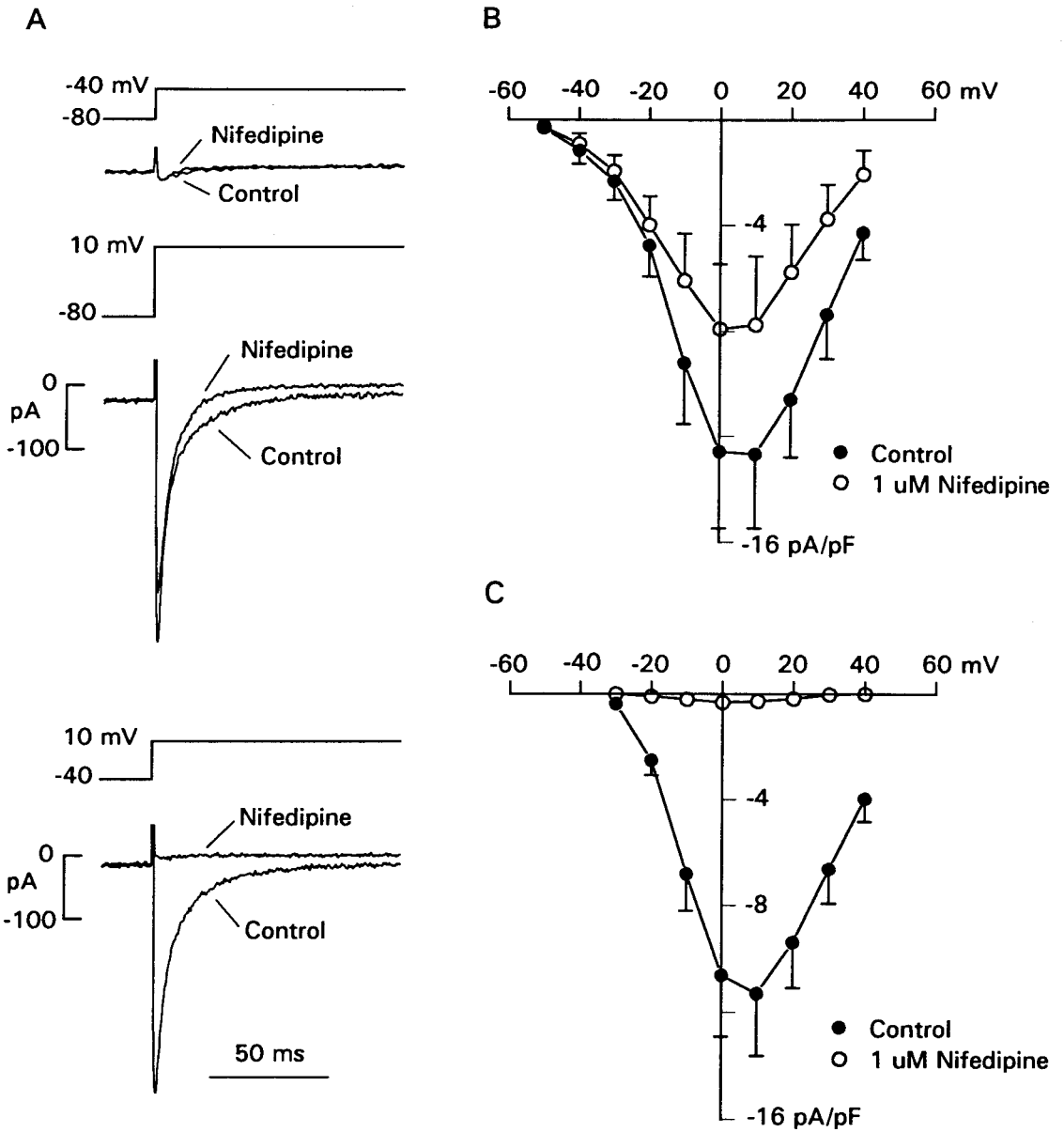


Figure 29. Effects of nifedipine on $I_{Ca,T}$ and $I_{Ca,L}$. A: (top) effect of $1 \mu\text{M}$ nifedipine on $I_{Ca,T}$ elicited by depolarizing clamp to -40 mV from V_h of -80 mV. Middle: effect of $1 \mu\text{M}$ nifedipine on $I_{Ca,L}$ elicited by depolarizing clamps to $+10$ mV from V_h of -80 mV. Bottom: effect of $1 \mu\text{M}$ nifedipine on $I_{Ca,L}$ elicited by depolarizing clamps to $+10$ mV with a 1 -sec conditioning pulse to -40 mV. B & C: I-V relationships in control (●) and in the presence of $1 \mu\text{M}$ nifedipine (○) from V_h of -80 mV without conditioning pulse (B) and with a 1 -sec conditioning pulse to -40 mV (C).

a conditioning pulse in control (●) and in the presence of 1 μM nifedipine (○) ($n=4$). Fig 29C shows the I-V relationships with a 1-s conditioning pulse to -40 mV in control (●) and in the presence of 1 μM nifedipine (○) ($n=4$).

Effect of nickel. Low concentrations of Ni^{2+} have been reported to specifically block $I_{\text{Ca,T}}$ in SA node pacemaker cells (90). However, others have shown that 40 μM Ni^{2+} could not block $I_{\text{Ca,T}}$, and higher concentrations reduced both $I_{\text{Ca,T}}$ and $I_{\text{Ca,L}}$ (79). In our experimental condition, 40 μM Ni^{2+} partially blocked $I_{\text{Ca,T}}$ at voltages of -50 and -40 mV (Figure 30A). At more positive potentials, Ni^{2+} had little effect on $I_{\text{Ca,T}}$ and $I_{\text{Ca,L}}$. Figure 30B shows the peak current I-V relationships from a holding potential of -80 mV in control (●) and in the presence of 40 μM Ni^{2+} (○) from 5 cells. The results show that 40 μM Ni^{2+} inhibited $I_{\text{Ca,T}}$ elicited at -50 and -40 mV by $63 \pm 9\%$ and $44 \pm 3\%$, respectively. However, at -10 mV the maximal $I_{\text{Ca,T}}$ was inhibited by only 10%.

To determine the relative contribution of $I_{\text{Ca,T}}$ to latent atrial pacemaker activity, 40 μM Ni^{2+} was tested on spontaneous action potentials using a nystatin-perforated recording method. Figure 31A shows the control spontaneous action potentials. In panel B, 40 μM Ni^{2+} significantly increased pacemaker cycle length by specifically decreasing the late phase of diastolic depolarization. Similar effect of Ni^{2+} on pacemaker action potentials has been reported in SA node pacemaker cells (64,90). Panel C shows the recovery of pacemaker action potentials after washout of Ni^{2+} . In 6 cells tested, Ni^{2+} increased mean pacemaker cycle length from 855 ± 38 to 1427 ± 218 ms, which represents a $35 \pm 6\%$ decrease in spontaneous rate ($P < 0.05$). Following washout of Ni^{2+} , cycle length returned to 863 ± 41 ms.

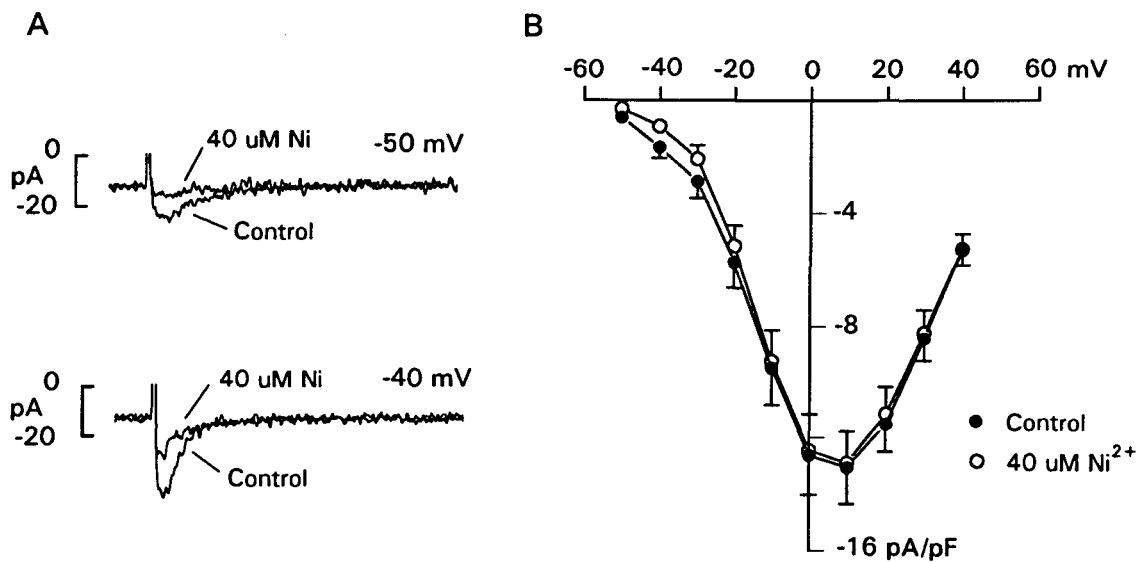


Figure 30. Effect of nickel (Ni^{2+}) on $I_{\text{Ca,T}}$. A: Effect of 40 $\mu\text{M Ni}^{2+}$ on $I_{\text{Ca,T}}$ elicited by depolarizing clamps to -50 mV (top) and -40 mV (bottom) from V_h of -80 mV. B: I-V relationships in control (●) and in the presence of 40 $\mu\text{M Ni}^{2+}$ (○).

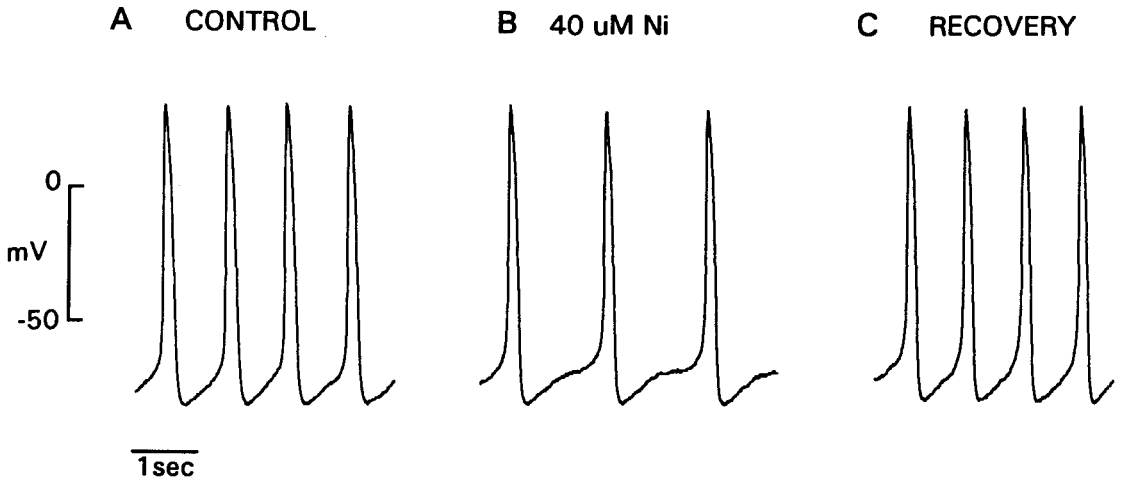


Figure 31. Effect of Ni^{2+} on spontaneous action potentials. A: control pacemaker action potentials. B: in the presence of $40 \mu\text{M}$ Ni. C: recovery following washout of Ni^{2+} .

4. Fast Na⁺ Current.

A TTX-sensitive fast Na⁺ current has been recorded in SA node pacemaker cells (48,160), as well as in tricuspid valve pacemaker cells. The following experiment was performed primarily to determine whether the fast Na⁺ current is present in atrial latent pacemaker cells. No attempt was made to quantitatively analyze the fast Na⁺ current. Figure 32 shows a recording of fast Na⁺ current in a latent pacemaker cell. In this experiment, Ca²⁺ currents were eliminated by 2 mM Co²⁺ (90) (see Figure 28). The cell was held at -100 mV and clamped to -40 mV. This depolarizing clamp elicited a very large inward current (about 12 nA) that activated rapidly with a peak at about 0.5 ms after start of the clamp. This current was blocked by 30 μM TTX and therefore is attributed to fast Na⁺ current. The TTX-sensitive Na⁺ current was observed in all latent pacemaker cells studied (n=10). Under the present experimental conditions (137 Na⁺ and 35°C) the Na⁺ current could not be clamped adequately.

5. Na-Ca Exchange Current.

Figure 33A shows selected current signals recorded from a pacemaker cell clamped from a holding potential (V_h) of -40 mV to more positive voltages using nystatin recording method. Depolarization to -30 mV elicited a very small inward current that slowly decayed with time. At -20 mV, two phases of inward current were evident; an initial, rapidly activating component followed by a slower secondary component. The secondary component developed slowly and decayed over about 100 ms. A clear separation of the two components is evident at -10 mV. Following the initial inward current, which peaked at about 5 ms, there was an initial rapid relaxation

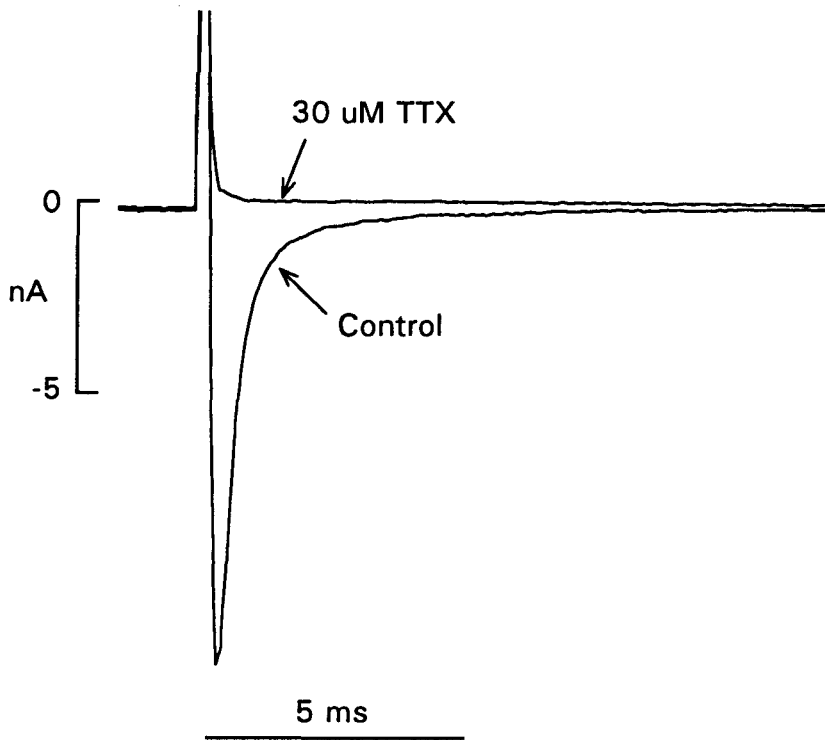


Figure 32. TTX-sensitive Na^+ current. TTX-sensitive Na^+ current was elicited by depolarizing clamp pulse to -40 mV from V_h of -100 mV. In $30 \mu\text{M}$ TTX the current was abolished. Extracellular solution contained 2 mM Co^{2+} to block Ca^{2+} currents.

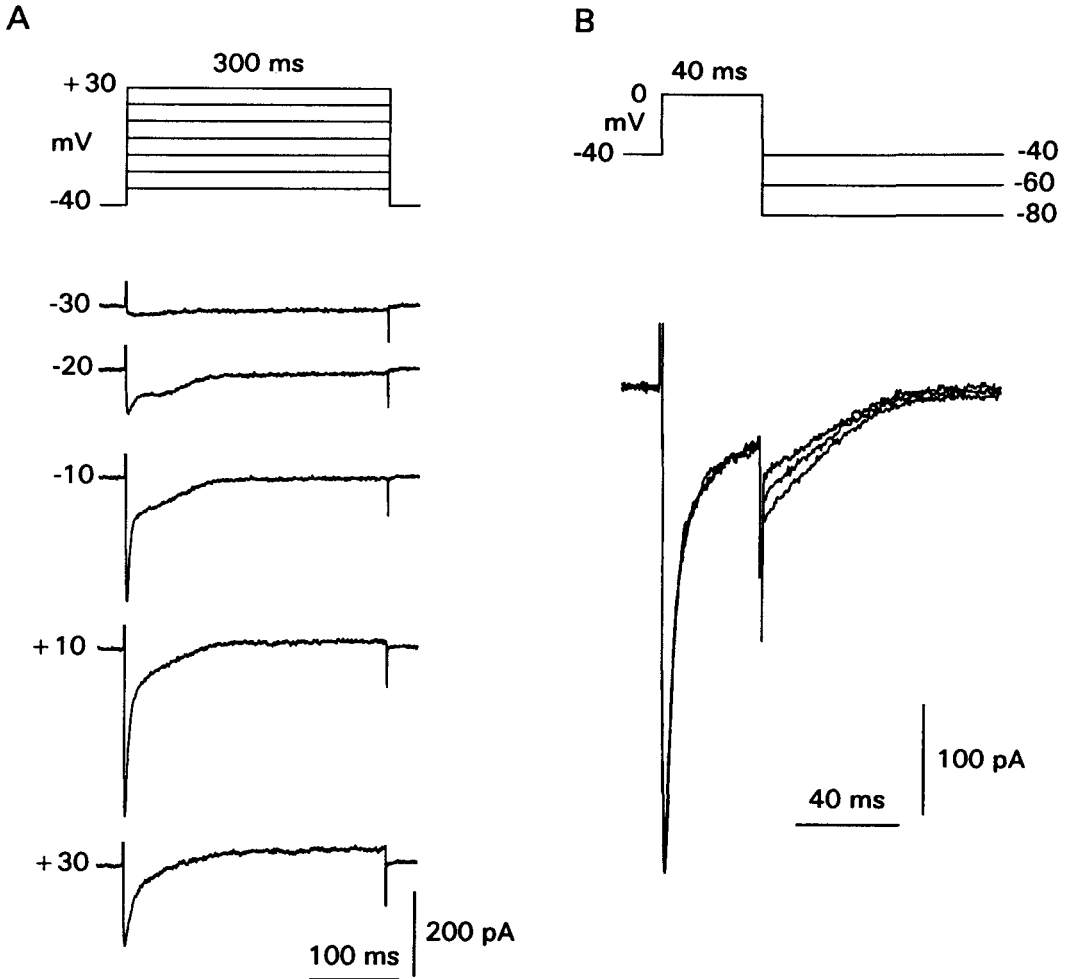


Figure 33. Slow inward currents recorded from a latent pacemaker cell. A: the voltage clamp protocol (top) and selected inward currents elicited by 300 ms depolarizing clamps from V_h of -40 to $+30$ mV in 10 mV steps (bottom). Depolarizations elicited $I_{Ca,L}$ that exhibited an initial rapid relaxation followed by a slower secondary inward current component. B: The same cell was clamped from V_h of -40 mV to 0 mV for 40 ms, and then repolarized to -40 , -60 , and -80 mV. Depolarization elicited $I_{Ca,L}$ that was followed upon repolarization by inward tail currents that slowly decayed with time. Peak inward tail current amplitude and the rate of current decay were increased at more negative voltages.

followed by a secondary component that decayed over about 100 ms. At more positive voltages the distinction between the two components became less apparent. The initial inward current can be attributed to activation of $I_{Ca,L}$. The secondary inward current is similar to that recorded in rabbit SA node (34), ferret ventricular trabeculae (3) and single guinea pig ventricular cells (78), and has been attributed to Na-Ca exchange. Experiments that will be presented below provide data to support these interpretations. Panel B shows that the secondary inward component appears as inward tail currents following short depolarizing clamp steps. Depolarizing steps to a fixed voltage elicited $I_{Ca,L}$ that were superimposed. Repolarization to different voltages elicited inward tail currents that slowly decayed with time. As the membrane was repolarized to more negative voltages, peak tail current amplitude increased and the rate of decay was accelerated. The absolute decay time of each tail current was essentially the same. With repolarization to -40 mV peak tail current amplitude was 61 ± 8.7 pA ($n=7$) and the time to decay back to baseline was 80-130 ms. In addition, the time course of the secondary inward currents elicited during depolarization (panel A) and the inward tail currents elicited upon repolarization (panel B) were similar. The time course of these inward currents is similar to the duration of the pacemaker action potential (189) (this study Figure 7). Similar tail currents have been recorded from atrial (69,82) and ventricular (78,82,155) cells and have been attributed to Na-Ca exchange.

Effect of EGTA on I_{NaCa} . To establish that these inward currents were, in fact, due to Na-Ca exchange we performed a variety of interventions that are known to alter Na-Ca exchange in other cardiac cells. If both the secondary inward currents and the

inward tail currents are due to Na-Ca exchange, then both currents should be dependent on intracellular Ca^{2+} . As shown in Figure 34, this point was tested by recording from two different pacemaker cells using two different recording methods. In panels A & B, the top current signals were recorded using a nystatin-perforated patch method where the membrane patch remained intact. The bottom traces in each panel were recorded from another pacemaker cell using a ruptured patch method where the cell interior was dialyzed with internal pipette solution containing 2 mM EGTA. In panel A (top), a 300 ms depolarizing clamp elicited $I_{\text{Ca,L}}$ with two components of decay: an initial rapid inactivation followed by a secondary slower component. The time to half decay for the rapid and slow components were 4.9 ± 0.4 and 41.2 ± 3.1 ms, respectively ($n=5$). Panel B (top) shows that following a 30 ms depolarizing clamp, repolarization to the holding potential elicited an inward tail current. These results are similar to those shown in Figure 33. Panels A & B (bottom) show that when a pacemaker cell was dialyzed with 2 mM EGTA, both the secondary inward component elicited during depolarization (panel A) and the inward tail current elicited upon repolarization (panel B) are abolished ($n=5$). It is evident that $I_{\text{Ca,L}}$ inactivation during depolarization is now smooth (panel A) and that repolarization elicits a very rapid deactivation of $I_{\text{Ca,L}}$ (panel B). These results support the hypothesis that both the secondary inward currents elicited during depolarization and the inward tail currents elicited upon repolarization are due to the same underlying mechanism and are dependent on intracellular Ca^{2+} . In the following experiments we used nystatin-perforated patch method to analyze I_{NaCa} .

Effect of ryanodine and low external Na^+ on I_{NaCa} . In mammalian cardiac

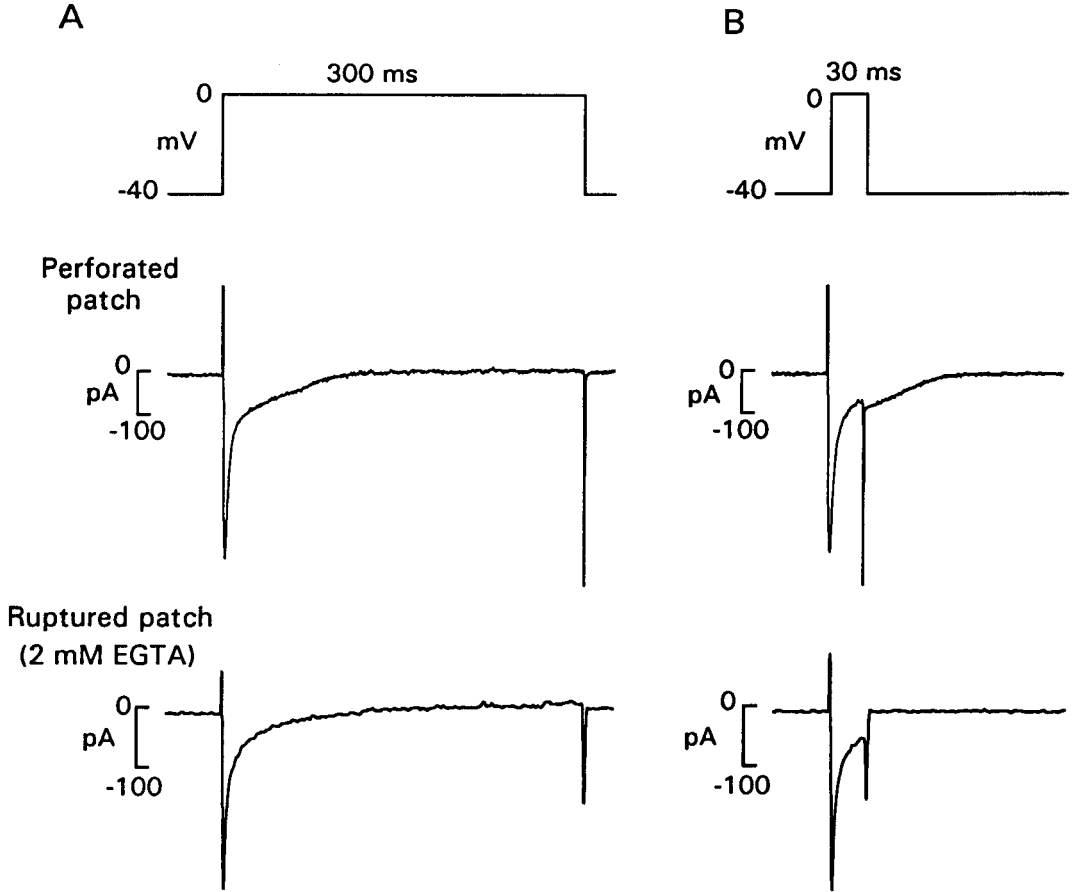


Figure 34. Slow inward currents recorded with two different whole-cell recording methods. A & B (top): pacemaker cells were clamped from V_h of -40 to 0 mV for 300 ms (A) and 30 ms (B), respectively. Middle panels: inward currents recorded with a nystatin-perforated patch recording method. Note the slowly decaying inward current that followed activation of $I_{Ca,L}$ (A) and the slowly decaying inward tail current elicited upon repolarization following short depolarizing clamps (B). Bottom panels: inward currents recorded a ruptured patch method where the cell was dialyzed with internal pipette solution containing 2 mM EGTA. Note that the secondary inward current (A) and the inward tail current (B) are abolished. Recordings with each method were obtained from different pacemaker cells.

cells, Na-Ca exchange currents have been shown to be mediated by SR Ca^{2+} release and carried by Na^+ influx (69,155). As shown in Figure 35A, under control conditions a short depolarizing clamp elicited $I_{\text{Ca,L}}$ that was followed upon repolarization to the holding potential by an inward tail current. When the same depolarizing clamp was delivered in the presence of 1 μM ryanodine, an agent that specifically interferes with SR Ca^{2+} release (182), the inward tail current was abolished ($n=6$). At the same time, peak $I_{\text{Ca,L}}$ amplitude was unchanged and the time course of $I_{\text{Ca,L}}$ inactivation was slowed slightly. The slower $I_{\text{Ca,L}}$ inactivation is consistent with a decrease in Ca^{2+} -mediated inactivation of $I_{\text{Ca,L}}$. That $I_{\text{Ca,L}}$ inactivation in the presence of ryanodine crossed-over the control $I_{\text{Ca,L}}$ signal indicates that the ryanodine-sensitive Na-Ca exchange current was already contributing to the late phase of $I_{\text{Ca,L}}$ inactivation. In addition, ryanodine abolished contractile activity. These records also show that $I_{\text{Ca,L}}$ deactivation is very rapid and therefore does not contribute to tail currents elicited on repolarization. In panel B, a similar experimental protocol was used to determine whether external Na^+ is a possible charge carrier for the inward tail current. Two possible mechanisms may be responsible for a Ca^{2+} -mediated Na^+ influx; activation of non-specific cation channels (43,73) or stimulation of Na-Ca exchange (126). To help distinguish between these two possibilities, external Na^+ was replaced with lithium because lithium can carry charge via Ca^{2+} -activated non-specific cation channels (73) but is unavailable for Na-Ca exchange (126). Reducing external Na^+ from 137 to 20 mM significantly decreased tail current amplitude, without affecting peak $I_{\text{Ca,L}}$ amplitude ($n=4$). In addition, $I_{\text{Ca,L}}$ inactivation was enhanced, probably as a result of an increase in intracellular Ca^{2+}

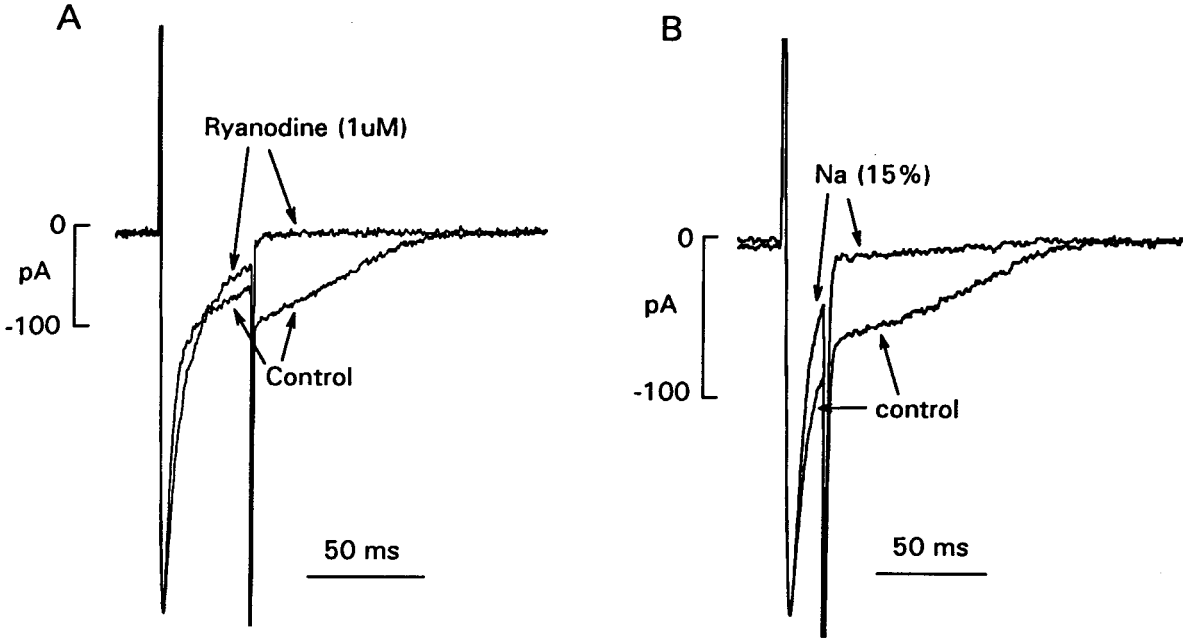


Figure 35. Effect of ryanodine and low external Na^+ on I_{NaCa} . A: Currents were elicited by depolarizing clamps from V_h of -40 to 0 mV for 40 ms. Under control conditions, depolarization elicited $I_{\text{Ca,L}}$ that was followed upon repolarization by a prominent inward tail current. The same cell was exposed to $1 \mu\text{M}$ ryanodine for approximately 10 min. Ryanodine abolished the inward tail current without affecting peak $I_{\text{Ca,L}}$ activation. B: Currents were elicited by depolarizing clamps from V_h of -40 to 0 mV for 20 ms. Extracellular Na^+ was decreased from 137 to 20 mM and replaced with equimolar concentrations of LiCl. Reducing external Na^+ significantly decreased the inward tail current without affecting peak $I_{\text{Ca,L}}$ activation. Recordings in panel A & B were obtained from two different pacemaker cells.

induced by low external Na^+ . Because the intracellular Ca^{2+} was not buffered via dialysis with the internal pipette solution, these records were obtained during relatively brief exposures to low external Na^+ . Longer exposures resulted in sustained contracture and cell death, probably due to rising levels of intracellular Ca^{2+} . These results, as well as those described below, indicate that the inward tail currents are separate from $I_{\text{Ca,L}}$, and carried by a Na^+ influx mediated by SR Ca^{2+} release. These properties are consistent with those of Na-Ca exchange currents (I_{NaCa}) described in both ventricular (78,82,155) and atrial cells (69,82) in a variety of species and experimental conditions.

Effect of clamp duration on I_{NaCa} . In Figure 36, we investigated the dependence of I_{NaCa} on the duration of the preceding depolarization. As shown in the top row, following a 2 ms depolarizing clamp there was little, if any, tail current. Prolonging the depolarization to 10 ms clearly elicited $I_{\text{Ca,L}}$ that peaked at about 5 ms. Repolarization interrupted $I_{\text{Ca,L}}$ inactivation and elicited a prominent I_{NaCa} tail that developed slowly. I_{NaCa} tail current peaked at about 30 ms (measured from repolarization) and then decayed to zero within about 100 ms. As the clamp duration was prolonged, repolarization occurred at later times during the time course of I_{NaCa} development and decay. With a 40 ms clamp, repolarization occurred at approximately the peak of I_{NaCa} development, and therefore I_{NaCa} decayed without an initial delay in onset. As clamp duration was increased to 80 and 120 ms, peak I_{NaCa} tail amplitude progressively decreased. Note, however, that the time course of each tail current was superimposable, except for the initial portion of the tail currents elicited following very short clamps. With longer clamp durations, I_{NaCa} appeared *during* depolarization as a

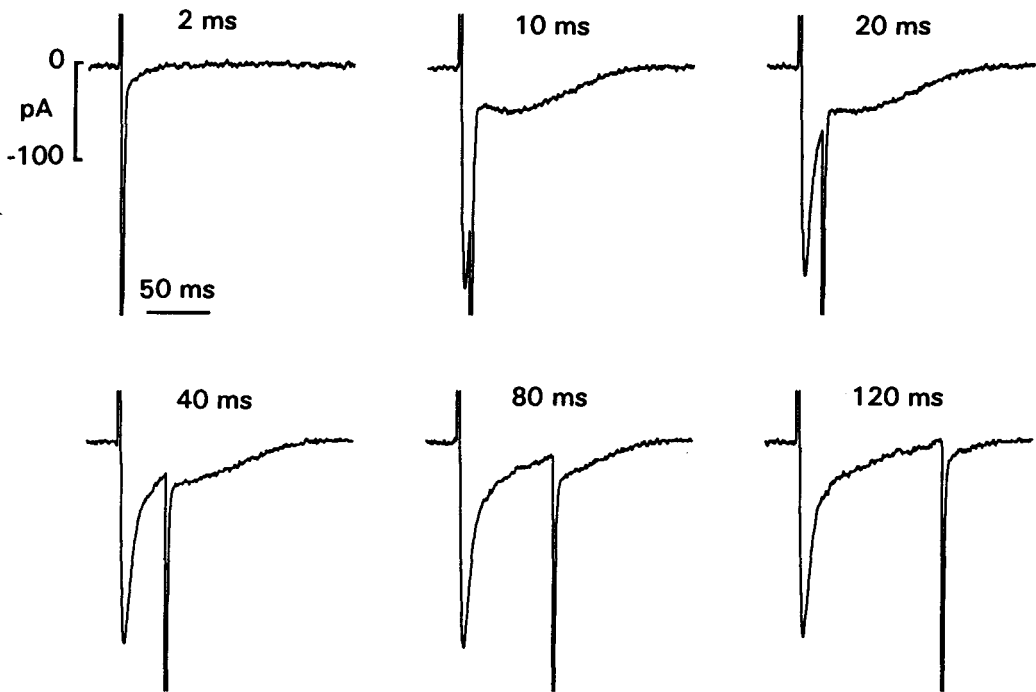


Figure 36. Effect of depolarizing clamp duration on I_{NaCa} . A pacemaker cell was clamped from V_h of -40 to 0 mV for different durations between 2 and 120 ms, as indicated in each panel. I_{NaCa} tail currents were elicited upon repolarization to -40 mV. Clamp duration had little effect on the time course of I_{NaCa} decay for clamps steps ≥ 10 ms.

secondary, slowly decaying inward current, similar to that shown in Figure 33A. In addition, the time course of I_{NaCa} elicited during depolarization and I_{NaCa} tails elicited upon repolarization were similar (see 80 ms clamp). A total of 4 cells showed similar results. These findings indicate that the mechanisms responsible for triggering I_{NaCa} are fully activated by clamps as short as 10 ms, or long enough to activate peak $I_{\text{Ca,L}}$. In addition, once peak $I_{\text{Ca,L}}$ is attained, repolarization has little effect on the time course or absolute decay time of I_{NaCa} . These results are similar to those reported for ventricular myocytes from guinea pig (78) and rat (66). In rabbit ventricular myocytes, longer clamp durations accelerated the time course of I_{NaCa} decay, but clamp duration had little effect on tail currents recorded from rabbit atrial myocytes (82).

Voltage dependent activation of $I_{\text{Ca,L}}$ and I_{NaCa} . Because activation of $I_{\text{Ca,L}}$ is essential for SR Ca^{2+} release and subsequent stimulation of I_{NaCa} , we investigated the voltage-dependence of $I_{\text{Ca,L}}$ and I_{NaCa} . Figure 37A (top) shows the voltage clamp protocol used. $I_{\text{Ca,L}}$ was elicited by short clamps to progressively more positive voltages and I_{NaCa} was elicited upon repolarization to the holding potential. Panel A (bottom) shows original current records, and panel B shows the I-V relationship of peak $I_{\text{Ca,L}}$ and I_{NaCa} obtained in 7 cells. As expected, $I_{\text{Ca,L}}$ amplitude increased at voltages more positive than -40 mV, reached a maximum at 0 mV and then declined almost linearly at more positive voltages. In contrast, I_{NaCa} amplitude increased following clamps up to -10 mV and then remained relatively constant until 20 mV. At more positive voltages (30 & 40 mV) I_{NaCa} declined slightly. $I_{\text{Ca,L}}$ exhibited a bell-shaped voltage dependence compared with a relatively flat voltage relation for I_{NaCa} . These findings indicate that

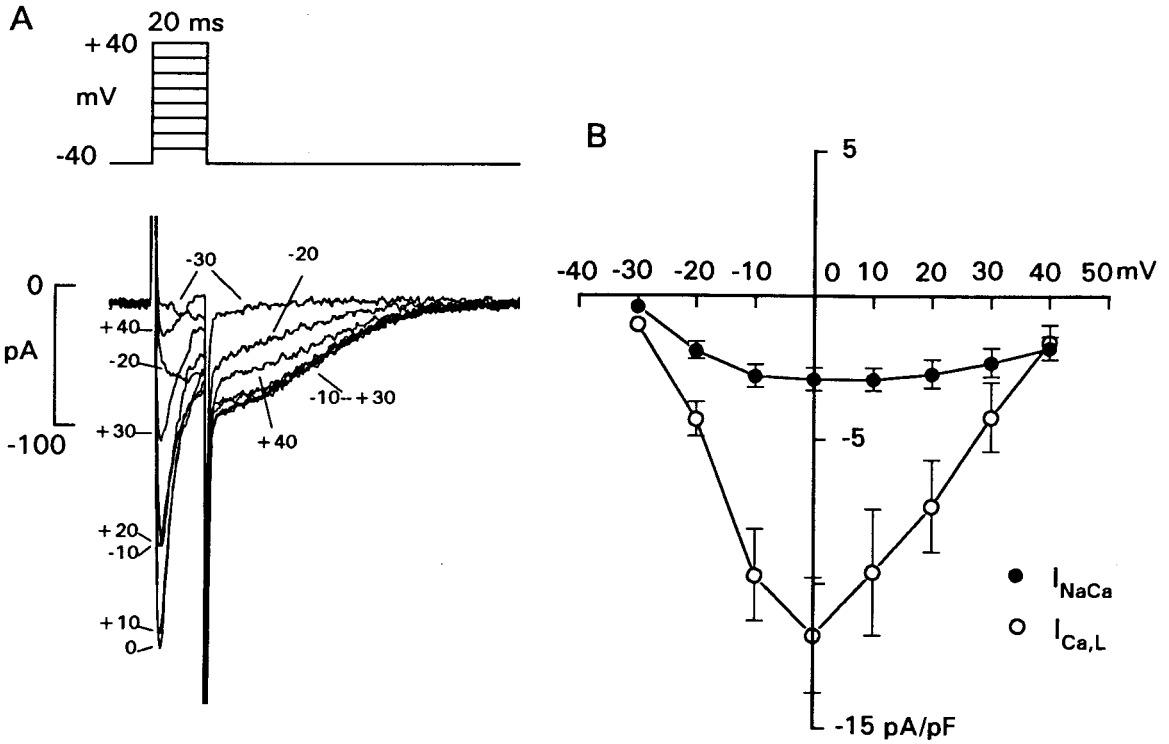


Figure 37. Voltage-dependence of $I_{Ca,L}$ and I_{NaCa} . A: voltage clamp protocol and original current recordings showing $I_{Ca,L}$ and I_{NaCa} . Cells were clamped from V_h of -40 to 40 mV for 20 ms durations in 10 mV increments. B: I-V relationships for $I_{Ca,L}$ (○) and I_{NaCa} (●) obtained from 7 cells. Currents are normalized against cell capacitance and expressed as current density (pA/pF). Maximum I_{NaCa} and $I_{Ca,L}$ were 2.9 ± 0.4 pA/pF and 11.8 ± 2.0 pA/pF, respectively.

I_{NaCa} is not proportional on a beat-to-beat basis to $I_{\text{Ca,L}}$, and suggest that only a fraction of $I_{\text{Ca,L}}$ may be required to activate I_{NaCa} . This interpretation is similar to that reported in rabbit atrial cells (69) and guinea pig ventricular cells (72), and consistent with similar relationships between the voltage dependence of $I_{\text{Ca,L}}$ and intracellular Ca^{2+} transients (39,67). Others, however, have shown a closer correlation between $I_{\text{Ca,L}}$ and intracellular Ca^{2+} (18,37).

Time course of $I_{\text{Ca,L}}$ and I_{NaCa} recovery. Another way of distinguishing between $I_{\text{Ca,L}}$ and I_{NaCa} is to determine their time course of recovery. This was tested by delivering two identical voltage clamp pulses separated by a variable time interval. The graph in Figure 38 shows that the recovery of I_{NaCa} is significantly slower than the recovery of $I_{\text{Ca,L}}$ ($n=3$). At the shortest interpulse interval tested of 200 ms, $I_{\text{Ca,L}}$ was 73% of its fully recovered value at a time when the recovery of I_{NaCa} was only 38% complete. Peak $I_{\text{Ca,L}}$ recovered to unity by 2 sec while I_{NaCa} required 5 sec to fully recover. In addition, the ratio of $I_{\text{Ca,L}}$ amplitude was slightly greater than unity at about 5 sec indicating that $I_{\text{Ca,L}}$ amplitude was enhanced above rested control levels. The overshoot in $I_{\text{Ca,L}}$ recovery has been reported by others (78,209), and is thought to reflect a facilitatory effect of intracellular Ca^{2+} (209).

Effect of cadmium on $I_{\text{Ca,L}}$ and I_{NaCa} . The relationship between $I_{\text{Ca,L}}$ and I_{NaCa} was studied further by using low concentrations of cadmium (Cd^{2+}), a divalent cation that exerts a relatively specific block of $I_{\text{Ca,L}}$ (135). The graph shown in Figure 39 plots peak $I_{\text{Ca,L}}$ and I_{NaCa} against time, before (point a) and during (points b-d) exposure to 50 μM Cd^{2+} . The current recordings at the bottom of the Figure (panels

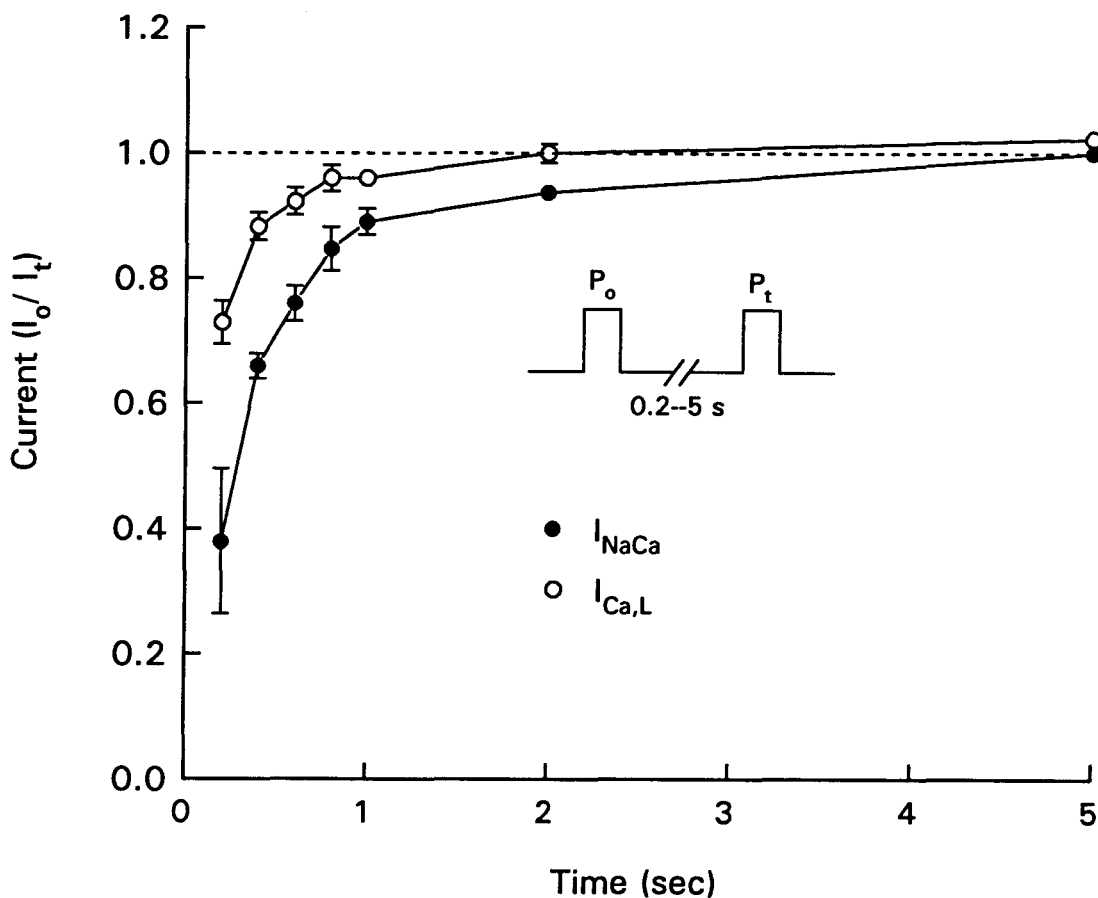


Figure 38: Recovery characteristics of I_{NaCa} and $I_{Ca,L}$. Cells were stimulated with two identical voltage clamp pulses delivered from V_h of -40 to 0 mV for 20 ms, every 30 sec. The initial conditioning pulse (P_o) and the test pulse (P_t) were separated by a variable time interval ranging from 200 ms to 5 sec. The shortest time interval of 200 ms was long enough to allow full decay of I_{NaCa} and $I_{Ca,L}$ after (P_o) and before the (P_t). The peak current response to P_t was normalized against the peak response to P_o , and the current ratio was plotted against the interpulse time interval.

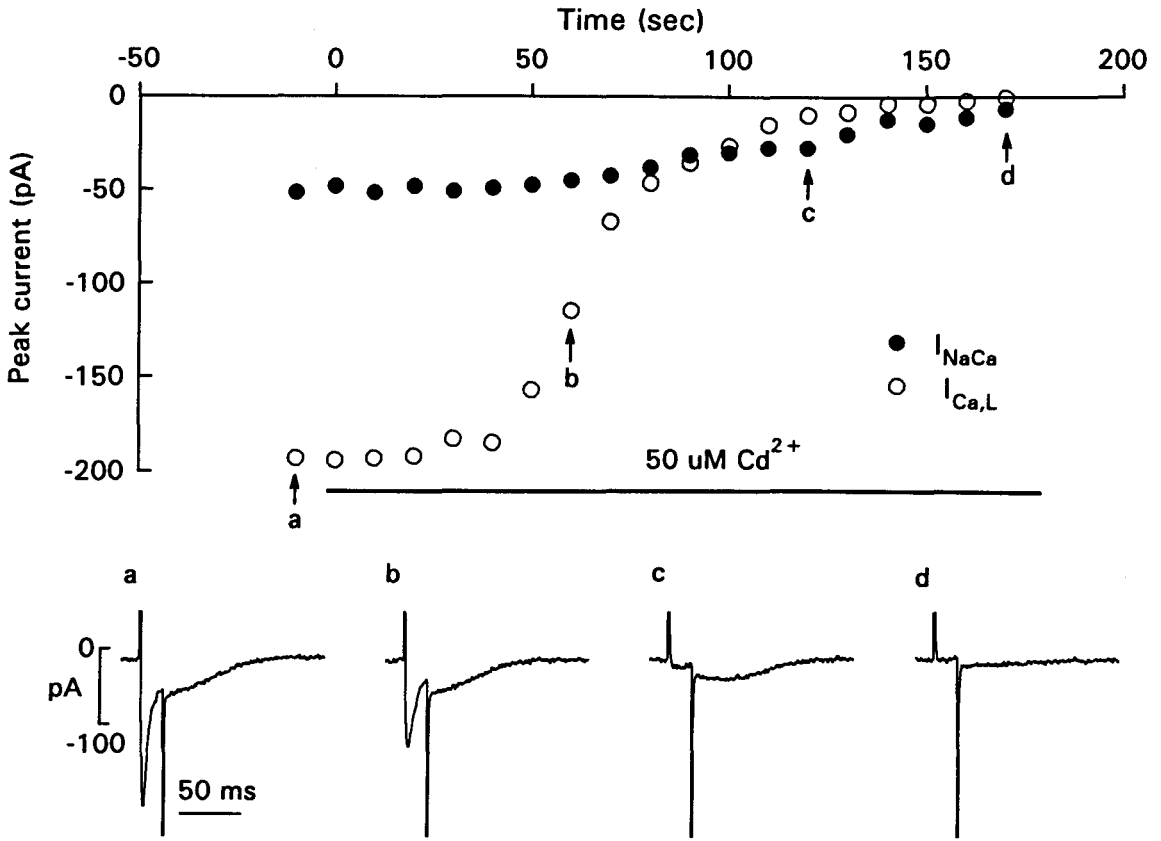


Figure 39: Effects of cadmium (Cd^{2+}) on I_{NaCa} and $I_{\text{Ca,L}}$. Peak I_{NaCa} and $I_{\text{Ca,L}}$ are plotted against time before (a) and during (b-d) exposure to 50 μM Cd^{2+} . At the bottom of the figure are selected current traces recorded at corresponding times before (a) and during exposure to Cd^{2+} (b-d). $I_{\text{Ca,L}}$ was elicited by depolarizing clamps from V_h of -40 to 0 mV for 20 ms, and I_{NaCa} was elicited upon repolarization to -40 mV. The inhibition of $I_{\text{Ca,L}}$ induced by Cd^{2+} does not correlate in time with changes in I_{NaCa} .

a-d) were obtained at various times during the experiment and correspond to points a-d in the graph. Under control conditions (panel a) a depolarizing pulse elicited typical $I_{Ca,L}$ followed by I_{NaCa} . At 1 min of exposure to Cd^{2+} , peak $I_{Ca,L}$ was reduced by about 40%, while I_{NaCa} was not significantly changed in amplitude or time course. By 2 min of exposure to Cd^{2+} , peak $I_{Ca,L}$ was decreased by more than 95% while I_{NaCa} was reduced by about 50% and still plainly discernable. Both $I_{Ca,L}$ and I_{NaCa} were abolished after nearly 3 min of exposure to Cd^{2+} (panel d). Similar results were obtained in a total of 4 cells. These experiments clearly demonstrate that the amplitude and time course of I_{NaCa} are not proportional to $I_{Ca,L}$ amplitude on a beat-to-beat basis. However, over a steady-state period of time Ca^{2+} influx through $I_{Ca,L}$ is essential to maintain I_{NaCa} . In addition, the fact that I_{NaCa} can be elicited at a time when more than 95% of $I_{Ca,L}$ is inhibited suggests that only a very small amount of Ca^{2+} influx may be needed to trigger SR Ca^{2+} release, or that a mechanism other than $I_{Ca,L}$ may be operating. Similar findings have been reported in rabbit atrial cells when diltiazem was used to block $I_{Ca,L}$ (69).

Effect of isoproterenol on $I_{Ca,L}$ and I_{NaCa} . Beta-adrenergic stimulation increases $I_{Ca,L}$, SR Ca^{2+} uptake and intracellular Ca^{2+} transients (37) and thereby should enhance I_{NaCa} . Figure 40 shows the steady-state effects of 3 different concentrations of isoproterenol (ISO) on $I_{Ca,L}$ and I_{NaCa} in 3 different pacemaker cells. In panel A, exposure to a relatively low concentration of $10^{-8}M$ ISO increased peak $I_{Ca,L}$ amplitude by about 44% ($n=2$). However, there was no discernable effect on I_{NaCa} amplitude or time course. In panel B, $5 \times 10^{-8}M$ ISO elicited a significantly larger

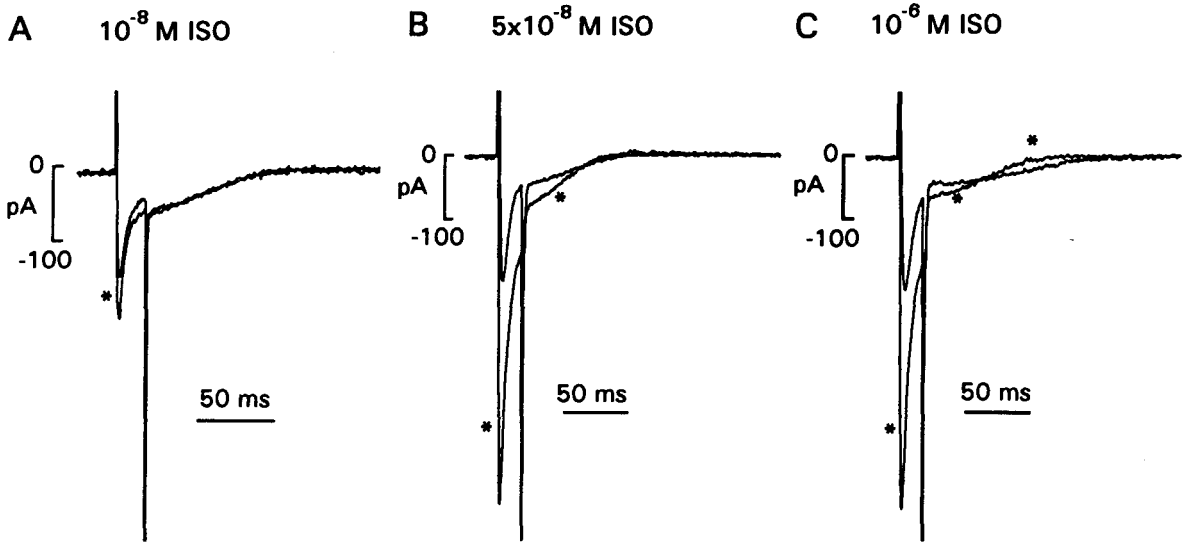


Figure 40: Effects of 3 different concentrations of ISO on I_{NaCa} and $I_{Ca,L}$. Currents were elicited by depolarizing clamps from V_h of -40 to 0 mV for 20 ms, and then repolarization to -40 mV. Results with each ISO concentration were obtained from 3 different pacemaker cells. In each panel, currents recorded in control and in the presence of ISO (*) are superimposed.

increase in $I_{Ca,L}$ amplitude (≈ 3 fold) that was accompanied by an increase in peak I_{NaCa} amplitude and an acceleration in the rate of I_{NaCa} decay ($n=4$). In addition, the absolute decay time of I_{NaCa} was slightly shorter than control. This is more evident in panel C, where $10^{-6}M$ ISO elicited a similarly large increase in peak $I_{Ca,L}$ amplitude, along with an increase in peak I_{NaCa} amplitude (from -51 ± 10 pA to -81 ± 18 pA, $n=4$), an acceleration in the rate of I_{NaCa} decay and a markedly shorter absolute decay time (from 89 ± 13 ms to 66 ± 10 ms, $n=4$). The increase in I_{NaCa} amplitude and rate of decay are consistent with the effects of catecholamines to increase the amplitude of the intracellular Ca^{2+} transient, and SR Ca^{2+} uptake, respectively (37). In addition, these findings clearly illustrate that I_{NaCa} is modulated by β -adrenergic receptor stimulation, and therefore may be, as shown below, important in the regulation of latent pacemaker function.

Time and voltage dependence of I_{NaCa} recovery. In the following experiments we sought to determine the possible contribution of I_{NaCa} to the pacemaker potential. Experiments presented earlier (Figure 38) showed that I_{NaCa} recovered over a time course that was relatively long (≈ 5 sec) in relation to the normal pacemaker cycle length. In those experiments, however, the cell was rested for steady-state times (30 sec) between paired pulse stimulations and the holding potential was -40 mV. This raised the question of whether the time course of I_{NaCa} recovery was more rapid under spontaneous conditions, and therefore compatible with the pacemaker cycle length. In addition, Na-Ca exchange is a voltage-dependent process, where the exchange mechanism is stimulated at more negative voltages (7,19). It was, therefore, important to know whether the level

of the diastolic membrane voltage influences the time course of I_{NaCa} recovery during the pacemaker cycle. As shown in Figure 41A (top), free-running pacemaker action potentials were clamped during diastole at either -40 or -70 mV (maximum diastolic potential) for variable periods of time. Panel A shows selected current signals where $I_{\text{Ca,L}}$ and I_{NaCa} were elicited from either -40 or -70 mV at 0.2, 1 and 20 sec after the last spontaneous action potential. In panel B, the graph shows that I_{NaCa} elicited at times from 0.2 to 2 sec progressively increased in amplitude whether the membrane was held at -40 or -70 mV. However, at any given time I_{NaCa} amplitude was larger when elicited from -70 than from -40 mV. The original current records also show that peak $I_{\text{Ca,L}}$ at 0.2 sec was larger when elicited from -70 than from -40 mV. It therefore seems likely that under the present experimental conditions, the voltage-dependent recovery of $I_{\text{Ca,L}}$ (37,170) may be one important factor determining the rate of recovery of I_{NaCa} at early times (≤ 2 sec). Note also, however, that at -70 mV I_{NaCa} amplitude increased significantly between 0.2 and 1 sec, even though $I_{\text{Ca,L}}$ amplitude was almost fully recovered at 0.2 sec. These findings indicate that other processes that are primarily time-dependent may also be operating (see Discussion). At 1 sec, I_{NaCa} amplitude was about 98% of maximum and peak $I_{\text{Ca,L}}$ amplitude was completely recovered whether elicited from -70 or -40 mV. At times > 2 sec I_{NaCa} amplitude depended strongly on membrane voltage. When elicited from -40 mV I_{NaCa} decreased slightly over time. At 20 sec I_{NaCa} was reduced by about 10% of maximum. In contrast, when the membrane was held at -70 mV I_{NaCa} decreased by about 60% of maximum over the same 20 sec. It is unlikely that this decrease in I_{NaCa} can be attributed to time- or voltage-dependent

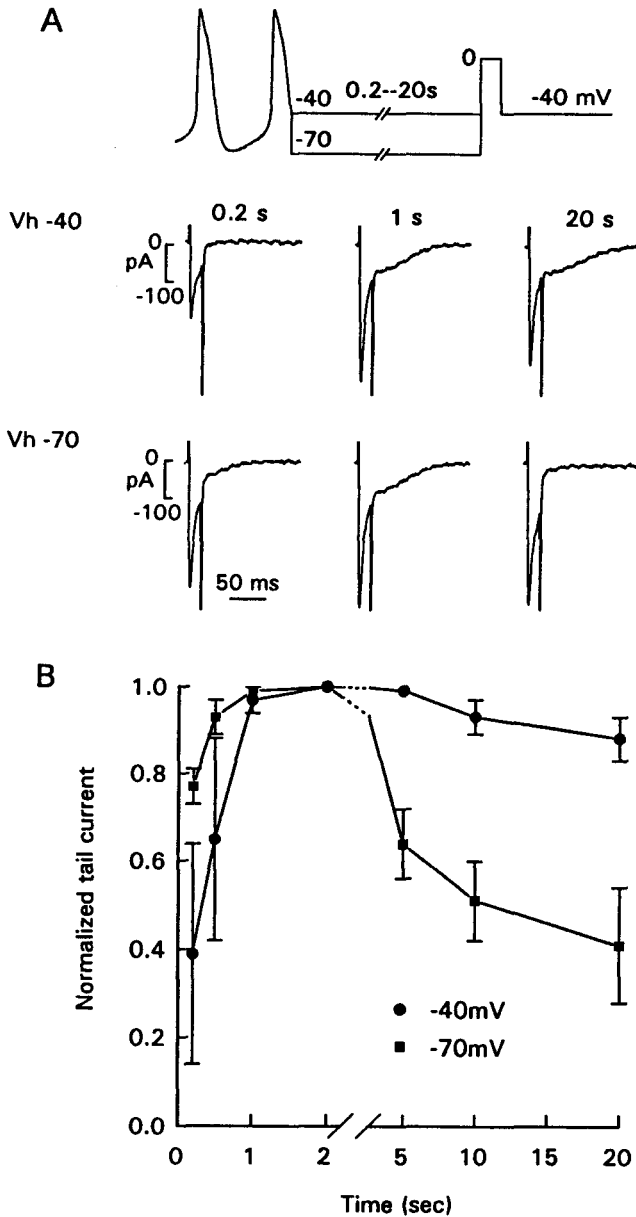


Figure 41: Dependence of I_{NaCa} recovery on diastolic time and voltage. A: voltage clamp protocol and selected current recordings. After at least 5 spontaneous action potentials a pacemaker cell was held at either -40 or -70 mV for various times during diastole between 0.2 and 20 sec. I_{NaCa} tails were elicited following 20 ms depolarizing clamps from V_h of -40 to 0 mV and returned to -40 mV. B: peak I_{NaCa} obtained from -40 mV ($n=2$) and -70 mV ($n=5$) are plotted against the diastolic time at each potential. Current amplitudes are normalized against the maximum current amplitude. External solution contained $20 \mu\text{M}$ TTX.

changes in $I_{Ca,L}$. Thus, the records in panel A show that at -70 mV peak $I_{Ca,L}$ amplitude at 1 and 20 sec were the same, yet I_{NaCa} amplitude was significantly reduced at 20 sec compared to 1 sec. In addition, at 20 sec peak $I_{Ca,L}$ amplitude was slightly larger when elicited from -70 mV than from -40 mV, yet I_{NaCa} amplitude was just the opposite. Similar results were obtained when spontaneous action potentials were simulated with 5 conditioning pulses that had parameters similar to action potentials ($n=5$; data not shown). The finding that I_{NaCa} recovery required 2 s in these experiments, compared with 5 sec in the paired pulse experiments (Figure 38) is probably related to the different experimental conditions. The paired pulse protocol examined the rested recovery characteristics of I_{NaCa} whereas the present experiments examined the mechanisms operating during repetitive pacemaker activity.

To summarize, these experiments indicate that under spontaneous conditions I_{NaCa} recovers over a period of approximately 1 sec. In addition, the recovery of I_{NaCa} is more rapid when elicited from more negative voltages. At times >2 sec, I_{NaCa} amplitude exhibits a voltage-dependent decay over time that is consistent with a voltage-dependent decrease in intracellular Ca^{2+} mediated by Na-Ca exchange (105).

Effect of ryanodine on pacemaker action potentials. To assess the relative contribution of I_{NaCa} to pacemaker function, free-running pacemaker action potentials were interrupted during the late phase of diastolic depolarization by clamping the membrane potential at -50 mV. As shown in Figure 42A, control pacemaker action potentials exhibited a spontaneous cycle length of 760 ms. In panel A (bottom), clamping at -50 mV resulted in a small (about 9 pA) transient inward current that

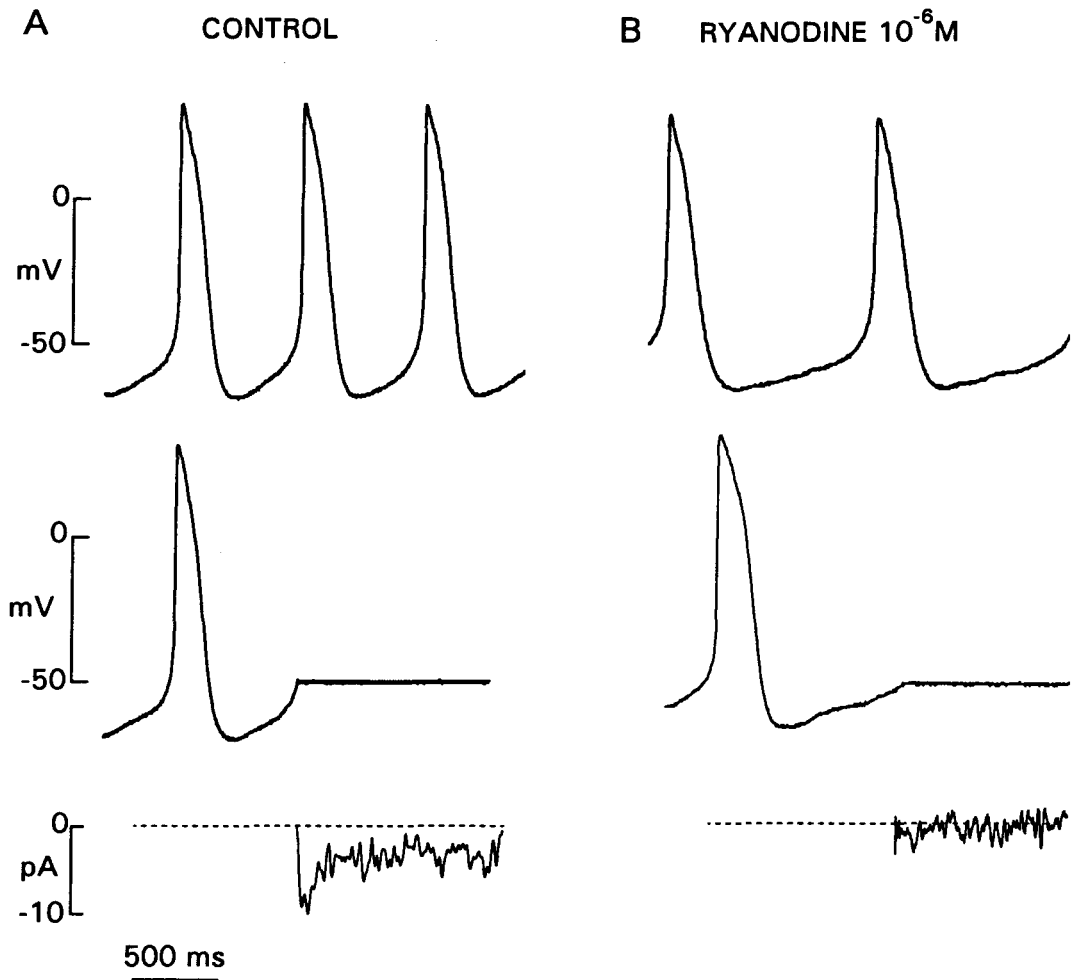


Figure 42: Effect of ryanodine on spontaneous pacemaker action potentials and currents recorded at -50 mV. A: control pacemaker action potentials (top) and current recorded at -50 mV (bottom). B: Exposure to $1 \mu\text{M}$ ryanodine.

decayed to a background net inward current level (about 2-3 pA). In panel B (top) the same pacemaker cell was clamped in the presence of 1 μ M ryanodine. Ryanodine caused a small positive shift in maximum diastolic potential, significantly decreased the slope of diastolic depolarization and increased cycle length to 1220 ms. Note that ryanodine primarily inhibited the late phase of diastolic depolarization. In the 4 cells tested, ryanodine decreased diastolic slope and increased pacemaker cycle length from 819 ± 43 to 1313 ± 217 ms (+60%; $p < 0.05$). That ryanodine significantly slowed but did not stop pacemaker activity indicates that a ryanodine-sensitive component contributes but is not essential to pacemaker activity. These findings are similar to those obtained in multicellular atrial pacemaker preparations (189). As shown in panel B (bottom), ryanodine also abolished the transient inward current and background inward current recorded at -50 mV.

Effect of isoproterenol on pacemaker action potentials. If I_{NaCa} contributes to pacemaker function, then ISO should enhance both I_{NaCa} and the slope of diastolic depolarization, and both responses should be abolished by ryanodine. Figure 43A shows a control recording where a pacemaker action potential (top) is clamped during the late diastolic slope at -50 mV, resulting in a small transient inward current (bottom). In panel B, exposure to 5×10^{-8} M ISO elicited a significant increase in the slope of diastolic depolarization (top) and a decrease in spontaneous cycle length from 792 ± 73 to 519 ± 41 ms, which is a $52 \pm 6.4\%$ increase in spontaneous rate ($n=5$). This was associated with a 3 fold increase in the transient peak inward current elicited at -50 mV (bottom). This inward current peaked at about 40 ms and required about 125 ms to

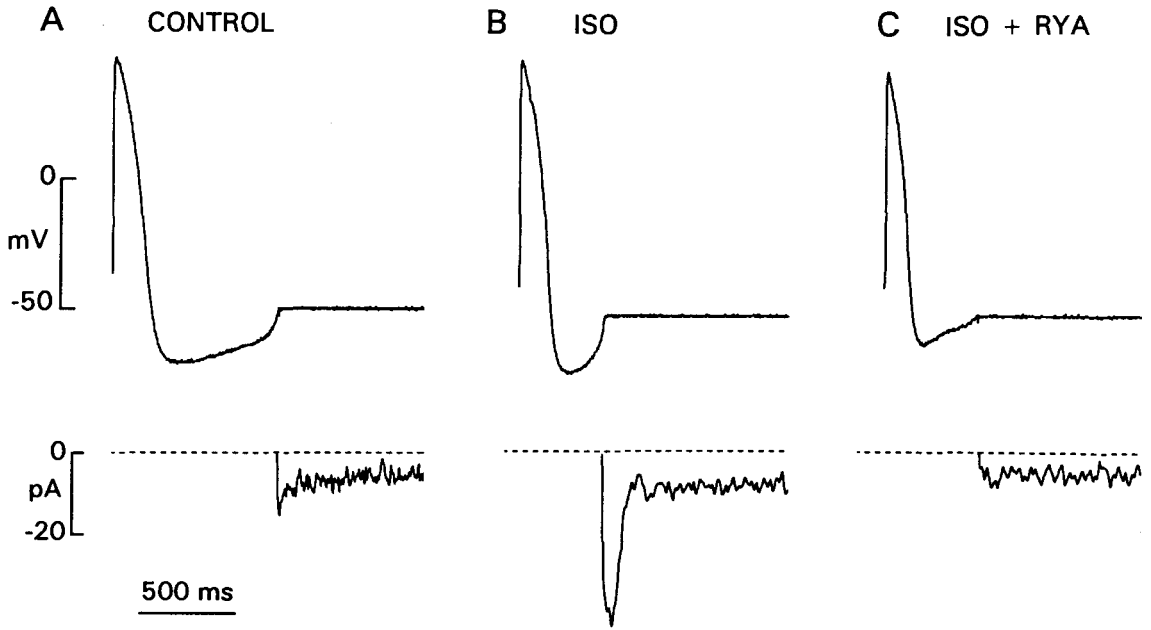


Figure 43: Effect of isoproterenol (ISO) on spontaneous pacemaker action potentials and currents recorded at -50 mV. A: Control action potentials and currents. B: Effect of 5×10^{-8} M ISO. C: Effect of 5×10^{-8} M ISO plus $1 \mu\text{M}$ ryanodine.

decay. In addition, ISO elicited an increase in the background inward current recorded at -50 mV. In panel C, addition of $1 \mu\text{M}$ ryanodine to the ISO-containing perfusate shifted the maximum diastolic potential more positive, significantly decreased the slope of diastolic depolarization (top) and abolished the transient inward current elicited at -50 mV (bottom). Similar results were observed in a total of 3 cells. Although ryanodine also decreased the background inward current at -50 mV to control levels, there remained a ryanodine-insensitive background inward current component. This ryanodine-insensitive current may result from a Na^+ -dependent Cl^- current induced by isoproterenol, that is not dependent on Na-Ca exchange (4,95,96). These results and those of the previous experiment suggest that I_{NaCa} contributes significantly to the diastolic slope of latent pacemaker cells and is an important component mediating β -adrenergic regulation of latent pacemaker automaticity.

CHAPTER V

DISCUSSION

As reviewed earlier, previous experiments on multicellular preparations have provided insights into the electrophysiological properties of atrial latent pacemakers. However, because of the limitations inherent to multicellular preparations it is not possible to perform a quantitative analysis of the ionic currents potentially responsible for latent pacemaker activity. In the present work, we sought to use single cell isolation and patch clamp techniques to determine the electrophysiological mechanisms underlying latent pacemaker function.

A. Isolation of Single Latent Atrial Pacemaker Cells.

In the present experiments, we have isolated latent pacemaker cells from the Eustachian ridge of cat right atrium. Cells isolated from the Eustachian ridge were both pacemaker and quiescent atrial cells. Latent pacemaker cells were easily distinguished and selected for study based primarily on their spontaneous activity and morphological appearance. Pacemaker cells always exhibited rhythmic beating associated with distinct contractile responses. In addition, pacemaker cells were elongated with tapered ends, had diameters of less than 10 μm , and appeared somewhat bent or crinkled, without obvious striations. These morphological characteristics are similar to those reported for

SA node pacemaker cells (12,47,48). Latent pacemaker cells did not become rounded when exposed to normal Ca^{2+} concentrations, as described in some studies of SA node (89,159) and in a study of pacemaker cells isolated from tricuspid valve (1). In addition, they were not morphologically similar to latent pacemaker cells isolated from rabbit crista terminalis (85). Eustachian ridge pacemaker cells displayed passive membrane properties that are similar to those reported for SA node cells (48,213). These results, therefore, suggest that latent pacemaker cells in the Eustachian ridge are morphologically and electrophysiologically similar to SA node pacemaker cells. This idea gains further support from studies of multicellular preparations which have shown that the Eustachian ridge contains P cell types (188,199) that are not morphologically different from SA node P cells (188). In addition, both Eustachian ridge (188) and SA node (188,206) P cells have been correlated with pacemaker activity. Latent pacemaker cells also exhibited action potentials that are similar to those recorded from multicellular Eustachian ridge pacemaker preparations (188,189). Collectively, these findings suggest that the latent pacemaker cells studied here may be similar to those in SA node.

B. Input Resistance and I_{K1} Current.

Latent atrial pacemaker cells exhibited very high input resistances. Similar high input resistance has been reported in other cardiac pacemaker cells (84,85,159,213,226). Voltage clamp experiments show that in response to hyperpolarization, latent atrial pacemaker cells exhibited very little, if any, instantaneous or background current. This suggests that latent atrial pacemaker cells lack the inward rectifier potassium current, I_{K1} . The lack of I_{K1} was confirmed by the fact that barium had no effect on the initial inward

current elicited by hyperpolarization. The lack of I_{K1} is a common feature of both SA node (172) as well as other latent atrial pacemakers (85,226). Wu *et al.* (226) showed that in myocytes isolated from the cat right atrium, 93% of the quiescent atrial cells studied exhibited prominent I_{K1} current, whereas 94% of atrial cells that exhibited spontaneous pacemaker activity lacked I_{K1} current. Apparently, the lack of background K^+ conductance is a requirement for atrial pacemaker function. This feature would contribute to the relatively low maximum diastolic potential and high input resistance of these cells. In addition, a high input resistance would also mean that very small current flowing across the cell membrane will elicit a relatively large change in membrane voltage.

C. I_f Current

The present findings show that the vast majority of latent pacemaker cells in the Eustachian ridge contained I_f . Only about 6% of the cells that exhibited pacemaker activity failed to exhibit significant I_f . In this regard, Wu *et al.* (226) have shown that the cat right atrium may contain two types of latent atrial pacemakers; those exhibiting I_f and those lacking I_f . Giles & van Ginneken (85) have also shown that I_f is not present in latent pacemaker cells isolated from rabbit crista terminalis. The fact that such a high percentage of pacemaker cells in the Eustachian ridge exhibit I_f emphasizes the functional importance of this region.

I_f recorded from latent atrial pacemaker cells exhibits many of the properties reported for I_f in SA node (59,89,213), Purkinje (36,51,52) and sinus venosus pacemakers (25). Thus, I_f : 1) activated at voltages more negative than -50 mV, 2) was

blocked by 2 mM Cs⁺, 3) exhibited a fully-activated I-V relationship that was approximately linear at voltages more negative than -30 mV and showed outward rectification at more positive voltages, 4) exhibited a reversal potential of -26 mV, 5) was carried by both Na⁺ and K⁺ ions, and 6) was increased by elevated K⁺ concentrations. Although many of the characteristics of I_f are similar to those reported in SA node pacemaker cells, the time course of activation in latent pacemakers was significantly slower than in SA node, e.g. at -70 mV the time constant of I_f activation was approximately 3 seconds while in SA node cells values closer to 1 second have been reported (89,213). In addition, the amplitude of I_f in latent pacemaker cells was significantly smaller than I_f reported in SA node pacemaker cells (59,213), even when I_f current is normalized to total cell capacitance. The smaller I_f amplitude in latent pacemaker cells was reflected also in a fully-activated channel conductance (1.75 nS) that was several times smaller than that reported in SA node (59,213). It is well known that latent atrial pacemakers exhibit a slower spontaneous rate than primary pacemaker activity. In multicellular tissues, a direct comparison of cat SA node and Eustachian ridge pacemaker activity showed that SA node cycle length was 434 ms whereas latent pacemaker cycle length was 948 ms (188). It should be noted that the pacemaker cycle lengths recorded from multicellular Eustachian ridge tissues (948 ms) and those recorded from single Eustachian ridge pacemakers (901 ms) are not different from one another. The relatively slow time course and small amplitude of I_f activation may be responsible, at least in part, for the relatively long cycle length of latent compared to primary pacemakers. Interestingly, the time course of I_f activation in latent atrial pacemakers is

comparable to ventricular Purkinje pacemaker cells (36). It thus appears that a relatively slow time course of I_f activation may be a common feature of both atrial and ventricular latent pacemaker activities. The slower time course of I_f activation in latent atrial pacemakers may be due to a smaller opening (alpha) rate constant in the pacemaker voltage range (Figure 15D) compared with that reported in SA node cells (89).

Several lines of evidence indicate that I_f contributes importantly to right atrial latent pacemaker function. First, I_f was activated well within the latent pacemaker voltage range (-70 to -55 mV). In addition, blocking I_f with 2 mM Cs^+ decreased the slope of diastolic depolarization, and resulted in consistent and significant (50%) decreases in spontaneous rate, suggesting that I_f contributes significantly to initiating the pacemaker potential. An analysis of the inward current components in SA node pacemaker cells by DiFrancesco (57) also indicates that I_f makes the largest contribution toward initiating the pacemaker potential. In contrast to the present results, studies in multicellular (171) and single SA node cell preparations (89) have shown that 2 mM Cs^+ elicited only small decreases in spontaneous rate. van Ginneken & Giles (213) have also reported that in single SA node cells 1 mM Cs^+ elicited inconsistent slowing in spontaneous rate among different cells. However, Denyer & Brown (49) used recording techniques similar to those in the present study and found that in rabbit SA node cells, 2 mM Cs^+ consistently slowed spontaneous rate by about 20-30%. The fact that Cs^+ exerted a quantitatively greater effect in latent than in SA node pacemakers suggests that I_f may contribute more to latent than to primary pacemaker function. A possible explanation for these findings is that latent pacemakers exhibit a more negative

pacemaker voltage range compared to primary pacemaker cells. A similar conclusion was proposed by Anumonwo *et al.* (1) who found that 2 mM Cs⁺ elicited a fourfold increase in cycle length of latent pacemakers isolated from tricuspid valve, which exhibited a maximum diastolic potential of about -82 mV. van Ginneken and Giles (213) also found that when SA node pacemaker cells were hyperpolarized by about 10 mV, Cs⁺ was more effective in inhibiting spontaneous activity. In the present study, the maximum diastolic potential of latent pacemakers averaged about -68 mV. This value is more negative than those reported for SA node pacemaker cells (159,213), and similar to those reported in SA node by others (48). This apparent discrepancy may be explained by a proposal of Denyer & Brown (48) that pacemaker cells isolated from the SA node may not be derived from the central nodal region, which have been shown in multicellular preparations to have a less negative maximum diastolic potential and slower upstroke velocity (22,175). However, measurements of maximum diastolic potentials should be viewed cautiously because of differing experimental techniques and conditions among different laboratories.

Recent reports have provided evidence to support the role of I_f as a pacemaker current (49,57,213). DiFrancesco (57) showed that in SA node cells the diastolic membrane potential depolarizes at a rate of about 100 mV/s, which requires only 0.1 pA/pF or 3 pA of inward current in a cell with a mean capacitance of 30 pF. In the present experiments, the diastolic slope of latent pacemaker cells was about 35 mV/s and cell capacitance was 28 pF. The calculated current required to elicit this response is only 0.03 pA/pF or 1 pA. Therefore, latent pacemakers require only about one-third the

inward current required by the SA node. The present experiments also show that pacemaker activity continued even after I_f was significantly blocked by Cs^+ . Apparently, I_f contributes significantly, but it is neither essential nor the only mechanism contributing to latent pacemaker activity. Similar findings have been reported in multicellular Eustachian ridge preparations (189), SA node pacemaker cells (49,213), and tricuspid valve pacemaker cells (1).

In the present experiments, when the ruptured patch method was used to record I_f , the response of I_f to ISO was variable. Similar findings have been reported in SA node pacemaker cells (59). However, when the nystatin-perforated patch recording method was used, ISO consistently increased I_f amplitude and shifted the activation curve to more positive voltages in all cells studied. These results suggest that some intracellular substances, which are important in mediating the effect of ISO, may be washed out when using the ruptured patch recording method. It is well known that the effects of β -adrenergic agonists on I_f are mediated by increased intracellular cAMP levels, which in turn activate protein kinase A (41,89). Therefore, the negative response of I_f to ISO in some of the ruptured patch experiments may be due to the loss of these substances. In addition, the rundown of I_f seen in ruptured patch experiments may also be related to the loss of these substances. With the nystatin recording method, the loss of intracellular substances was minimized. Thus, under these recording conditions I_f exhibited little run-down and its response to ISO was consistently observed in all cells studied. With the nystatin recording method ISO also increased the spontaneous rate of latent pacemaker action potentials. Our results suggest that the positive chronotropic

effect of ISO on latent pacemaker activity is mediated, at least in part, via an increase of I_f amplitude in the pacemaker voltage range.

D. I_K current.

In the present experiments, we have analyzed the delayed rectifier potassium current, I_K , in latent atrial pacemaker cells. The activation threshold of I_K was about -40 mV and the current was fully activated at about $+30$ mV. The activation curve showed a half-maximal activation voltage of -8.6 mV. The activation voltage range is more positive than that of rabbit SA node pacemaker cells (200), but is more negative than that of guinea pig SA node pacemaker cells (2). In rabbit SA node pacemaker cells I_K exhibits a threshold of -50 mV and is fully activated at about 0 mV with a half maximal voltage of -25 mV (200). In guinea pig SA node I_K exhibits a threshold of -20 mV and is fully activated at $+80$ mV with a half maximal potential of $+30$ mV (2). The large difference between the voltage dependence of I_K activation in rabbit and guinea pig SA node pacemaker cells may be related to two distinct components of I_K : $I_{K,r}$ and $I_{K,s}$ (193,194). $I_{K,r}$ activates very rapidly during depolarization and is blocked by an antiarrhythmic agent, E-4031. In contrast, $I_{K,s}$ activates relatively slowly and is insensitive to E-4031. The half-maximal activation voltage of $I_{K,r}$ was -21.5 mV which is more negative than that of $I_{K,s}$ ($+15$ mV). I_K of rabbit SA node cells shares many characteristics with $I_{K,r}$ (200), while I_K of guinea pig SA node cells has properties similar to $I_{K,s}$ (2). Further experiments are needed to clarify whether I_K of latent pacemaker cells resembles $I_{K,r}$, $I_{K,s}$, or a composite of two components.

I_K of latent pacemaker cells did not exhibit inactivation. Similar results have been

reported in guinea pig SA node pacemaker cells (2) and other types of cardiac cells (84,107,149,201). In contrast, in rabbit SA node pacemaker cells I_K exhibited inactivation at voltages more positive than 0 mV (200). The fully-activated I-V relationship of I_K in latent pacemaker cells displayed inward rectification at voltages more positive than -30 mV. Similar results have been reported in SA node pacemaker cells (159). In rabbit SA node pacemaker cells, this inward rectification is attributed to the inactivation of I_K at more positive voltages (200). Because I_K of latent pacemaker cells does not exhibit inactivation, other mechanisms may be involved in the inward rectification of I_K . For example, the inward rectification of I_{K1} has been shown to be related to intracellular magnesium ions (148).

The usual method of determining the reversal potential of I_K is to activate I_K with a large depolarizing clamp and then repolarize the cell to different voltages. However, in latent pacemaker cells repolarization to voltages more negative than about -50 mV elicits both I_K tail currents and I_f activation. Clearly, activation of I_f can influence measurements of the I_K reversal potential. In studies of SA node pacemaker cells, the I_K reversal potential was measured in those cells in which activation of I_f was not significant (159,200). Because I_f is a major characteristic of latent pacemaker cells, those cells with small I_f may not represent typical latent pacemakers. In addition, even small I_f may affect accurate measurement of the I_K reversal potential. Therefore, in the present experiments the I_K reversal potential was measured using a voltage clamp protocol which separated I_K tail currents from I_f activation. I_K tail currents obtained by this protocol exhibited a reversal potential of -78 mV. This value is close to the

calculated K^+ equilibrium potential and suggests that I_K is primarily carried by K^+ ions. The results also show that a tenfold change in $[K^+]_o$ elicited a 52 mV change in the reversal potential. Similar values have been reported in guinea pig ventricular cells (149), frog sinus venosus (84) and atrial cells (107). These results further support the idea that K^+ is the major charge carrier for I_K . However, the fact that the reversal potential of I_K is slightly more positive than the calculated K^+ equilibrium potential and that the change in reversal potential is less than 61 mV suggest that I_K channels may not be purely selective for K^+ . Matsuura *et al.* (149) found that removal of extracellular Na^+ resulted in a negative shift in the I_K reversal potential in guinea pig ventricular cells, suggesting that Na^+ ions may also contribute in part to I_K .

The present work shows that in the pacemaker voltage range of latent pacemakers, the time course of I_K deactivation is coincident with the initial phase of diastolic depolarization. This finding is similar to that in rabbit SA node (33,159,169) and frog sinus venosus pacemaker cells (84). The decay of I_K is thought to contribute to diastolic depolarization by reducing outward current (33). However, to elicit depolarization of the membrane potential the net current must be inward. Therefore, the decay of I_K must be associated with an inward current component. At present, the nature of the inward current component is not clear. Recently, Hagiwara *et al.* (91) have found an inward background current in rabbit SA node pacemaker cells. This current is a time-independent current which exhibits a reversal potential of -21 mV at physiological concentrations of intracellular K^+ and extracellular Na^+ . Thus, this background current may provide an inward current in the pacemaker potential range. However, DiFrancesco

(57) found that the instantaneous background current is outward in the pacemaker voltage range of SA node cells. He proposed that I_f may represent the only inward current source at voltages within the primary pacemaker range. The present work supports the role of I_f as an inward current component in the latent pacemaker voltage range, but does not exclude other possible sources of inward current.

Experiments on multicellular preparations have also shown that SA node (143,217-219) as well as latent atrial pacemakers (139) are relatively insensitive to elevated extracellular K^+ . We therefore tested the effects of elevated K^+ on pacemaker action potentials recorded from single latent pacemaker cells. The primary effect of elevated K^+ on action potential configuration was to shift the maximum diastolic potential about 10 mV more positive and increase the spontaneous rate by 27%. From these results, it is evident that latent atrial pacemaker activity recorded from single cells is also relatively insensitive to high K^+ . Similar insensitivity to elevated K^+ in SA node preparations has been attributed to a lack of background K^+ conductance (172). As shown in this study and by others (85,226), latent pacemaker cells also lack significant background K^+ conductance. This feature may therefore account for their relative insensitivity to high K^+ as well. Experiments on multicellular Eustachian ridge preparations (139) have shown that high K^+ induces a similar depolarization of maximum diastolic potential and an increase rather than a decrease in pacemaker cycle length, as shown here. It seems likely that the slowing in rate recorded in multicellular tissues results from a secondary increase in K^+ conductance in surrounding atrial muscle. This effect would be expected to shunt current flowing during diastole and thereby

depress diastolic slope of the pacemaker cells. The present results show that elevated K^+ also shifted the I_K reversal potential to more positive voltages, resulting in a more positive maximum diastolic potential. Because the maximum diastolic potential moved closer to the I_K reversal potential, the driving force on K^+ was reduced and the I_K tail current amplitude at maximum diastolic potential was decreased. This effect may contribute to the increase in spontaneous rate induced by high K^+ observed in single latent pacemaker cells. As shown in the earlier experiments, elevated extracellular K^+ also increased I_f . This raises the possibility that I_f may also contribute to the K^+ -induced increase in spontaneous rate recorded from single pacemaker cells. On the other hand, although I_f is enhanced by high K^+ , the more positive diastolic potential would be expected to reduce the contribution of I_f activation. The K^+ -induced increase in I_f may also contribute to the more positive maximum diastolic potential in elevated K^+ .

E. Ca^{2+} Currents.

The present experiments demonstrate the existence of both $I_{Ca,T}$ and $I_{Ca,L}$ in latent pacemaker cells. The Ca^{2+} currents cannot be attributed to fast Na^+ current (see Figure 32), because both internal and external solutions were Na-free and external solution contained 30 μM TTX. In addition, in the presence of 2 mM Co^{2+} , depolarizing clamps failed to elicit any inward current, indicating that Na^+ current was completely eliminated under our experimental conditions. $I_{Ca,T}$ and $I_{Ca,L}$ were distinguished by their voltage dependence of activation and inactivation. $I_{Ca,T}$ was activated primarily at more negative voltages with a threshold of about -50 mV and maximal amplitude at -10 mV, whereas $I_{Ca,L}$ current was activated primarily at more

positive voltages with a threshold of about -30 mV and maximal amplitude at $+10$ mV. The half-maximal activation and inactivation voltages of $I_{Ca,T}$ were significantly more negative than those of $I_{Ca,L}$, indicating that the two currents can be largely separated by their voltage dependence. In latent pacemaker cells, the half-maximal activation voltage for $I_{Ca,T}$ is about -31 mV, which is more negative than that of SA node pacemaker cells (-23 mV) (90), but is more positive than that of cultured SA node pacemaker cells (-38 mV) (79). The half-maximal inactivation voltage for $I_{Ca,T}$ is about -57 mV, which is more positive than that of SA node pacemaker cells (-75 mV) (90), but is comparable to that of cultured SA node pacemaker cells (-59 mV) (79).

The maximum $I_{Ca,T}$ current density in latent pacemaker cells was 3.3 pA/pF which is comparable to that of SA node pacemaker cells (2.6 pA/pF) (90) and Purkinje cells (2.9 pA/pF) (210). However, $I_{Ca,T}$ current density of latent pacemaker cells was about 5 times larger than that of working atrial muscle cells. Tseng and Boyden (210) have reported that $I_{Ca,T}$ current density of Purkinje cells is about two times larger than that of ventricular cells. Hagiwara *et al.* (90) also report that $I_{Ca,T}$ current density of rabbit SA pacemaker cells appears to be about 10 times larger than that of canine atrial cells (10). These results indicate that $I_{Ca,T}$ current density is relatively high in cardiac pacemaker cells and is a common feature among primary as well as latent atrial and ventricular pacemakers. The high $I_{Ca,T}$ current density in pacemaker cells may be related to their function as pacemakers.

In the present experiments, 40 μ M Ni^{2+} significantly inhibited $I_{Ca,T}$ currents elicited at relatively negative voltages (-50 to -40 mV). At more positive voltages, 40

$\mu\text{M Ni}^{2+}$ had less effect on $I_{\text{Ca,T}}$. Many authors have reported that low concentrations of Ni^{2+} selectively block $I_{\text{Ca,T}}$ in cardiac cells (26,90,124,225). Others, however, have reported that low concentrations of Ni^{2+} have less selective blocking effect (99,156,210) or no effect (79) on $I_{\text{Ca,T}}$. In SA node pacemaker cells $40 \mu\text{M Ni}^{2+}$ completely blocks $I_{\text{Ca,T}}$ at all voltages without affecting $I_{\text{Ca,L}}$ (90). In contrast, in cultured SA node pacemaker cells $40 \mu\text{M Ni}^{2+}$ has no effect on $I_{\text{Ca,T}}$, and higher concentrations reduce both $I_{\text{Ca,T}}$ and $I_{\text{Ca,L}}$ (79). In Purkinje cells, $50 \mu\text{M Ni}^{2+}$ inhibited $I_{\text{Ca,T}}$ and $I_{\text{Ca,L}}$ by 47% and 11%, respectively. Elevating the concentration of Ni^{2+} to $500 \mu\text{M}$ caused a further reduction of $I_{\text{Ca,T}}$ and $I_{\text{Ca,L}}$ by 72% and 28%, respectively (210).

The present experiments show that $40 \mu\text{M Ni}^{2+}$ significantly increased spontaneous cycle length of latent pacemaker action potential by decreasing the slope of late phase of diastolic depolarization. Similar results have been reported in SA node pacemaker cells, where $40 \mu\text{M Ni}^{2+}$ inhibited $I_{\text{Ca,T}}$ and prolonged spontaneous cycle by decreasing the late slope of diastolic depolarization (90). However, in SA node pacemaker cells the prolongation was only 14.4%, while in the present study the spontaneous cycle length of latent pacemaker cells was prolonged by 66.9%. These results suggest that $I_{\text{Ca,T}}$ may contribute more to latent than primary pacemakers activity. This may be related to the fact that the latent pacemakers exhibit a relatively more negative maximum diastolic potential. In this regard, in SA node pacemaker cells, the effect of Ni^{2+} was more pronounced when the cell was hyperpolarized by injecting a constant current, indicating that $I_{\text{Ca,T}}$ contributes more to pacemaker activity at more negative voltages (90).

F. Na-Ca exchange current.

In studies of Na-Ca exchange current it is important to use a recording method that minimizes interference with the normal intracellular Ca^{2+} buffering mechanisms. This can be accomplished by using conventional microelectrodes as reported in rat and guinea pig ventricular cells (72,78,155). However, it is not practical to use microelectrodes to record from single atrial pacemaker cells due to their relatively small dimensions (diameters $< 10 \mu\text{m}$). Na-Ca exchange currents have also been recorded by using a ruptured patch/whole-cell recording method, where the EGTA concentration in the pipette solution was lowered to micromolar levels (69) or omitted (82). Even with this precaution, the ruptured patch method suffers from two significant drawbacks; 1) rundown of $I_{\text{Ca,L}}$, and 2) disruption of endogenous cellular Ca^{2+} buffering mechanisms. Each of these effects may influence the normal intracellular Ca^{2+} transient. In the present experiments the nystatin-perforated patch recording technique was used to record Na-Ca exchange current. This method prevents rundown of Ca^{2+} current and maintains endogenous Ca^{2+} buffering mechanisms during recording of whole cell currents (104,130). Therefore, the nystatin-perforated patch recording technique provides an essentially non-invasive method of analyzing Na-Ca exchange under conditions that are as close to physiological as possible, and thereby may provide a more accurate view of its contribution in atrial pacemaker function.

I_{NaCa} was recorded as either a secondary inward current following peak activation of $I_{\text{Ca,L}}$ or as a slowly decaying inward tail current elicited upon repolarization following short depolarizing steps. Similar recordings have been reported in multicellular

preparations (3,34) and single cardiac myocytes (66,69,72,78,82,155). As in these previous studies, the present experiments indicate that the slow inward currents are due to Na-Ca exchange and are mediated by SR Ca^{2+} release. Thus, inward currents were: (i) abolished by dialyzing the cell interior with EGTA to buffer intracellular Ca^{2+} , (ii) abolished by ryanodine, an agent that effectively eliminates SR Ca^{2+} release, and (iii) significantly decreased by substituting lithium for external Na^+ . Tail currents also exhibited a voltage-dependence that is consistent with Na-Ca exchange (45). Thus, repolarization to more negative voltages enhanced peak tail current amplitude and accelerated the rate of current decay (Figure 33). That low external Na^+ inhibited inward tail currents indicates that the current was carried by Na^+ rather than an intracellular Ca^{2+} -activated Cl^- conductance (231). The finding that tail currents were blocked by substituting lithium for Na^+ further indicates that the primary underlying mechanism is Na-Ca exchange (126) rather than a non-specific cation channel (73).

Several of the present findings indicate that I_{NaCa} amplitude is not proportional to $I_{\text{Ca,L}}$ on a beat-to-beat basis and that only a fraction of $I_{\text{Ca,L}}$ is required to initiate I_{NaCa} . Thus, the voltage dependent characteristics of $I_{\text{Ca,L}}$ and I_{NaCa} differed significantly from one another. $I_{\text{Ca,L}}$ exhibited a bell-shaped voltage relationship while that of I_{NaCa} was relatively flat, especially between -10 and $+30$ mV. The present results also showed that I_{NaCa} and $I_{\text{Ca,L}}$ did not correlate in time when cells were exposed to cadmium (Figure 39). For example, when cadmium had blocked about 95% of $I_{\text{Ca,L}}$, I_{NaCa} amplitude was reduced by only 50%. Similar results have been reported in atrial (69) and ventricular myocytes (72,155). Moreover, because the rested recovery

time of I_{NaCa} was significantly slower than that of $I_{\text{Ca,L}}$, significant $I_{\text{Ca,L}}$ could be recorded at a time when I_{NaCa} was markedly smaller. These experiments as well as others (15,67,72) indicate that I_{NaCa} (and intracellular Ca^{2+}) is relatively insensitive to changes in $I_{\text{Ca,L}}$. The present results agree with a proposal by Earm and Noble (70) that Ca-mediated SR Ca^{2+} release is partly regenerative and therefore there is a non-linear relationship between $I_{\text{Ca,L}}$ and SR Ca^{2+} release. Moreover, the amount of SR Ca^{2+} available for release and the magnitude of SR Ca^{2+} release appear to be more important than the magnitude of the Ca^{2+} influx that triggers the release (15,72).

The present work also shows that the duration of the depolarizing pulse has no effect on the time course of I_{NaCa} elicited upon repolarization (Figure 36). If the clamp duration was sufficiently long (≥ 10 ms) to activate peak $I_{\text{Ca,L}}$, repolarization elicited I_{NaCa} tail currents that were, for the most part, superimposable regardless of the preceding clamp duration. If we assume that I_{NaCa} follows the time course of intracellular Ca^{2+} released by the SR (66), then the present findings suggest that once $I_{\text{Ca,L}}$ initiates SR Ca^{2+} release, it becomes regenerative and goes to completion regardless of pulse duration. This idea is generally consistent with reports in ventricular myocytes that repolarization does not affect peak levels of intracellular Ca^{2+} (67) as long as peak $I_{\text{Ca,L}}$ is reached. In contrast, Cannell *et al.* (39) have shown that in rat ventricular myocytes, repolarization following clamps as long as 20 ms (long enough to reach peak $I_{\text{Ca,L}}$) can alter peak intracellular Ca^{2+} amplitude and longer clamps can accelerate the rate of intracellular Ca^{2+} decline. This voltage-dependent decline in intracellular Ca^{2+} does not appear to be due to a voltage-dependent stimulation of Na-Ca

exchange (17).

Based on the voltage range in which I_{NaCa} is activated during depolarization and its time course of decay, it seems likely that I_{NaCa} contributes to the duration of latent pacemaker action potentials (189). Na-Ca exchange currents have been proposed to contribute to action potential duration in atrial (69) and ventricular myocytes (66,72,155). The present experiments indicate that I_{NaCa} also contributes to the diastolic phase of the cycle. Thus, in cells beating spontaneously, or repetitively stimulated, I_{NaCa} increasingly recovers during diastole at times compatible with the normal pacemaker cycle length. This early recovery of I_{NaCa} exhibited both time- and voltage-dependent properties. One factor contributing to I_{NaCa} recovery appears to be the time- and voltage-dependent recovery from inactivation of $I_{\text{Ca,L}}$. It is well known that $I_{\text{Ca,L}}$ recovery is more rapid at more negative voltages (170,209). However, I_{NaCa} recovery also exhibits a time-dependent component. Thus, I_{NaCa} amplitude progressively increased at early times, even though $I_{\text{Ca,L}}$ was almost fully recovered within about 200 ms. It therefore seems likely that other time-dependent processes such as the recovery of SR Ca^{2+} release channels (77) and/or the re-uptake of Ca^{2+} into the SR, contribute to the time course of I_{NaCa} recovery. The paired pulse recovery experiments (Figure 38) also show that time-dependent processes, other than recovery of $I_{\text{Ca,L}}$, contribute to I_{NaCa} recovery. At times later than 2 sec, I_{NaCa} amplitude exhibited a voltage-dependent decline over time, where I_{NaCa} decayed more rapidly at -70 than at -40 mV. This voltage-dependent decrease in I_{NaCa} is consistent with a voltage-dependent loss of intracellular Ca^{2+} . Of the possible mechanisms that may be responsible for a decline in intracellular Ca^{2+} , i.e.

Ca-ATPase, SR uptake, and Na-Ca exchange, only Na-Ca exchange has been shown to be voltage-sensitive (7,45,198). Shattock and Bers (198) have reported that extrusion of Ca^{2+} by Na-Ca exchange occurs when the resting membrane potential is more negative than the equilibrium potential of Na-Ca exchange. The finding that I_{NaCa} is dependent on SR Ca^{2+} (Figure 35) suggests that the voltage-dependent decline in I_{NaCa} is associated with a decline in SR Ca^{2+} content. This idea is consistent with the diastolic loss of SR Ca^{2+} via Na-Ca exchange that is thought to underlie the decay of contraction amplitude with time, i.e. rest decay (105,198). In relation to pacemaker function, the present findings indicate that at times that are compatible with the normal pacemaker cycle length (<1 sec), SR Ca^{2+} and I_{NaCa} recover and increase over time. In addition, the voltage to which the pacemaker cell repolarizes is an important determinant of the time course of I_{NaCa} recovery. At voltages consistent with the normal maximum diastolic potential (-70 mV) I_{NaCa} is essentially fully recovered for the next pacemaker cycle.

The present results show that inhibition of SR Ca^{2+} release by ryanodine depresses the slope of diastolic depolarization, resulting in a significant increase in pacemaker cycle length. This is similar to that obtained in multicellular pacemaker tissues (189). In addition, ryanodine abolished a transient inward current and a background current flowing during the late diastolic depolarization (Figure 42). These results suggest that a component mediated by SR Ca^{2+} release and presumably due to I_{NaCa} contributes to the diastolic slope. This raises the question of how I_{NaCa} contributes during the pacemaker potential. The answer may be related to the voltage-dependent extrusion of intracellular Ca^{2+} that is mediated by Na-Ca exchange during diastole.

Thus, as the pacemaker action potential repolarizes to the maximum diastolic potential, Na-Ca exchange is stimulated to extrude Ca^{2+} . As discussed above, this loss of intracellular Ca^{2+} is linked to a loss of SR Ca^{2+} (105). An extrusion of Ca^{2+} that is mediated via Na-Ca exchange is expected to generate a small but functionally significant I_{NaCa} inward current during the diastolic phase of the cycle. Based on passive membrane properties and the slope of diastolic depolarization, calculations indicate that about 1 pA of total current is required to generate the pacemaker potential in latent atrial pacemaker cells. Therefore, I_{NaCa} could generate less than 1 pA and still make a significant contribution to pacemaker function. This idea is consistent with the present experimental observations and those reported previously (189) that inhibition of SR function by ryanodine slows but does not stop pacemaker activity. Because SR Ca^{2+} and therefore I_{NaCa} becomes more available with time, the contribution of I_{NaCa} to the diastolic slope will be more evident at later times in the diastolic phase of the pacemaker cycle. This hypothesis is consistent with the present as well as previous results (189) which show that the inhibitory effects of ryanodine are more evident during the late phase of the pacemaker potential.

The idea that a component of latent atrial pacemaker activity is mediated by SR Ca^{2+} release assumes additional significance in light of our previous ultrastructural studies of the cat Eustachian ridge (188). Those studies showed that although latent pacemakers were morphometrically similar to SA nodal pacemaker cells, latent pacemakers exhibited prominent subsarcolemmal cisternae that were not seen in SA node cells. In addition, the subsarcolemmal cisternae in latent pacemakers were arranged in

a unique architecture, where two cisternae were directly apposed to one another on each side of the cell membranes of two adjacent cells. This structural arrangement may somehow facilitate the way in which Ca^{2+} is handled by latent pacemaker cells during repetitive activity. The structures between the cisternae and sarcolemma, i.e. "feet" proteins, have been shown to be the site at which ryanodine binds to Ca^{2+} release channels (111,134). The relationship between SR structure and pacemaker function is further supported by the finding that SA node cells lack similar SR structures and ryanodine elicits only a small increase (+12%) in SA node pacemaker cycle length compared with latent atrial pacemakers (139). The fact that ryanodine has qualitatively similar effects on single latent pacemaker cells as those reported in multicellular preparations (189) indicates that the apposition of SR between pacemaker cells is not essential for basal pacemaker activity. However, the effect of ryanodine reported here in single pacemaker cells is quantitatively smaller than in multicellular preparations. This may be related to the loss of a functional communication between latent pacemaker cells when they are studied in isolation. Consequently, the contribution of I_{NaCa} to latent atrial pacemaker activity may be somewhat underestimated in the present single cell experiments.

Finally, these experiments showed that isoproterenol induced an increase in the slope of diastolic depolarization and a concomitant increase in inward current. The fact that ryanodine abolished the inward current and significantly decreased the diastolic slope, suggests that SR Ca^{2+} release and presumably I_{NaCa} , mediated at least part of the effects of isoproterenol. This is consistent with the effects of isoproterenol to directly

stimulate $I_{Ca,L}$ and SR Ca^{2+} uptake (37) and thereby increase SR Ca^{2+} content. Loading the SR with Ca^{2+} would enhance the diastolic leak of SR Ca^{2+} and the concomitant inward current generated by Ca^{2+} extrusion via Na-Ca exchange. Of course, isoproterenol affects many other current systems such as I_f and $I_{Ca,L}$ that may directly affect pacemaker activity. Nevertheless, these results suggest that adrenergic regulation of latent pacemaker function may be partially mediated via I_{NaCa} .

SUMMARY AND CONCLUSIONS

Single latent pacemaker cells have been isolated from the Eustachian ridge of cat right atrium using Langendorff perfusion and enzyme dispersion techniques. Whole-cell patch clamp techniques were used to study ionic currents underlying pacemaker activity of these cells. All cells studied beat rhythmically and exhibited normal morphological and electrophysiological characteristics. Pacemaker action potentials recorded from single latent pacemaker cells were similar to those recorded from multicellular preparations. Pacemaker cells were elongated with tapered ends and appeared bent or crinkled without obvious striations. The morphological and passive membrane properties of latent pacemaker cells were similar to those of SA node pacemaker cells.

Hyperpolarizing clamps elicited I_f with little, if any, background I_{K1} current. Activation of I_f was well within the pacemaker voltage range. The fully-activated current-voltage (I-V) relationship was approximately linear at voltages more negative than -30 mV and showed outward rectification at more positive voltages. The time constant of I_f activation at -70 mV was 3.3 sec, which is much slower than that of SA node pacemaker cells. Reducing extracellular Na^+ or K^+ shifted the reversal potential more negative, and increasing extracellular K^+ exerted the opposite effect. Reducing extracellular Na^+ decreased I_f amplitude and the slope of the fully-activated I-V relationship, and elevated extracellular K^+ increased I_f amplitude and the slope of the

fully-activated I-V relationship. Cesium (2 mM) inhibited I_f in a voltage dependent manner and decreased the slope of diastolic depolarization, resulting in a 48% decrease in spontaneous rate.

When the ruptured patch method was used, isoproterenol (ISO; 1 μ M) elicited variable changes in I_f among different cells, resulting in no net change in mean current amplitude and no significant change in the I_f activation curve. When using a nystatin-perforated patch recording method, however, ISO increased I_f consistently in all cells studied and increased the spontaneous rate of pacemaker action potentials by 58%. In addition, ISO elicited a positive shift in the I_f activation curve. Therefore, variabilities in the response of I_f to ISO may result from loss of internal constituents when using the ruptured patch method.

Depolarizing clamps from a holding potential of -40 mV elicited L-type Ca^{2+} current ($I_{\text{Ca,L}}$) followed by an increasing outward current, I_{K} . The voltage dependence of I_{K} activation was between -40 and $+30$ mV. The fully-activated I_{K} I-V relationship was linear between -100 and -30 mV and exhibited inward rectification at more positive voltages. Repolarization to voltages more negative than -60 mV elicited tail currents that consisted of both I_{K} deactivation and I_f activation. Subtraction protocols were used to isolate I_{K} deactivating tail currents. In $5.4 [\text{K}^+]_o$, I_{K} tail currents exhibited a reversal potential of -78 mV. The reversal potential of I_{K} exhibited a linear relationship with $\log [\text{K}^+]_o$ and a slope of 51.5 mV per tenfold change in $[\text{K}^+]_o$. At voltages compatible with the pacemaker maximum diastolic potential (-70 mV), current attributable to I_{K} deactivation was relatively small and decayed more rapidly than activation of I_f .

Two types of Ca^{2+} currents ($I_{\text{Ca,T}}$ and $I_{\text{Ca,L}}$) were recorded in single latent pacemaker cells. $I_{\text{Ca,T}}$ and $I_{\text{Ca,L}}$ were distinguished by their voltage dependence of activation and inactivation. $I_{\text{Ca,T}}$ was activated primarily at more negative voltages with a threshold about -50 mV and maximal amplitude at -10 mV, whereas $I_{\text{Ca,L}}$ was activated primarily at more positive voltages with a threshold about -30 mV and maximal amplitude at $+10$ mV. The density of $I_{\text{Ca,T}}$ in latent pacemaker cells was about 5 times larger than that in working atrial muscle cells. Both Ca^{2+} currents were blocked by 2 mM Co^{2+} . Nifedipine blocked $I_{\text{Ca,L}}$ in a voltage dependent manner. Low concentrations of Ni^{2+} ($40 \mu\text{M}$) inhibited $I_{\text{Ca,T}}$ at voltages of -50 and -40 mV, but the inhibitory effect was less at more positive voltages. Ni^{2+} ($40 \mu\text{M}$) also significantly increased the spontaneous cycle length of latent pacemaker action potentials by decreasing the slope of the late phase of the diastolic potential.

A nystatin-perforated patch recording method was used to study Na-Ca exchange current (I_{NaCa}). The nystatin method avoids alterations in intracellular Ca^{2+} , cellular constituents and run down of ionic currents. Depolarizing voltage clamp pulses from -40 mV elicited $I_{\text{Ca,L}}$ that exhibited an initial rapid phase of inactivation followed by a secondary slower inward current component that decayed over about 100 ms. The secondary inward component appeared as a slowly decaying inward tail current following short (10–40 ms) depolarizing clamp steps. Slowly decaying inward currents were abolished by dialyzing the cell with EGTA, by depleting SR Ca^{2+} with ryanodine, and by replacing 85% of external Na^+ with lithium. These findings suggest that the inward current is due to Na-Ca exchange mediated by SR Ca^{2+} release. Isoproterenol

$\geq 5 \times 10^{-8} \text{M}$ significantly increased peak $I_{\text{Ca,L}}$ amplitude and peak I_{NaCa} amplitude, and accelerated I_{NaCa} rate of decay. During diastole, I_{NaCa} exhibited a voltage-dependent increase in amplitude over time. At times > 2 sec, I_{NaCa} exhibited a voltage-dependent decline in amplitude over time. That is, when elicited from -40 mV I_{NaCa} decreased by 10% of maximum, whereas from -70 mV, I_{NaCa} decreased by 60% of maximum. Interruption of free-running pacemaker action potentials during the late phase of diastolic depolarization (-50 mV) elicited a small, transient inward current that decayed to a background inward current. Ryanodine decreased diastolic slope, increased pacemaker cycle length and abolished the inward currents. Isoproterenol induced an increase in diastolic slope and inward current (at -50 mV) that was inhibited by ryanodine.

CONCLUSIONS

1. The present study demonstrates the isolation of Ca^{2+} -tolerant latent pacemaker cells from the Eustachian ridge of the cat right atrium. Latent pacemakers appear morphologically and electrophysiologically similar, though not identical, to pacemaker cells isolated from SA node.

2. I_f of latent pacemaker cells is activated within the pacemaker voltage range and contributes significantly to latent pacemaker function. The relatively slow time course of activation and small amplitude of I_f may explain, in part, the relatively long spontaneous cycle length of latent atrial pacemakers. The positive chronotropic effect of isoproterenol is mediated in part by stimulation of I_f .

3. Latent atrial pacemaker cells exhibit prominent I_K activation during depolarization. Repolarization elicits tail currents that consist of both I_K deactivation and I_f activation. At the maximum diastolic potential the current attributable to I_K deactivation is relatively small and decays more rapidly than activation of I_f . I_K may contribute to the repolarization and initial phase of diastolic depolarization in latent pacemaker cells. In addition, a reduction in I_K tail current amplitude may contribute to the acceleration of spontaneous rate induced by elevated external K^+ .

4. Both $I_{Ca,T}$ and $I_{Ca,L}$ are present in latent pacemaker cells. $I_{Ca,T}$ current density of latent pacemaker cells is significantly larger than that of working atrial cells. $I_{Ca,T}$ exhibits a "window" current within the latent pacemaker voltage range and thereby may contribute to the late phase of diastolic depolarization.

5. A slow inward current attributable to Na-Ca exchange is recorded in latent pacemaker cells. The time course and voltage-dependence of I_{NaCa} suggest that it may contribute to the duration of the pacemaker action potential. In addition, I_{NaCa} contributes significantly to the slope of diastolic depolarization and may partially mediate the positive chronotropic response to isoproterenol of latent atrial pacemakers.

BIBLIOGRAPHY

1. Anumonwo, J.M.B., M. Delmar, and J. Jalife. Electrophysiology of single heart cells from the rabbit tricuspid valve. *J. Physiol.* **425**: 145-167, 1990.
2. Anumonwo, J.M.B., L.C. Freeman, W.M. Kwok, and R.S. Kass. Delayed rectification in single cells isolated from guinea pig sinoatrial node. *Am. J. Physiol.* **262**: H921-H925, 1992.
3. Arlock, P. and D. Noble. Two components of "second inward current" in ferret papillary muscle. *J. Physiol.* **369**: 88P, 1985.
4. Bahinski, A., A.C. Nairn, P. Greengard, and D.C. Gadsby. Chloride conductance regulated by cyclic AMP-dependent protein kinase in cardiac myocytes. *Nature* **340**: 718-721, 1989.
5. Balke, C.W. and W.G. Wier. Ryanodine does not affect calcium current in guinea pig ventricular myocytes in which Ca^{2+} is buffered. *Circ. Res.* **68**: 897-902, 1991.
6. Balsler, J.R., P.B. Bennett, and D.M. Roden. Time-dependent outward current in guinea pig ventricular myocytes. Gating kinetics of the delayed rectifier. *J. Gen. Physiol.* **96**: 835-863, 1990.
7. Barceñas-Ruiz, L., D.J. Beuckelmann, and W.G. Wier. Sodium-calcium exchange in heart: membrane currents and changes in $[Ca^{2+}]_i$. *Science* **238**: 1720-1722, 1987.
8. Bassett, A.L., J.J. Fenoglio, A.L. Wit, R.J. Myerburg, and H. Gelband. Electrophysiologic and ultrastructural characteristics of the canine tricuspid valve. *Am. J. Physiol.* **230**: 1366-1377, 1976.
9. Baumgarten, C.M. and G. Isenberg. Depletion and accumulation of potassium in the extracellular clefts of cardiac Purkinje fibres during voltage-clamp hyperpolarization and depolarization. *Pflügers Arch.* **368**: 19-31, 1977.
10. Bean, B.P. Two kinds of calcium channels in canine atrial cells: Differences in kinetics, selectivity, and pharmacology. *J. Gen. Physiol.* **86**: 1-30, 1985.

11. Belardinelli, L, U Klockner, and G Isenberg. Modulation of potassium and calcium currents in atrial and nodal cells. *Isolated Adult Cardiomyocytes 2*: 155-180, 1989.
12. Belardinelli, L., W.R. Giles, and A. West. Ionic mechanisms of adenosine actions in pacemaker cells from rabbit heart. *J. Physiol.* **405**: 615-633, 1988.
13. Bennett, P.B. and T.B. Begenisich. Catecholamines modulate the delayed rectifying potassium current (IK) in guinea pig ventricular myocytes. *Pflügers Arch.* **410**: 217-219, 1987.
14. Berkowitz, G.A. and R.D. Nathan. Sodium current in primary pacemaker cells isolated from the rabbit sinoatrial node. *Circ.* **82**: III-748, 1990.
15. Berlin, J.R., M.B. Cannell, and W.J. Lederer. Voltage dependent changes in intracellular calcium on single cardiac myocytes measured with fluorescent calcium indicators. In: *Biology of isolated adult cardiac myocytes*, edited by W.A. Clark, R.S. Decker, and T.K. Borg. New York: Elsevier Science Publishing Co., 1988, p. 366-369.
16. Bers, D.M. and J.H.B. Bridge. Relaxation of rabbit ventricular muscle by Na-Ca exchange and sarcoplasmic reticulum Ca-pump: ryanodine and voltage sensitivity. *Circ. Res.* **65**: 334-342, 1989.
17. Bers, D.M., W.J. Lederer, and J.R. Berlin. Intracellular Ca transients in rat cardiac myocytes: role of Na-Ca exchange, the calcium current, and the sarcoplasmic reticulum. *Am. J. Physiol.* **258**: C944-C954, 1990.
18. Beuckelmann, D.J. and W.G. Wier. Mechanism of release of calcium from sarcoplasmic reticulum of guinea-pig cardiac cells. *J. Physiol.* **405**: 233-255, 1988.
19. Beuckelmann, D.J. and W.G. Wier. Sodium-calcium exchange in guinea-pig cardiac cells: exchange current and changes in intracellular Ca^{2+} . *J. Physiol.* **414**: 499-520, 1989.
20. Biermans, G., J. Vereecke, and E. Carmeliet. The mechanisms of the inactivation of the inward-rectifying K current during hyperpolarizing steps in guinea-pig ventricular myocytes. *Pflügers Arch.* **410**: 604-613, 1987.
21. Blaustein, M.P., R. Pipolo, and J.P. Reeves. *Sodium-Calcium exchange*. New York: The New York Academy of Sciences, 1991,

22. Bleeker, W.K., A.J.C. Mackaay, M. Masson-Pevet, L.N. Bouman, and A.E. Becker. Functional and morphological organization of the rabbit sinus node. *Circ. Res.* **46**: 11-22, 1980.
23. Boineau, J.P., R.B. Schuessler, D.B. Hackel, C.B. Miller, C.W. Brockus, and A.C. Wylds. Widespread distribution and rate differentiation of the atrial pacemaker complex. *Am. J. Physiol.* **239**: H406-H415, 1980.
24. Boineau, J.P., R.B. Schuessler, C.R. Mooney, A.C. Wylds, C.R. Miller, R.D. Hudson, J.M. Burroughs and C.W. Brockus. Multicentric origin of the atrial depolarization wave: the pacemaker complex. *Circ.* **58**: 1036-1048, 1978.
25. Bois, P. and J. Lenfant. Isolated cells of the frog sinus venosus: properties of the inward current activated during hyperpolarization. *Pflügers Arch.* **416**: 339-346, 1990.
26. Bonvallet, R. A low threshold calcium current recorded at physiological Ca concentrations in single frog atrial cells. *Pflügers Arch.* **408**: 540-542, 1987.
27. Borman, M.C. and W.J. Meek. Coronary sinus rhythm: rhythm subsequent to destruction by radon of the sino-auricular nodes in dogs. *Arch. Intern. Med.* **47**: 957, 1931.
28. Brennecke, R. and B. Lindemann. Theory of a membrane-voltage clamp with discontinuous feedback through a pulse current clamp. *Rev. Sci. Instr.* **45**: 184-188, 1974.
29. Brennecke, R. and B. Lindemann. Design of a fast voltage clamp for biological membrane, using discontinuous feedback. *Rev. Sci. Instr.* **45**: 656-661, 1974.
30. Brooks, C.McC. and H.H. Lu. *The Sinoatrial Pacemaker of the Heart*. Springfield: Charles C. Thomas, 1972, p. 1-179.
31. Brown, H.F. and D. DiFrancesco. Voltage-clamp investigations of membrane currents underlying pace-maker activity in rabbit sino-atrial node. *J. Physiol.* **308**: 331-351, 1980.
32. Brown, H.F., D. DiFrancesco, and S.J. Noble. How does adrenaline accelerate the heart. *Nature* **280**: 235-236, 1979.
33. Brown, H.F., J. Kimura, D. Noble, S.J. Noble, and A. Taupignon. The ionic currents underlying pacemaker activity in rabbit sino-atrial node: experimental results and computer simulations. *Proc. R. Soc. Lond. B* **222**: 329-347, 1984.

34. Brown, H.F., J. Kimura, D. Noble, S.J. Noble, and A. Taupignon. The slow inward current, i_{si} , in the rabbit sino-atrial node investigated by voltage clamp and computer simulation. *Proc. R. Soc. Lond. B* **222**: 305-328, 1984.
35. Brown, H.F., K. Kimura, and S. Noble. The relative contributions of various time-dependent membrane currents to pacemaker activity in the sino atrial node. In: *Cardiac Rate and Rhythm: Physiological, Morphological and Developmental Aspects*, edited by L.N. Bouman and H.J. Jongasma. Boston: Martinus-Nijoff, 1982, p. 53-68.
36. Callewaert, G., E. Carmeliet, and J. Vereecke. Single cardiac Purkinje cells: general electrophysiology and voltage-clamp analysis of the pace-maker current. *J. Physiol.* **349**: 643-661, 1984.
37. Callewaert, G., L. Cleemann, and M. Morad. Epinephrine enhances Ca^{2+} current-regulated Ca^{2+} release and Ca^{2+} reuptake in rat ventricular myocytes. *Proc. Natl. Acad. Sci. USA* **85**: 2009-2013, 1988.
38. Campbell, D.L., R.L. Rasmusson, and H.C. Strauss. Ionic current mechanisms generating vertebrate primary cardiac pacemaker activity at the single cell level: an integrative view. *Annu. Rev. Physiol.* **54**: 279-302, 1992.
39. Cannell, M.B., J.R. Berlin, and W.J. Lederer. Effect of membrane potential changes on the calcium transient in single rat cardiac muscle cells. *Science* **238**: 1419-1423, 1987.
40. Cass, A., A. Finkelstein, and V. Krespi. The ion permeability induced in thin lipid membranes by the polyene antibiotics nystatin and amphotericin B. *J. Gen. Physiol.* **56**: 100-124, 1970.
41. Chang, F., I.S. Cohen, D. DiFrancesco, M.R. Rosen, and C. Tromba. Effects of protein kinase inhibitors on canine Purkinje fibre pacemaker depolarization and the pacemaker current $i(f)$. *J. Physiol.* **440**: 367-384, 1991.
42. Cohen, I., J. Daut, and D. Noble. The effects of potassium and temperature on the pace-maker current, iK_2 , in Purkinje fibres. *J. Physiol.* **260**: 55-74, 1976.
43. Colquhoun, D., E. Neher, H. Reuter, and C.F. Stevens. Inward current channels activated by intracellular Ca in cultured cardiac cells. *Nature* **294**: 752-754, 1981.
44. Cranefield, P.F. Does spontaneous activity arise from phase 4 depolarization or from triggering? In: *The Sinus Node: Structure, Function and Clinical Relevance*, edited by F.I.M. Bonke. Boston: Martinus-Nijoff, 1978, p. 348-356.

45. Crespo, L.M., C.J. Grantham, and M.B. Cannell. Kinetics, stoichiometry and role of the Na-Ca exchange mechanism in isolated cardiac myocytes. *Nature* **345**: 618-621, 1990.
46. De Mello, W.C. and B.F. Hoffman. Potassium ions and electrical activity of specialized cardiac fibers. *Am. J. Physiol.* **199**: 1125-1130, 1960.
47. Denyer, J.C. and H.F. Brown. An method for isolating rabbit sino-atrial node cells which maintains their natural shape. *Jap. J. Physiol.* **37**: 963-965, 1987.
48. Denyer, J.C. and H.F. Brown. Rabbit sino-atrial node cells: isolation and electrophysiological properties. *J. Physiol.* **428**: 405-424, 1990.
49. Denyer, J.C. and H.F. Brown. Pacemaking in rabbit isolated sino-atrial node cells during Cs⁺ Block of the hyperpolarization-activated current i_f . *J. Physiol.* **429**: 401-409, 1990.
50. Denyer, J.C. and H.F. Brown. Calcium 'window' current in rabbit isolated sino-atrial node cells. *J. Physiol.* **429**: 21P, 1990.
51. DiFrancesco, D. A study of the ionic nature of the pace-maker current in calf Purkinje fibres. *J. Physiol.* **314**: 377-393, 1981.
52. DiFrancesco, D. A new interpretation of the pace-maker current i_{K2} in Purkinje fibres. *J. Physiol.* **314**: 359-376, 1981.
53. DiFrancesco, D. Block and activation of the pace-maker channel in calf purkinje fibers: effects of potassium, caesium and rubidium. *J. Physiol.* **329**: 485-507, 1982.
54. DiFrancesco, D. The current i_{K2} in Purkinje fobres reinterpreted and identified with the current i_f in the sinus node. In: *Cardiac Rate and Rhythm: Physiological, Morphological and Developmental Aspects*, edited by L.N. Bouman and H.J. Jongasma. Boston: Martinus-Nijoff, 1982, p. 69-91.
55. DiFrancesco, D. Characterization of the pace-maker current kinetics in calf Purkinje fibres. *J. Physiol.* **348**: 341-367, 1984.
56. DiFrancesco, D. The cardiac hyperpolarizing-activated current, i_f . Origins and developments. *Prog. Biophys. Mol. Biol.* **46**: 163-183, 1985.
57. DiFrancesco, D. The contribution of the 'pacemaker' current (i_f) to generation of spontaneous activity in rabbit sino-atrial node myocytes. *J. Physiol.* **434**: 23-40, 1991.

58. DiFrancesco, D. and A. Ferroni. Delayed activation of the cardiac pacemaker current and its dependence on conditioning pre-hyperpolarizations. *Pflügers Arch.* **396**: 265-267, 1983.
59. DiFrancesco, D., A. Ferroni, M. Mazzanti, and C. Tromba. Properties of the hyperpolarizing-activated current (i_f) in cells isolated from the rabbit sino-atrial node. *J. Physiol.* **377**: 61-88, 1986.
60. DiFrancesco, D. and D. Noble. A model of cardiac electrical activity incorporating ionic pumps and concentration changes. *Phil. Trans. R. Soc. Lond. B* **307**: 353-398, 1985.
61. DiFrancesco, D., A. Noma, and W. Trautwein. Kinetics and magnitude of the time-dependent potassium current in the rabbit sino-atrial node. *Pflügers Arch.* **381**: 271-279, 1979.
62. DiFrancesco, D., M. Ohba, and C. Ojeda. Measurement and significance of the reversal potential for the pacemaker current (i_{K2}) in sheep Purkinje fibers. *J. Physiol.* **297**: 135-162, 1979.
63. DiFrancesco, D. and C. Ojeda. Properties of the current i_f in the sino-atrial node of the rabbit compared with those of the current i_{K2} in Purkinje fibres. *J. Physiol.* **308**: 353-367, 1980.
64. Doerr, T., R. Denger, and W. Trautwein. Calcium currents in single SA node cells of the rabbit heart studied with action potential clamp. *Pflügers Arch.* **413**: 599-603, 1989.
65. Draper, M.H. and S. Weidmann. Cardiac resting and action potentials recorded with an intracellular electrode. *J. Physiol.* **115**: 74-94, 1951.
66. DuBell, W.H., M.R. Boyett, H.A. Spurgeon, A. Talo, M.D. Stern, and E.G. Lakatta. The cytosolic calcium transient modulates the action potential of rat ventricular myocytes. *J. Physiol.* **436**: 347-369, 1991.
67. DuBell, W.H. and S.R. Houser. Voltage and beat dependence of Ca^{2+} transient in feline ventricular myocytes. *Am. J. Physiol.* **257**: H746-H759, 1989.
68. Duchatelle-Gourdon, I., H.C. Hartzell, and A.A. Lagrutta. Modulation of the delayed rectifier potassium current in frog cardiomyocytes by β -adrenergic agonists and magnesium. *J. Physiol.* **415**: 251-274, 1989.
69. Earm, Y.E., W.K. Ho, and I.S. So. Inward current generated by Na-Ca

- exchange during the action potential in single atrial cells of the rabbit. *Proc. R. Soc. Lond. B* **240**: 61-81, 1990.
70. Earm, Y.E. and D. Noble. A model of the single atrial cell: relation between calcium current and calcium release. *Proc. R. Soc. Lond. B* **240**: 83-96, 1990.
71. Earm, Y.E., Y. Shimoni, and A.J. Spindler. A pace-maker-like current in the sheep atrium and its modulation by catecholamines. *J. Physiol.* **342**: 569-590, 1983.
72. Egan, T.M., D. Noble, S.J. Noble, T. Powell, A.J. Spindler, and V.W. Twist. Sodium-calcium exchange during the action potential in guinea-pig ventricular cells. *J. Physiol.* **411**: 639-661, 1989.
73. Ehara, T., A. Noma, and K. Ono. Calcium-activated nonselective cation channel in ventricular cells isolated from adult guinea-pig hearts. *J. Physiol.* **403**: 117-133, 1988.
74. Euler, D.E., S.B. Jones, W.P. Gunnar, J.M. Loeb, D.K. Murdock, and W.C. Randall. Cardiac arrhythmias in the conscious dog after excision of the sinoatrial node and crista terminalis. *Circ.* **59**: 468-475, 1979.
75. Eyster, J.A.E. and W.J. Meek. The origin and conduction of the heart beat. *Physiol. Rev.* **1**: 1-43, 1921.
76. Eyster, J.A.E. and W.J. Meek. Studies on the origin and conduction of the cardiac impulse. VIII. The permanent rhythm following destruction of the sino-auricular node. *Am. J. Physiol.* **61**: 117-129, 1922.
77. Fabiato, A. Time and calcium dependence of activation and inactivation of calcium-induced release of calcium from sarcoplasmic reticulum of a skinned canine cardiac purkinje. *J. Gen. Physiol.* **85**: 247-290, 1985.
78. Fedida, D., D. Noble, Y. Shimoni, and A.J. Spindler. Inward current related to contraction in guinea-pig ventricular myocytes. *J. Physiol.* **385**: 565-589, 1987.
79. Fermini, B. and R.D. Nathan. Removal of sialic acid alters both T- and L-type calcium currents in cardiac myocytes. *Am. J. Physiol.* **260**: H735-H743, 1991.
80. Finkel, A.S. and S.J. Redman. Theory and operation of a single microelectrode voltage clamp. *J. Neurosci. Methods* **11**: 101-127, 1984.
81. Frace, A.M., F. Maruoka, and A. Noma. External K increases Na conductance of the hyperpolarization-activated current in rabbit cardiac pacemaker cells.

Pflügers Arch. 421: 97-99, 1992.

82. Giles, W. and Y. Shimoni. Slow inward tail currents in rabbit cardiac cells. *J. Physiol.* 417: 447-463, 1989.
83. Giles, W., A. van Ginneken, and E.F. Shibata. Ionic currents underlying cardiac pacemaker activity: a summary of voltage-clamp data from single cells. In: *Cardiac Muscle: The Regulation of Excitation and Contraction*, edited by R. Nathan. London, England: Academic Press, Inc., 1986, p. 1-27.
84. Giles, W.R. and E.F. Shibata. Voltage clamp of bull-frog cardiac pace-maker cells: a quantitative analysis of potassium currents. *J. Physiol.* 368: 265-292, 1985.
85. Giles, W.R. and A.C.G. van Ginneken. A transient outward current in isolated cells from the crista terminalis of rabbit heart. *J. Physiol.* 368: 243-264, 1985.
86. Gintant, G.A., N.B. Datyner, and I.S. Cohen. Gating of delayed rectification in acutely isolated canine cardiac Purkinje myocytes. Evidence for a single voltage-gated conductance. *Biophys. J.* 48: 1059-1064, 1985.
87. Glitsch, H.G., H. Pusch, T. Schumacher, and F. Verdonck. An identification of the K activated Na pump current in sheep Purkinje fibers. *Pflügers Arch.* 394: 256-263, 1982.
88. Hagiwara, N. and H. Irisawa. Na-Ca exchange current in sinoatrial node cell of rabbit. *Circ.* 78: II-123, 1988.
89. Hagiwara, N. and H. Irisawa. Modulation by intracellular Ca^{2+} of the hyperpolarization-activated inward current in rabbit single sino-atrial node cells. *J. Physiol.* 409: 121-141, 1989.
90. Hagiwara, N., H. Irisawa, and M. Kameyama. Contribution of two types of calcium currents to the pacemaker potentials of rabbit sino-atrial node cells. *J. Physiol.* 395: 233-253, 1988.
91. Hagiwara, N., H. Irisawa, H. Kasanuki, and S. Hosoda. Background current in sino-atrial node cells of the rabbit heart. *J. Physiol.* 448: 53-72, 1992.
92. Halliwell, J.V., T.D. Plant, and N.B. Standen. Voltage clamp techniques. In: *Microelectrode Techniques*, edited by N.B. Standen, P.T.A. Gray, and M.J. Whitaker. Cambridge: The Company of Biologists Limited, 1987, p. 13-28.
93. Hamill, O.P., A. Marty, E. Neher, B. Sakmann, and F.J. Sigworth. Improved

patch-clamp techniques for high resolution current recording from cells and cell-free membrane patches. *Pflügers Arch.* **391**: 85-100, 1981.

94. Hart, G. The kinetics and temperature dependence of the pace-maker current, i_f sheep Purkinje fibers. *J. Physiol.* **337**: 401-416, 1983.
95. Harvey, R.D., C.D. Clark, and J.R. Hume. Chloride current in mammalian cardiac myocytes. Novel mechanism for autonomic regulation of action potential duration and resting membrane potential. *J. Gen. Physiol.* **95**: 1077-1102, 1990.
96. Harvey, R.D. and J.R. Hume. Autonomic regulation of a chloride current in heart. *Science* **244**: 983-985, 1989.
97. Harvey, R.D. and J.R. Hume. Autonomic regulation of delayed rectifier K^+ current in mammalian heart involves G proteins. *Am. J. Physiol.* **257**: H818-H823, 1989.
98. Hecht, H.H. Normal and abnormal transmembrane potentials of the spontaneously beating heart. *New York Acad. Sci.* **65**: 700, 1957.
99. Hirano, Y., H.A. Fozzard, and C.T. January. Characteristics of L- and T-type Ca^{2+} currents in canine cardiac Purkinje cells. *Am. J. Physiol.* **256**: H1478-H1492, 1989.
100. Hiraoka, M. and T. Sano. Role of the sinoatrial ring bundle in internodal conduction. *Am. J. Physiol.* **231**: 319-325, 1976.
101. Hogan, P.M. and L.D. Davis. Evidence for specialized fibers in the canine right atrium. *Circ. Res.* **23**: 387-396, 1968.
102. Hogan, P.M. and L.D. Davis. Electrophysiological characteristics of canine atrial plateau fibers. *Circ. Res.* **28**: 62-73, 1971.
103. Holz, R. and A. Finkelstein. The water and nonelectrolyte permeability induced in thin lipid membrane by the polyene antibiotics nystatin and amphotericin. *J. Gen. Physiol.* **56**: 125-145, 1970.
104. Horn, R. and A. Marty. Muscarinic activation of ionic currents measured by a new whole-cell recording method. *J. Gen. Physiol.* **92**: 145-159, 1988.
105. Hryshko, L.V., V. Stiffel, and D.M. Bers. Rapid cooling contractures as an index of sarcoplasmic reticulum calcium content in rabbit ventricular myocytes. *Am. J. Physiol.* **257**: H1369-H1377, 1989.

106. Hume, J.R. Component of whole cell Ca current due to electrogenic Na-Ca-exchange in cardiac myocytes. *Am. J. Physiol.* **252**: H666-H670, 1987.
107. Hume, J.R., W. Giles, K. Robinson, E.F. Shibata, R.D. Nathan, K. Kanai, and R. Rasmusson. A time- and voltage-dependent K^+ current in single cardiac cells from bullfrog atrium. *J. Gen. Physiol.* **88**: 777-798, 1986.
108. Hume, J.R. and A. Uehara. "Creep currents" in single frog atrial cells may be generated by electrogenic Na/Ca exchange. *J. Gen. Physiol.* **87**: 857-884, 1986.
109. Hume, J.R. and A. Uehara. Properties of "creep currents" in single frog atrial cells. *J. Gen. Physiol.* **87**: 833-855, 1986.
110. Iijima, T. and N. Taira. Effects of Manganese ions and diltiazem on the spontaneous action potential of the canine atrio-ventricular node cell. *J. Mol. Cell. Cardiol.* **15**: 863-866, 1983.
111. Inui, M., A. Saito, and S. Fleischer. Isolation of the ryanodine receptor from cardiac sarcoplasmic reticulum and identity with feet structures. *J. Biol. Chem.* **262**: 15637-15642, 1987.
112. Irisawa, H. and W.R. Giles. Sinus and atrioventricular node cell: Cellular electrophysiology. In: *Cardiac Electrophysiology From Cell to Bedside*, edited by D.P. Zipes and J. Jalife. Philadelphia: W.B. Saunders Company, 1990, p. 95-102.
113. Irisawa, H., T. Nakayama, and A. Noma. Membrane currents of single pacemaker cells from rabbit SA and AV nodes. In: *Electrophysiology of single cardiac cells*, edited by D. Noble and T. Powell. New York: Academic Press, 1987, p. 167-186.
114. Isenberg, G. and U. Klockner. Calcium tolerant ventricular myocytes prepared by preincubation in a "KB Medium". *Pflügers Arch.* **395**: 6-18, 1982.
115. Isenberg, G. and U. Klockner. Calcium currents of isolated bovine ventricular myocytes are fast and of large amplitude. *Pflügers Arch.* **395**: 30-41, 1982.
116. Ishikawa, S., K. Sawada, Y. Tanahashi, J. Tsuzuki, M. Hattori, R. Kato, and I. Toyama. Experimental studies on sick sinus syndrome: relationship of extent of right atrial lesions to subsidiary pacemaker shift and its function. *Am. Heart J.* **105**: 593-602, 1983.
117. James, T.N. Anatomy of the human sinus node. *Anat. Rec.* **141**: 469-495, 1961.
118. James, T.N. and L. Sherf. Ultrastructure of the human atrioventricular node.

Circ. **37**: 1049-1070, 1968.

119. James, T.N., L. Sherf, G. Fine, and A.R. Morales. Comparative ultrastructure of the sinus node in man and dog. *Circ.* **34**: 139-163, 1966.
120. Jones, S.B., D.E. Euler, E. Hardie, W.C. Randall, and G. Brynjolfsson. Comparison of SA nodal and subsidiary atrial pacemaker function and location in the dog. *Am. J. Physiol.* **234**: H471-H476, 1978.
121. Jones, S.B., D.E. Euler, W.C. Randall, G. Brynjolfsson, and E.L. Hardie. Atrial ectopic foci in the canine heart: hierarchy of pacemaker automaticity. *Am. J. Physiol.* **238**: H788-H793, 1980.
122. Kameyama, M., F. Hofmann, and W. Trautwein. On the mechanism of β -adrenergic regulation of the Ca channels in the guinea-pig heart. *Pflügers Arch.* **405**: 285-293, 1985.
123. Kameyama, M., T. Kiyosue, and M. Soejima. Inward rectifier K channel in the rabbit ventricular cells. *Jap. J. Physiol.* **33**: 1039-1056, 1983.
124. Kawano, S. and R.L. DeHaan. Low-threshold current is major calcium current in chick ventricle cells. *Am. J. Physiol.* H1505-H1508, 1989.
125. Kenyon, J.L. and W.R. Gibbons. 4-aminopyridine and the early outward current of sheep cardiac Purkinje fibers. *J. Gen. Physiol.* **73**: 139-157, 1979.
126. Kimura, J., S. Miyamae, and A. Noma. Identification of sodium-calcium exchange current in single ventricular cells of guinea-pig. *J. Physiol.* **384**: 199-222, 1987.
127. Kimura, J., A. Noma, and H. Irisawa. Na-Ca exchange current in mammalian heart cells. *Nature* **319**: 596-597, 1986.
128. Kokubun, S., M. Nishimura, A. Noma, and H. Irisawa. The spontaneous action potential of the rabbit atrioventricular node cells. *Jap. J. Physiol.* **30**: 529-540, 1980.
129. Kokubun, S., M. Nishimura, A. Noma, and H. Irisawa. Membrane currents in the rabbit atrioventricular node cell. *Pflügers Arch.* **393**: 15-22, 1982.
130. Korn, S.J. and R. Horn. Influence of sodium-calcium exchange on calcium current rundown and the duration of the calcium-dependent chloride currents in pituitary cells, studied with whole cell and perforated patch recording. *J. Gen. Physiol.* **94**: 789-812, 1989.

131. Kreitner, D. Evidence for the existence of a rapid sodium channel in the membrane of rabbit sinoatrial cells. *J. Mol. Cell. Cardiol.* **7**: 655-662, 1975.
132. Kreitner, D. Electrophysiological study of the two main pacemaker mechanisms in the rabbit sinus node. *Cardiovas. Res.* **19**: 304-318, 1985.
133. Kurachi, Y. Voltage-dependent activation of the inward-rectifier potassium channel in the ventricular cell membrane of guinea-pig heart. *J. Physiol.* **366**: 365-385, 1985.
134. Lai, F.A., H. Erickson, B.A. Block, and G. Meissner. Evidence for a junctional feet-ryanodine receptor complex from sarcoplasmic reticulum. *Biochem. Biophys. Res. Comm.* **143**: 704-709, 1987.
135. Lansman, J.B., P. Hess, and R.W. Tsien. Blockade of current through single calcium channels by Cd^{2+} , Mg^{2+} , and Ca^{2+} . *J. Gen. Physiol.* **88**: 321-347, 1986.
136. Lewis, T., B.S. Oppenheimer, and A. Oppenheimer. The site of origin of the mammalian heart-beat; the pacemaker in the dog. *Heart* **2**: 147-169, 1910.
137. Lipp, P. and L. Pott. Voltage dependence of sodium-calcium exchange current in guinea-pig atrial myocytes determined by means of an inhibitor. *J. Physiol.* **403**: 355-366, 1988.
138. Lipp, P. and L. Pott. Transient inward current in guinea-pig atrial myocytes reflects a change of sodium-calcium exchange current. *J. Physiol.* **397**: 601-630, 1988.
139. Lipsius, S.L. Mechanisms of atrial subsidiary pacemaker function. In: *Cellular Pathophysiology*, edited by M.M. Sayeed. Boca Raton, Florida: CRC Press, 1989, p. 1-39.
140. Lipsius, S.L. and D.S. Rubenstein. Cyclic brady dysrhythmias generated by atrial subsidiary pacemakers. *J. Electrophysiol.* **2**: 90-103, 1988.
141. Lipsius, S.L. and M. Vassalle. Characterization of a two-component upstroke in the sinus node subsidiary pacemakers. In: *The sinus node*, edited by F.I.M. Bonke. Hague: Nijhoff, 1978, p. 233-244.
142. Lipsius, S.L. and M. Vassalle. Dual excitatory channels in the sinus node. *J. Mol. Cell. Cardiol.* **10**: 753-767, 1978.

143. Lu, H.H. Shifts in pacemaker dominance within the sinoatrial region of cat and rabbit hearts resulting from increase of extracellular potassium. *Circ. Res.* **26**: 339-346, 1970.
144. Makarychev, V.A., I.L. Kosharskaya, and L.S. Ul'yaninskii. Automatic activity of pacemaker cells of the atrioventricular valves of the rabbit heart. *Bull. Exp. Biol. Med.* **81**: 517-520, 1976.
145. Marban, E. and W. G. Wier. Ryanodine as a tool to determine the contributions of calcium entry and calcium release to the calcium transient and contraction of cardiac Purkinje fibers. *Circ. Res.* **56**: 133-138, 1985.
146. Masson-Pevet, M.A., W.K. Bleeker, E. Besselsen, B.W. Treytel, and H.J. Jongsma. Pacemaker cell types in the rabbit sinus node: A correlative ultrastructural and electrophysiological study. *J. Mol. Cell. Cardiol.* **16**: 53-63, 1984.
147. Masson-Pevet, M., W.K. Bleeker, A.J.C. Mackaay, L.N. Bouman, and J.M. Houtkooper. Sinus node and atrium cells from the rabbit heart: A quantitative electron microscopic description after electrophysiological localization. *J. Mol. Cell. Cardiol.* **11**: 555-568, 1979.
148. Matsuda, H., A. Saigusa, and H. Irisawa. Ohmic conductance through the inwardly rectifying K channel and blocking by internal Mg^{2+} . *Nature* **325**: 156-159, 1987.
149. Matsuura, H., T. Ehara, and Y. Imoto. An analysis of the delayed outward current in single ventricular cells of the guinea-pig. *Pflügers Arch.* **410**: 596-603, 1987.
150. Maylie, J. and M. Morad. Ionic currents responsible for the generation of pacemaker current in the rabbit sino-atrial node. *J. Physiol.* **355**: 215-235, 1984.
151. McAllister, R.E. and D. Noble. The time and voltage dependence of the slow outward current in cardiac Purkinje fibres. *J. Physiol.* **186**: 632-662, 1966.
152. McDonald, T F and W. Trautwein. The potassium current underlying delayed rectification in cat ventricular muscle. *J. Physiol.* **274**: 217-246, 1978.
153. Mechmann, S. and L. Pott. Identification of Na-Ca exchange current in single cardiac myocytes. *Nature* **319**: 597-599, 1986.
154. Meek, W.J. and J.A.E. Eyster. Experiments on the origin and propagation of the impulse in the heart. III. The effect of vagal stimulation on the location of the

- pacemaker in auriculo-ventricular rhythm, and the effect of vagal stimulation on this rhythm. *Heart* **5**: 227-244, 1913.
155. Mitchell, M.R., T. Powell, D.A. Terrar, and V.W. Twist. Calcium-activated inward current and contraction in rat and guinea-pig ventricular myocytes. *J. Physiol.* **391**: 545-560, 1987.
 156. Mitra, R. and M. Morad. Two types of calcium channels in guinea pig ventricular myocytes. *Proc. Natl. Acad. Sci. USA* **83**: 5340-5344, 1986.
 157. Muramatsu, H. and R.D. Nathan. Characterization of sodium current in primary pacemaker cells isolated from the sinoatrial node. *Biophys. J.* **59**: 98a, 1991.
 158. Muramatsu, H. and R.D. Nathan. Role of a TTX-sensitive sodium current in primary pacemaker cells of the rabbit sinoatrial node. *Biophys. J.* **61**: A306, 1992.
 159. Nakayama, T., Y. Kurachi, A. Noma, and H. Irisawa. Action potential and membrane currents of single pacemaker cells of the rabbit heart. *Pflügers Arch.* **402**: 248-257, 1984.
 160. Nathan, R.D. Two electrophysiologically distinct types of cultured pacemaker cells from rabbit sinoatrial node. *Am. J. Physiol.* **250**: H325-H329, 1986.
 161. Nilius, B., P. Hess, J.B. Lansman, and R.W. Tsien. A novel type of cardiac calcium channel in ventricular cells. *Nature* **316**: 443-446, 1985.
 162. Noble, D. Electrical properties of cardiac muscle attributable to inward going (anomalous) rectification. *J. Cell. Comp. Physiol.* **66**: 127-136, 1965.
 163. Noble, D. Potassium accumulation and depletion in frog atrial muscle. *J. Physiol.* **258**: 579-613, 1976.
 164. Noble, D. The surprising heart: A review of recent progress in cardiac electrophysiology. *J. Physiol.* **353**: 1-50, 1984.
 165. Noble, D. Ionic basis of rhythmic activity in the heart. In: *Cardiac Electrophysiology and Arrhythmias*, edited by D. Zipes and J. Jalife. FL, USA.: Grune & Stratton Inc., 1985, p. 3-11.
 166. Noble, D. and R.W. Tsien. The kinetics and rectifier properties of the slow potassium current in cardiac Purkinje fibres. *J. Physiol.* **195**: 185-214, 1968.
 167. Noble, D. and R.W. Tsien. Outward membrane currents activated in the plateau

- range of potentials in cardiac Purkinje fibres. *J. Physiol.* **200**: 205-231, 1969.
168. Noble, D. and R.W. Tsien. Reconstruction of the repolarization process in cardiac Purkinje fibres based on voltage clamp measurements of membrane current. *J. Physiol.* **200**: 233-254, 1969.
169. Noma, A. and H. Irisawa. A time- and voltage-dependent potassium current in the rabbit sinoatrial node cell. *Pflügers Arch.* **366**: 251-258, 1976.
170. Noma, A., H. Kotake, S. Kokubun, and H. Irisawa. Kinetics and rectification of the slow inward current in the rabbit sinoatrial node cell. *Jap. J. Physiol.* **31**: 491-500, 1981.
171. Noma, A., M. Morad, and H. Irisawa. Does the "pacemaker current" generate the diastolic depolarization in the rabbit s.a. node cells? *Pflügers Arch.* **397**: 190-194, 1983.
172. Noma, A., T. Nakayama, Y. Kurachi, and H. Irisawa. Resting K conductance in pacemaker and non-pacemaker heart cells of the Rabbit. *Jap. J. Physiol.* **34**: 245-254, 1984.
173. Oei, H.I., A.C.G. Van Ginneken, H.J. Jongasma, and L.N. Bouman. Mechanisms of impulse generation in isolated cells from the rabbit sinoatrial node. *J. Mol. Cell. Cardiol.* **21**: 1137-1149, 1989.
174. Ojeda, C. and O. Rougier. Kinetic analysis of the delayed outward currents in frog atrium. Existence of two types of preparation. *J. Physiol.* **239**: 51207-73, 1974.
175. Opthof, T., B. DeJonge, M. Masson-Pevet, H.J. Jongasma, and L.N. Bouman. Functional and morphological organization of the cat sinoatrial node. *J. Mol. Cell. Cardiol.* **18**: 1015-1031, 1986.
176. Osterrieder, W., Q-F. Yang, and W. Trautwein. Effects of barium on the membrane current in the rabbit s-a node. *Pflügers Arch.* **394**: 78-84, 1982.
177. Paes de Carvalho, A., W.C. DeMello, and B. Hoffman. Electrophysiological evidence for specialized fiber types in rabbit atrium. *Am. J. Physiol.* **196**: 483-488, 1959.
178. Peper, K. and W. Trautwein. A note on the pace-maker current in Purkinje fibres. *Pflügers Arch.* **309**: 356-361, 1969.
179. Randall, W.C., L.E. Rinkema, S.B. Jones, J.F. Moran, and G. Brynjolfsson.

- Functional characterization of atrial pacemaker activity. *Am. J. Physiol.* **242**: H98-H106, 1982.
180. Randall, W.C., J. Talano, M.P. Kaye, D.E. Euler, S.B. Jones, and G. Brynjolfsson. Cardiac pacemakers in the absence of the SA node: responses to exercise and autonomic blockade. *Am. J. Physiol.* **234**: H465-H470, 1978.
181. Randall, W.C., W.H. Wehrmacher, and S.B. Jones. Hierarchy of supraventricular pacemakers. *J. Thorac. Cardiovas. Surg.* **82**: 797-800, 1981.
182. Rousseau, E., J.S. Smith, and G. Meissner. Ryanodine modifies conductance and gating behavior of single Ca^{2+} release channel. *Am. J. Physiol.* **253**: C364-C368, 1987.
183. Rozanski, G.J. Electrophysiological properties of automatic fibers in rabbit atrioventricular valves. *Am. J. Physiol.* **253**: H720-H727, 1987.
184. Rozanski, G.J. and J. Jalife. Automaticity in atrioventricular valve leaflets of rabbit heart. *Am. J. Physiol.* **19**: H397-H406, 1986.
185. Rozanski, G.J. and S.L. Lipsius. Electrophysiology of functional subsidiary pacemakers in canine right atrium. *Am. J. Physiol.* **249**: H594-H603, 1985.
186. Rozanski, G.J., S.L. Lipsius, and W.C. Randall. Functional characteristics of sinoatrial and subsidiary pacemaker activity in the canine right atrium. *Circ.* **67**: 1378-1387, 1983.
187. Rozanski, G.J., S.L. Lipsius, W.C. Randall, and S.B. Jones. Alterations in subsidiary pacemaker function after prolonged subsidiary pacemaker dominance in the canine right atrium. *J. Am. Coll. Cardiol.* **4**: 535-542, 1984.
188. Rubenstein, D.S., L.M. Fox, J.A. McNulty, and S.L. Lipsius. Electrophysiology and ultrastructure of Eustachian ridge from cat right atrium: a comparison with SA node. *J. Mol. Cell. Cardiol.* **19**: 965-976, 1987.
189. Rubenstein, D.S. and S.L. Lipsius. Mechanisms of automaticity in subsidiary pacemakers from cat right atrium. *Circ. Res.* **64**: 648-657, 1989.
190. Sakmann, B., A. Noma, and W. Trautwein. Acetylcholine activation of single muscarinic K channels in isolated pacemaker cells of the mammalian heart. *Nature* **303**: 250-253, 1983.
191. Sakmann, B. and G. Trube. Voltage-dependent inactivation of inward-rectifying single-channel current in the guinea-pig heart cell membrane. *J. Physiol.* **347**:

659-683, 1984.

192. Sakmann, B. and G. Trube. Conductance properties of single inwardly rectifying potassium channels in ventricular cells from guinea-pig heart. *J. Physiol.* **347**: 641-657, 1984.
193. Sanguinetti, M.C. and N.K. Jurkiewicz. Two components of cardiac delayed rectifier K^+ current. Differential sensitivity to block by class III antiarrhythmic agents. *J. Gen. Physiol.* **96**: 195-215, 1990.
194. Sanguinetti, M.C. and N.K. Jurkiewicz. Delayed rectifier outward K^+ current is composed of two currents in guinea pig atrial cells. *Am. J. Physiol.* **260**: H393-H399, 1991.
195. Sano, T., M. Tasaki, M. Ono, H. Tsuchihashi, N. Takayama, and T. Simamoto. Resting and action potential in the region of the atrioventricular node. *Proc. Jpn. Acad.* **34**: 558-563, 1958.
196. Sealy, W.C., R.J. Bache, A.V. Seaber, and S.K. Bhattacharga. The atrial pacemaking site after surgical exclusion of the sinoatrial node. *J. Thorac. Cardiovasc. Surg.* **65**: 841-850, 1973.
197. Sealy, W.C. and A.V. Seaber. Cardiac rhythm following exclusion of the sinoatrial node and most of the right atrium from the remainder of the heart. *J. Thorac. Cardiovasc. Surg.* **77**: 436-447, 1979.
198. Shattock, M.J. and D.M. Bers. Rat vs. rabbit ventricle: Ca flux and intracellular Na assessed by ion-selective microelectrodes. *Am. J. Physiol.* **256**: C813-C822, 1989.
199. Sherf, L. and T.N. James. Fine structure of cells and their histologic organization within internodal pathways of the heart: Clinical and electrocardiographic implications. *Am. J. Cardiol.* **44**: 345-369, 1979.
200. Shibasaki, T. Conductance and kinetics of delayed rectifier potassium channels in nodal cells of the rabbit heart. *J. Physiol.* **387**: 227-250, 1987.
201. Simmons, M.A., T. Creazzo, and H.C. Hartzell. A time-dependent and voltage-sensitive K^+ current in single cells from frog atrium. *J. Gen. Physiol.* **88**: 739-755, 1986.
202. Soejima, M. and A. Noma. Mode of regulation of the ACh-sensitive K channel by the muscarinic receptor in the rabbit atrial cells. *Pflügers Arch.* **400**: 424-431, 1984.

203. Sterba, J.A., L.E. Rinkema, and W.C. Randall. Influence of cardiac denervation on subsidiary atrial pacemaker stabilization. *Am. J. Physiol.* **247**: H523-H530, 1984.
204. Takano, M. and A. Noma. Distribution of the isoprenaline-induced chloride current in rabbit heart. *Pflügers Arch.* **420**: 223-226, 1992.
205. Taniguchi, J., S. Kokubin, A. Noma, and H. Irisawa. Spontaneously active cells isolated from the sino-atrial and atrio-ventricular nodes of the rabbit heart. *Jap. J. Physiol.* **31**: 547-558, 1981.
206. Taylor, J.J., L.S. D'Agrosa, and E.M. Burns. The pacemaker cell of the sinoatrial node of the rabbit. *Am. J. Physiol.* **235**: H407-H412, 1978.
207. Trautwein, W. and D.G. Kassebaum. On the mechanism of spontaneous impulse generation in the pacemaker of the heart. *J. Gen. Physiol.* **45**: 317-330, 1961.
208. Tse, W.W. Evidence of presence of automatic fibers in the canine atrioventricular node. *Am. J. Physiol.* **225**: 716-723, 1973.
209. Tseng, G. Calcium current restitution in mammalian ventricular myocytes is modulated by intracellular calcium. *Circ. Res.* **63**: 468-482, 1988.
210. Tseng, G. and A. Boyden. Multiple types of Ca^{2+} currents in single canine purkinje cells. *Circ. Res.* **65**, No. 6: 1735-1750, 1989.
211. Urthaler, F. and T.N. James. Hierarchy of supraventricular pacemakers. *J. Thorac. Cardiovas. Surg.* **80**: 750-753, 1980.
212. Urthaler, F., C.R. Katholi, J. Macy, J.r., and T.N. James. Mathematical relationship between automaticity of the sinus node and the AV junction. *Am. Heart J.* **86**: 189-195, 1973.
213. Van Ginneken, A.C.G. and W. Giles. Voltage clamp measurements of the hyperpolarization-activated inward current I_f in single cells from rabbit sino-atrial node. *J. Physiol.* **434**: 57-83, 1991.
214. Vassalle, M. Analysis of cardiac pacemaker potential using a "voltage clamp" technique. *Am. J. Physiol.* **210**: 1335-1341, 1966.
215. Vassalle, M. Electrogenic suppression of automaticity in sheep and dog Purkinje fibers. *Circ. Res.* **27**: 361-377, 1970.

216. Vassalle, M. The relationship among cardiac pacemakers. Overdrive suppression. *Circ. Res.* **41**: 269-277, 1977.
217. Vassalle, M., K. Greenspan, S. Jomain, and B.F. Hoffman. Effect of potassium on automaticity and conduction of canine hearts. *Am. J. Physiol.* **207**: 334-340, 1964.
218. Vassalle, M., J.K. Greineder, and J.H. Stuckey. Role of the sympathetic nervous system in the sinus node resistance to high potassium. *Circ. Res.* **32**: 348-355, 1973.
219. Vassalle, M. and B.F. Hoffman. The spread of sinus activation during potassium administration. *Circ. Res.* **17**: 285-295, 1965.
220. Walsh, K.B. and R.S. Kass. Distinct voltage-dependent regulation of a heart-delayed IK by protein kinases A and C. *Am. J. Physiol.* **261**: C1081-C1090, 1991.
221. West, T.C. Ultramicroelectrode recording from the cardiac pacemaker. *J Pharmacol. Exp. Ther.* **115**: 283-290, 1955.
222. Wier, W.G., D.T. Yue, and E. Marban. Effects of ryanodine on intracellular Ca transients on mammalian cardiac muscle. *Fed. Proc.* **44**: 2989-2993, 1985.
223. Wilson, W.A. and M.M. Goldner. Voltage clamping with a single microelectrode. *J. Neurobiol.* **6**: 411-422, 1975.
224. Wit, A.L. and P.F. Cranefield. Triggered and automatic activity in the canine coronary sinus. *Circ. Res.* **41**: 435-445, 1977.
225. Wu, J. and S.L. Lipsius. Effects of extracellular Mg^{2+} on T- and L-type Ca^{2+} currents in single atrial myocytes. *Am. J. Physiol.* **259**: H1842-H1850, 1990.
226. Wu, J., J. Vereecke, E. Carmeliet, and S.L. Lipsius. Ionic currents activated during hyperpolarization of single right atrial myocytes from cat heart. *Circ. Res.* **68**: 1059-1069, 1991.
227. Yamagishi, S. and T. Sano. Effect of tetrodotoxin on the pacemaker action potential of the sinus node. *Proc. Jap. Acad.* **42**: 1194-1196, 1966.
228. Yanagihara, K. and H. Irisawa. Inward current activated during hyperpolarization in the rabbit sinoatrial node cell. *Pflügers Arch.* **385**: 11-19, 1980.

229. Yanigahara, K. and H. Irisawa. Potassium current during the pacemaker depolarization in rabbit sino-atrial node cell. *Pflügers Arch.* **388**: 255-260, 1980.
230. Yatani, A and A M Brown. Regulation of cardiac pacemaker current I_f in excised membranes from sinoatrial node cells. *Am. J. Physiol.* H1947-H1951, 1990.
231. Zygmunt, A.C. and W.R. Gibbons. Calcium-activated chloride current in rabbit ventricular myocytes. *Circ. Res.* **68**: 424-437, 1991.

APPROVAL SHEET

The dissertation submitted by Zhengfeng Zhou has been read and approved by the following committee:

Dr. Stephen L. Lipsius, Director
Associate Professor, Physiology, Loyola University

Dr. Richard D. Nathan
Associate Professor, Physiology, Texas Tech University

Dr. J. Andrew Wasserstrom
Associate Professor, Medicine, Northwestern University

Dr. Charles L. Webber
Associate Professor, Physiology, Loyola University

Dr. David E. Euler
Associate Professor, Medicine/Physiology, Loyola University

The final copies have been examined by the director of the dissertation and the signature which appears below verifies the fact that any necessary changes have been incorporated and that the dissertation is now given final approval by the committee with reference to content and form.

The dissertation is therefore accepted in partial fulfillment of the requirements for the degree of Doctor of Philosophy.

10/13/92
Date


Director's signature